McNAIR SCHOLARS
RESEARCH JOURNAL

VOLUME X

Summer 2020

TEXAS A&M UNIVERSITY
CORPUS CHRISTI

TRIO

RONALD E. MCNAIR
POST-BACCALAUREATE
ACHIEVEMENT PROGRAM

BIOGRAPHY OF

Dr. Ronald E. McNair

HE OVERCAME OBSTACLES.

Dr. Ronald Erwin McNair, Physicist & Astronaut, dared to dream. As an African American growing up in a poor community in the South, he encountered discrimination early in his youth. Yet this did not stop him from pursuing his dream of becoming a scientist.

HE ACHIEVED ACADEMIC EXCELLENCE.

In 1971, he graduated magna cum laude from North Carolina AT&T State University with a B.S. degree in physics. Ronald McNair then enrolled in the Massachusetts Institute of Technology. In 1976, at the age of 26, he earned his Ph.D. degree in laser physics.

HE BECAME A LEADER IN HIS FIELD.

Dr. McNair soon became a recognized expert in laser physics while working as a staff physicist with Hughes Research Laboratory. He was selected by NASA for the space shuttle program in 1978 and was a mission specialist aboard the 1984 flight of the shuttle Challenger.

HE WAS RESPECTED AND COMMENDED.

For his achievements, Ronald McNair received three honorary doctorate degrees and many fellowships and accomodations. These distinctions include: Presidential Scholar, 1967-71; Ford Foundation Fellow, 1971-74; National Fellowship Fund Fellow, 1974-75, Omega Psi Phi Scholar of the Year, 1975; Distinguished National Scientist, National Society of Black Professional Engineers, 1979; and the Friend of Freedom Award, 1981.

HE EXCELLED IN MANY ASPECTS OF LIFE.

Ronald McNair also held a fifth degree black belt in karate and was an accomplished jazz saxophon-ist. He was married and was the dedicated father of a daughter and a son.

After his death in the Challenger explosion in January 1986, members of Congress provided funding for the Ronald E. McNair Post Baccalaureate Achievement Program to encourage college students with similar backgrounds to Dr. McNair to enroll in graduate studies. Thus, the program targets students of color and low income, first generation college students. This program is dedicated to the high standards of achievement inspired by Dr. McNair's life.

TABLE OF CONTENTS

2020 McNAIR RESEARCH ARTICLES

President/CEO

DR. KELLY M. MILLER

Inspired by the momentous achievements of Ronald E. McNair, the TAMUCC McNair Scholars Program continues to honor his legacy by equipping underrepresented undergraduate students with the tools necessary to realize their highest aspirations.

The ability to conduct scholarly research is central to success in a variety of academic fields and vital to the attainment of a graduate degree. Through faculty mentorship and the assistance of program staff, the McNair Scholars Program is helping students develop these essential skills as evidenced by the work presented in this research journal.

I would like to congratulate the McNair Scholars on their accomplishments and extend my sincerest appreciation to the McNair staff, Faculty Mentors, and the campus community for their continued support of the scholarly growth of our students.

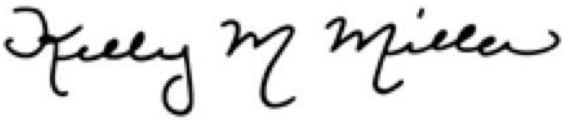

Dr. Kelly M. Miller
President/CEO

Provost and Vice President for Academic Affairs

DR. CLARENDA PHILLIPS

Texas A&M University-Corpus Christi is honored to host the McNair Scholars Program. Because the McNair Scholars Program prepares underrepresented students to pursue graduate degrees by emphasizing academic achievement, scholarly inquiry, and mentorship, we are excited to partner with the Program to develop the next generation of researchers. Research is a key activity for McNair scholars who seek to make a difference in the world by exploring an array of topics to find solutions for the problems that face our world.

From educating our children to managing ocean resources, our scholars provide an in depth perspective on education, psychology, health, technology, engineering, marine science and other scientific fields. The scholars included in this journal are among the most talented students at the Island University. They are our future leaders in higher education, and we are proud of what they have already accomplished.

I am grateful for the students' commitment to scholarly inquiry and discovery of new knowledge, the faculty mentors who have worked alongside these scholars, and the McNair Scholars Program staff. Reading through this journal, you too will see that the culmination of their efforts are exemplary.

Dr. Clarenda Phillips
Provost and Vice President for Academic Affairs

Associate Vice President for Academic Affairs

DR. GERARDO MORENO

This journal is the culmination of the summer 2020 research of the McNair Scholars Program. By engaging in undergraduate research these scholars have developed considerable critical thinking and methodological skills that will aid in their success in graduate school. This journal provides them an opportunity to have their research published and shared with the academic community.

The McNair scholars demonstrate a diversity of academic topics in this excellent undergraduate research. The McNair Scholars Program provides students access to nationwide conferences and graduate schools where they can present their original projects and meet doctoral faculty. Texas A&M University-Corpus Christi is proud of these researchers and understands the many challenges these underrepresented students face.

I am very honored to have each of the McNair scholars in the Academic Affairs family and you will see why as you read through this journal. Thank you scholars, faculty and staff for all your support for our outstanding students.

Dr. Gerardo Moreno
Associate Vice President for Academic Affairs

McNair Scholars Program Staff

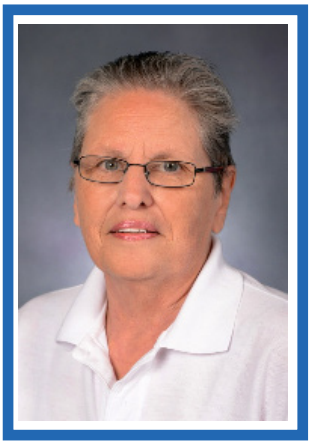

DR. PATRICIA SPANIOL-MATHEWS
PROGRAM DIRECTOR

DR. ANABEL HERNANDEZ
ASSISTANT DIRECTOR

APRIL RICHARDSON
GRADUATE RESEARCH ASSISTANT

McNair Scholars Journal Editors

DR. PATRICIA SPANIOL-MATHEWS
Senior Editor

DR. ANABEL HERNANDEZ
Editor

APRIL RICHARDSON
GRADUATE RESEARCH ASSISTANT

2020 McNAIR RESEARCH ARTICLES

Semantic Competition Between Interlingual Homographs

by Giselle Balderas

Abstract

Research on Retrieval Induced Forgetting (RIF) has been supported to be an adaptive response to resolve competition between a domain and subordinate language (Levy, McVeigh, Marful, & Anderson, 2006). When individuals are trying to remember a piece of information, the RIF resolves competition by inhibiting other related information from being recalled from memory. This RIF prediction is based on the results of Levy et al. 2007 in which naming a picture in Spanish impairs access to the English word for English dominant bilinguals. This study will contribute to the understanding of retrieval induced forgetting by looking at how bilinguals remember word-picture pairs when presented with interlingual homographs. A homograph is a word that is spelled the same as another word but may not pronounced the same and has different meanings. An interlingual homograph is a word that is spelled the same in two or more languages but is pronounced differently and has a different meaning in each language. An example of an interlingual homograph is the word PIE, which means foot in Spanish. The purpose of our study is to see if repeatedly retrieving one language specific meaning of an interlingual homograph will inhibit the ability to remember the other meaning of the same interlingual homograph. Instead of using a category with different examples, we are using an interlingual spelling with a different meaning. For example, the repeated retrieval of the concept of "foot" (i.e., foot picture) when presented with the word PIE may inhibit a Spanish-English bilingual reader's ability remember the concept of pastry, a language alternative meaning of PIE. This study will use pictures/drawings to trigger a particular concept: showing a picture of a foot to get the participant to think of the word PIE. We hypothesized the presentation of an interlingual homograph in a language ambiguous context will create competition. The results established a relation between a practiced and non-practiced interlingual homograph, with the practiced word having a faster recall than the opposing.

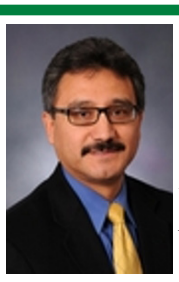

Mentor

Dr. Miguel Moreno

Associate Professor of Psychology

Department of Psychology and Sociology

Introduction

Recognition of the word *bug* can seem simple and easy; however, experience fails to capture the complexity of how words (whether spoken or written) are recognized. Word recognition relies on accessing our long-term memory for known words. Our memory for known words is referred to as the lexicon. New memory entries are added to the lexicon as we learn new words. Sometimes, the new memories we learn can look, sound, and have similar meanings to previously stored words in our lexicon. This redundancy can sometimes create a conflict as we try to recognize a word. For example, recognizing the word *bug* triggers the idea of insect but it can also trigger the idea of being an annoyance (e.g., bugging someone) and the idea of a secret listening device. These different meanings linked to the word *bug* might not be equal. One meaning might be more strongly connected to or a dominate meaning of the word bug compared to the other more weakly connected or subordinate meanings. For the word *bug*, the insect meaning is dominate and being an annoyance and the secret listening device are subordinate meanings. Regardless of dominate or subordinate, these ideas that are connected to a word are referred to as semantic meanings of a word. The different semantic meanings of a word can create a situation of competition in a word recognition event. The resolution between the competing semantic meanings may result in longer reaction times.

Retrieving a word can also activate other words; such that, retrieving one word can lead to the activation of other words that not only have similar meaning, but that sound or look similar. An example of this is the word *two* which has the same sound as *too* and *to*. The word *two* is an example of a homophone. A homophone is a word where the sound is the same as that of other words but look different when spelled. Because, *two, too*, and *to* share the same pronunciation or phonology, they illustrate a difference in orthography (Dx) because they are spelled differently. Sedivy (2014) explained as we recognize one word, we trigger the memory of other words that have overlapping orthographies. By triggering the memories of other words with similar features we create another type of conflict. For example, as we recognize the word *apply*, we may also trigger the memory for *apple, app*, and *appointment*. These triggered words that are similar (either in phonology or orthography) are referred to as the cohort candidates which are critical ideas of the cohort model of word recognition by William Marslen-Wilson (1987). In this model, recognition begins by the immediate and automatic activation of orthographic competitors (Sedivy, 2014). According to this model, language processing works quickly and incremental by creating a hypothesis of the most likely words (i.e., cohorts) to recognize as we are hearing or reading.

The automatic activation of cohort competitors can be influenced by using a prime. A prime can be anything that facilitates or influences the retrieval of a word. For example, presenting the word *spy* before showing the word *bug* to speed up the retrieval times to the word *bug*. In this example, the word *spy* is a semantic prime for the word *bug* because the semantic meaning of *spy* which includes the idea of secret overlaps with one of the meanings of *bug* to secretly record. Semantic priming can also be used with pictures of a particular meaning to help retrieve a word. In the Dell'Acqua and Grainger study, (1999) pictures (e.g., *grape*) were used to prime the naming of the words (e.g., *raisin*) and the results showed quicker naming to the word *raisin* when primed with the *grape* image. Because both *grape* and *raisin* are semantically similar, priming with a *grape* image can facilitate the retrieval of the pronunciation *raisin* with less conflict.

Sedivy (2014) wrote that several studies have also used specific primes, like a phonological prime. In a phonological prime example, the words, *dream, deem, and gleam* would prime for a faster retrieval of the word *cream*.

Another influence on word recognition performance is the neighborhood density effect. The neighborhood density effect occurs when the response time is slower to words that bear a stronger phonological similarity to other words (Sedivy, 2014) and therefore, more competitors. A phonological word holds these stronger similarities to other words by rhyme. As described earlier, an example of a phonological word is the word *cream*, which holds similar phonological structures to *dream* and *gleam*, because all words rhyme with cream. However, notice the word *cream* only differs to dream and gleam by the change of the first phoneme. A phoneme is a small unit of sound that distinguishes the meaning of a word (Sedivy, 2014). By changing the first phoneme for the words *cream*, *dream* and *gleam*, these words are then placed in a dense neighborhood. A dense neighborhood has a higher number of words that can be created by changing one phoneme, for example the word *cream* has the neighbor *dream*, because they only differ by one letter (e.g., the first letter) and therefore have less differences and higher resemblance. A neighborhood where the words have low resemblance represents a sparse neighborhood (Sedivy, 2014). The word stench comes from a sparse neighborhood. Unlike the word *cream*, there are very few words that can be created by only changing one letter thereby creating a very sparse neighborhood size. Therefore, in this example, the uniqueness of the word stench predicts a faster recognition time than the word cream which could illustrate the neighborhood density effect. This effect measures the neighborhood size of one word which is based on the number of words that can be generalized to another word.

Word primes are one of the few ways to facilitate the memory retrieval of one word while inhibit one or a whole category of other words. While priming for the facilitation of one word, the word's competitors will be adversely affected by inhibition. Inhibition is the suppression of a memory from being retrieved. For example, an individual can be presented with the category fruit, and asked to study the three examples from that category (e.g., apple, orange, banana). Practicing the memory retrieval of one fruit (e.g. orange), will inhibit the memory retrieval of the other previously studied fruit examples, while even inhibit the ability to remember fruit examples that were not previously presented (e.g., kiwi) (Anderson, 2003). This phenomenon is referred to as retrieval induced forgetting (RIF).

The retrieval-induced forgetting (RIF) phenomenon has been argued to be the cause of long-lasting forgetting of related items when repeatedly practicing certain items (Shivde & Anderson, 2001). According to the RIF, when practicing a category of words, those words are made hyperaccessible while at the same time inhibiting any competing items (Shivde & Anderson, 2001). In the Shivde and Anderson (2001) study, levels of retrieval competition was used on individuals by practicing retrieval on the dominant (e.g., *part of the body*) or subordinate meaning (e.g., to *weaponize*) of a homograph (e.g., *arm*). Again, a homograph represents words that are spelled similarly but may sound different and refer to different meanings. A dominant or subordinate homograph is based on the strength of connection between the word's spelling and a particular meaning. By having a strong connection or being hyperaccessible, a homographs' dominant meaning (e.g., *arm-shoulder*) inhibits the subordinate meaning (e.g., *arm-missile*). Shvide and Anderson (2001) sought to practice a homographs subordinate meaning (e.g., *arm-missile*) to inhibit the words dominant meaning (e.g., *shoulder*).

The authors choose to practice the subordinate meaning because more interference can be expected when trying to retrieve the non-practiced dominant meaning (Shvide & Anderson, 2001). Practicing a dominant meaning, which already requires less effort in recall, and then trying to retrieve the sub-ordinate meaning of a homograph should cause little interference and forgetting. Therefore, by studying the natural characteristics (the dominant or subdominate meanings) of a homograph the authors created different levels of retrieval competition (Shvide & Anderson, 2001). By practicing the retrieval of a word related to one meaning of a homograph, the authors applied it to the idea of RIF.

In the Levy et al. (2007) study, the RIF procedure was used to evaluate the inhibitory influence on interlingual labels (e.g., "snake" and "culebra") for the same concept (a picture of a snake). Participants practiced retrieving the labels for pictures in either English (the participants' dominate language) or Spanish (the participants' subordinate language). Participants' memory for the English labels of pictures that had been practiced in Spanish was tested by presenting a phonological prime that was not semantically related to the target label. For example, the word break was presented for 4 seconds and then participants were asked to come up with the first word that came to mind that rhymed with the previously viewed phonological prime (e.g., *break*) and matched a previously practiced picture. Because participants had been practicing naming the picture in Spanish, the hypothesis was that the practice of the label in one language would inhibit the ability to remember the English label for the same picture. In the present study similar presentations of words and pictures will be used to provide evidence for the role of RIF.

The Shvide and Anderson (1994) study also supported the role of inhibition in retrieval. Shvide and Anderson (1994) looked at a situation where one concept was more strongly connected to a word compared to another. Its study required an unbalanced situation. In Levy et al. (2007), there is also an unbalanced situation. In Levy et al. (2007), you have one concept and a dominant word form and a subordinate word form. Because the study used beginning level Spanish learners, a word was more hyperaccessible to represent a concept (*snake*) and another word that was far less accessible to represent the same concept (*culebra*). The natural imbalance in both studies represents a 1:2 ratio on their chosen words and meanings. In the Schvide and Anderson (1994) experiment, the ratio of one word with two meanings was used. Whereas Levy et al. (2007) conducted his experiments using two words and one meaning.

Furthermore, in the Levy et al. (2007) study the RIF effect was used to examine the retrieval between bilingual's lexicon. Again, the mental lexicon stores meanings and definitions of a word, and for bilinguals the lexicon stores two meanings of one word. Research from Smith (1997) also suggests bilinguals to have two separate, language-specific lexicons. Overall the findings from Smith (1997) suggests a word's spelling and sound is stored separately from a word's meaning. A bilingual lexico-semantic system aims to control both language systems, and the nature of how bilinguals control these two languages are still being studied.

The complexity in bilinguals lexico-semantic system has been studied in an attempt to explain the relationship between competing words in two languages. In a study done by Green (2003), the cross-language competition was discussed within bilinguals' lexico-semantic system. Green (2003) focused on how one can translate from one language to another while not saying the words of the language being translated. Green (2003) discussed the idea of bilinguals constructing a switch in language, allowing a person translating from one language to a second language without interference. Green (2003) explained that whenever we are translatingwith no interferences, then we have activated the controlling schema which inhibits the unwanted language.

Although, when faced with more complex words, for example interlingual homographs, the activation of controlling our schemas can be more difficult than explained by Green's (2003) study. Homographs can be defined by the complexity of having two words spelled the same as another word but not pronounced the same with different meanings. Whereas an interlingual homograph is a word that is spelled the same in two or more languages but is pronounced differently and has a different meaning in each language. An example of an interlingual homograph is the word *PIE*, which means foot in Spanish and a baked dish in English. The explanation for related items being inhibited, like homographs, is believed to be caused by retrieval competition, suggesting that inhibition settles interference (Shivde & Anderson, 2001).

Levy et al. (2007) suggested RIF to be the cause of first language attrition and used picture primes to retrieve or inhibit certain words. The prediction was supported with the results in which practicing naming a picture in Spanish impairs access to the English word for English-dominant bilinguals. While the participants only acquired a minimum of 1 year of college-level Spanish, an examination of participants with more Spanish fluency and experience outside of a classroom could exhibit more external validity. In the present study, participants' language fluency will be taken into consideration, while also looking into the use of pictures/ drawings to trigger a particular concept similar to Levy et al.'s (2007) study. Past studies have explained the suppression of competing items without the recourse to inhibition, yet for bilinguals the meaning selection is different than speakers of one language, monolinguals (Levy et al., 2007). The present study will contribute to the understanding of retrieval induced forgetting by looking at how bilinguals remember word-picture pairs when presented with interlingual homographs.

Method

Participants

A minimum of 20 participants, male and female who can read in Spanish and English, will be required for a sample. Participants in this study will be students from Texas A&M University Corpus-Christi. All participants in this study will be volunteers and will be reached out from Spanish Upper-Division courses. Unlike Levy et al.'s (2007) participants who only acquired a minimum of 1 year of college-level Spanish, an examination of participants with more Spanish fluency and experience outside of a classroom could exhibit more external validity. In the present study, participants' language fluency will be taken into consideration.

Stimuli and Material

The present study will use computers to assess each participants accuracy to four types of stimuli. This study will use picture-word pairs as a prime to trigger a particular concept. One stimulus will be the interlingual homograph words with a picture representing its English meaning that were shown at the study and were practiced. A second type of stimuli will involve matching interlingual homographs that were presented at the study with the picture reflecting its Spanish meaning but were not practiced. A third type of stimuli will involve interlingual homographs with pictures reflecting the Spanish meaning, which were presented in the study and practiced. The last type of stimuli will involve matching interlingual homographs presented in the study with pictures reflecting its English meaning but were not practiced.

Each word and drawing shown will be outlined with either blue or green. The color green will represent the words and pictures meaning in English, while a blue outline will reflect the word's meaning in Spanish.

For example, a participant will be shown the word PIE in blue letters and shown a drawing of a foot in blue lines to get the participants to think of the word PIE in Spanish.

Procedure

The following phases will take place for the design of the study: a study phase, a practice retrieval phase, and a memory phase. One at a time, picture-word pairs will be presented for several seconds in the study phase. Half of the participants will study a homograph and a picture, in green, with the meaning in English. The other half will study the same concepts but in Spanish and in blue. The study phase would last approximately 5 minutes with each homograph and drawing appearing twice for 5 seconds, followed by a 1 second pause between homographs. Next, the practice phase will prime to recall half of the words, each 10 times for a total of 10 minutes. To practice each word a drawing will be shown, and participants will type the word that corresponds to the picture. For example, if studied Spanish, then the picture of a foot will lead to the typing of PIE. Following a 5-minute distractor task involving simple math problems, the participants will then move on to the memory phase. All pictures from the study phase will be shown and the participants will type in the corresponding homograph that was studied with the drawing as quickly and accurately as possible.

Hypothesis

In our study we wanted to see if studying and practicing one particular meaning of an interlingual homograph will inhibit the ability to remember the other meaning of the same interlingual homograph. Unlike past studies, we will not be using categories with different examples and instead focus on interlingual spelling with different meanings. For example, if the concept and image of a "foot" is repeatedly retrieved with the word PIE, then a Spanish-English bilingual reader might inhibit the concept of a pastry, another meaning of PIE.

With the use of pictures/drawings to trigger a particular concept, a picture of a foot will get a participant to think of the word PIE. Therefore, we hypothesize that presentation of an interlingual homograph in a language ambiguous context will create competition.

Future limitations of the study might include obtaining data because our study involves Spanish-English bilingual readers, which might also result a small sample size. All future research limitations can be decreased by increasing samples or widening our population.

References

Anderson, M.C. (2003). Rethinking interference theory: Executive control and the mechanisms of forgetting. *Journal of Memory and Language, 49*, 415-445.

Dell'Acqua, R. & Grainger, J. (1999). Unconscious semantic priming from pictures. *Cognition, 73*, B1-B15.

Green, D.W. (1998). Mental control of the bilingual lexico-semantic system. Bilingualism: *Language and Cognition, 3*, 151-166.

Levy, B.J., McVeigh, N.D., Marful, A., & Anderson, M.C. (2007). Inhibiting your native language. *Psychological Science, 18*, 29-34.

Marslen-Wilson WD. (1987). Functional parallelism in spoken word-recognition. *Cognition, 25,* 71-102.

Sedivy, J. (2014). *Language in mind: An introduction to psycholinguistics.*

Shivde, G., & Anderson, C.M. (2011). The role of inhibition in meaning selection: Insight from retrieval-induced forgetting. *Journal of Experimental Psychology: Learning, Memory, and Cognition, 41*, 175-190.

Limpet Shell Characterization From 3D Scans

by: Julie Enriquez

Abstract

Limpets are considered bioindicators of their environment as their growth patterns and shell physical attributes are related to the environmental conditions that surround them. This research focuses on determining limpet shell attributes in an attempt to provide a tool for scientists to compare different shell characteristics within and across multiple shell locations. Seven physical measures are reported in this research based on 3D scanning data and computations through MATLAB programming tool. These measurements include inner shell volume, outer shell volume, solid shell volume, major axis, minor axis, height, and peak shift. The characteristics of nine shells collected from the same location are presented in this research. The attributes are analyzed statistically, and inner shell volume plotted against other significant attributes to observe correlations between the region where the animal grows and the shell attributes in large, medium and small sized shells. The preliminary results show that all attributes are directly related with inner shell volume. The lowest variance and highest correlation occur with data inner shell volume vs. outer shell volume. The highest variance and lowest correlation are observed with data representing inner shell volume with peak shift.

Mentor

Dr. Ruby Mehrubeoglu

Professor of Engineering

Department of Engineering

Collaborator

Patricia Cockett

Introduction

Limpet shells protect the animal from strong wave action as well as from dehydration. Limpet shell attributes provides an indication of its environmental conditions, as the animal spends its resources accordingly to either grow or to strengthen its shell (Harford, 2020). For example, extreme conditions cause erosion in the shell details which can vary across locations (Shanks, 1986). The physical measures of shell characteristics are of importance to scientists investigating trends across multiple sites, and for those involved in conservation efforts.

Several articles have been reviewed to effectively explore the methods used for quantitative characterization of irregularly shaped objects such as limpet shells, and to better understand previous approaches by researchers in relation to the following questions:

1. Why are nontraditional methods for volume computation needed for irregularly shaped objects?
2. What methods are used for volume computation of irregularly shaped objects?
3. How has 3D scanning ben used to measure object attributes?

There are objects with geometry that can be easily evaluated for their volume due to the symmetry involved in their shape. Some of these objects include a cube, cylinder, a sphere or a combination thereof. For objects such as these, the volume can be calculated using well-established formulae. In some cases, volume can be determined using the conventional water/liquid displacement method (Igathinathane, 2010). For small objects, water displacement method may introduce inaccuracies in observations due to the meniscus around the liquid-container boundary. For objects with irregular shapes, finding the volume can be challenging; since irregular geometries are diversely shaped, their volumes cannot be calculated simply or in a universal manner and there are no set rules to follow (Li, 2018). Conventional methods can also be harmful or destructive to an object.

Researchers are developing and utilizing unique methods for volume computation of irregularly shaped objects of all sizes. These methods include using 3D scanning technology and 2D imaging and image processing tools. The use the 3D and 2D methods have led to noninvasive and nondestructive volume measurement techniques.

2D imaging was used in determining morphological attributes of grapevine clusters (Tello, 2016).

2D imaging was also utilized for 3D image reconstruction, (Siswantoro, 2013) (Dang & Guo, 2014), Both applications included the use of 2D image histograms. Siswantoro (2013) exploited image histograms to determine a threshold value that would provide adequate image segmentation. The segmented pieces separated the object from the background. Dang and Guo (2014) applied histograms in a process called "histogram acceleration". This process uses a histogram of pictures to speed up the computations and reduce the singular points, at the same time, reducing the amount of color.

3D scanning technology has been implemented in healthcare applications (Treleaven & Wells, 2007), farming and ranching applications (Adamczak, 2018) (Le Cozler, 2019) (Tello, 2016), and in measuring marine objects (Reichert, 2016). One implementation of 3D scanning was by Pang (2014) who focused on the use of structured lighting and a turntable. The idea is to place the object on a turntable that would rotate a full 360O in increments of a set of user-specified degrees at a time. When the turntable rotates a certain degree, it pauses and a projector projects structured light patterns onto the object in which a camera captures partial scans of the object. The 2D scans are then fused to create a 3D object scan. Other 3D scanning methods exist that incorporate laser 3D scanners, some of which are handheld (Li (2018), Tello (2016), Reichert (2016), Xu (2017)).

3D scanners typically produce point clouds, which are data sets that represent the x, y, and z coordinates of an object. Li (2018) used two different volume calculation methods with point clouds. One method segmented the point clouds and the other sliced the point clouds. The results from this research showed that the slicing method was the better method in terms of accuracy, conciseness, reliability, and efficiency. Following 3D scanning, a software tool can be used that allows the user

to edit the point clouds generated by the scanners and fuse them together, as previously mentioned, to produce a solid 3D model.

A 3D model format commonly used involves stereolithography (STL). Users can generate triangular meshes directly from point clouds as well as an STL file. Sholts (2010) discussed a method of using different sized mesh triangles to calculate the surface area and volume of human craniums. Sholts concluded that decreasing the size of the triangular mesh produced more precise results. 3D scanning has also proved to be among effective methods for the applications of other researchers such as Spelitz, Shariff, and Stewart. Spelitz (2019) discussed the use of 3D scanning for 3D documentation and presentation of vessels. Shariff (2019) documented the use of a 3D foot scanner for anthropometric measurements. The effective measurements were used to propose a standard shoe sizing system for Malaysian women. Stewart (2015) discussed the use of a 3D body scanning system to determine the shape of offshore workers. The 3D scan measurements were used to bring awareness of the spacing conditions in offshore facilities. In a recent publication, Hennad et al. (2019) used 3D structured light scanner to scan limpet shells as is also accomplished in this research.

This paper focuses on the comparison of physical measurements among nine different limpet shells collected in Hawaii (Puanui) to investigate the statistics of attributes among three sizes of shells labeled as large, medium and small, and to investigate the correlation of inner shell volume where the animal resides with the other shell attribute measurements. Preliminary results showing measurement trends from different sized shells from a single location are presented. The tested attributes include 3D physical measures such as the inner shell volume where the animal resides, external shell volume which represents the maximum convex hull volume, and solid (physical) shell volume.

In addition, 1D attributes such as the largest long and short axes of the rim (oval opening) of each shell, height of the shell from its base or rim to its peak (apex), as well as peak shift from the center of the shell's opening to the maximum height as an indicator of asymmetry are measured from 3D scan data.

The rest of this paper describes the methods used, including the equipment, system calibration, scanning and data fusion, and measurement of attributes using MATLAB software tool. The results and conclusions are presented at the end.

Methods

3D Scanning System:

The scanning system consists of a HP 3D Structured Light Scanner Pro S3, HP 3D Calibration Panels (adjusts perspective distortion), HP 3D Automatic Turntable Pro (holds samples), and a HP 3D HD Camera Pro and LED Projector (light source). The hardware comes with a control software application to achieve computer-controlled scanning.

Figure 1 shows the components of the 3D structured light scanner system. Figure 2 represents a limpet shell on the turntable.

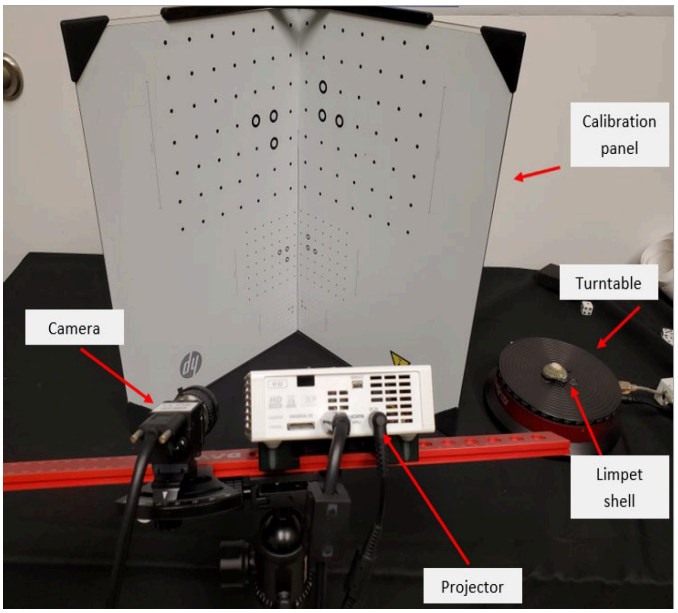

Figure 1. 3D structured light scanner system.

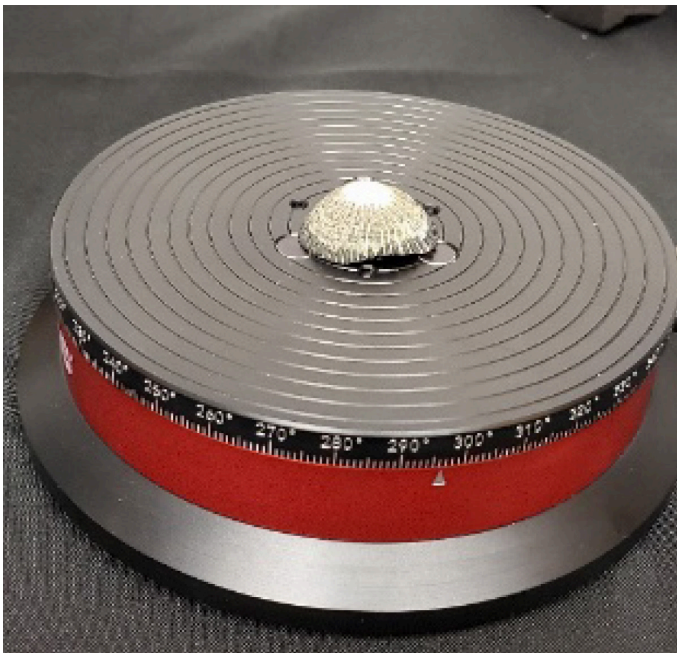

Figure 2. Automatic turntable with a limpet shell.

System Calibration

The system must be calibrated to account for perspective vision effects, and to represent the scanned keep the data in appropriate dimensional representation. The following procedure describes the steps involved in calibrating the system before meaningful 3D scans can be obtained:

1) Place a marker (a piece of blue tape) at the desired location for the turntable
2) Adjust focus and exposure levels (1/30 s) for HD Camera while object is in the frame
3) Mark the location of tripod to keep calibration parameters the same throughout the experiment
4) Remove the turntable and object and replace them with the calibration panel.
5) Calibrate with appropriate scale input into Calibr. Scale [mm]: box (60mm)

Scanning

The following list of steps summarizes the scanning procedure:

1) Scan background, including automatic turntable, so that it may be removed from the fusion model later.
2) Place the test sample (limpet shell) on the automatic turntable.
3) Select 10 scans (min) for each object, at partial rotation of 36˚ for 360˚ revolution, to create a full view of the object and check for adequate positioning. (See Fig. 3 for software-based scanning options.)

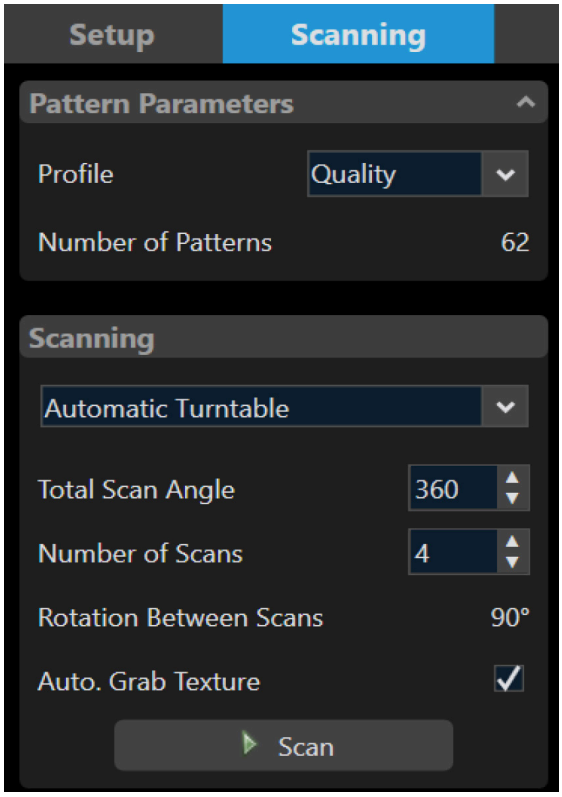

Figure 3. Software-based scanning options.

4) With proper positioning, run 36 more scans for each object, a partial rotation of 10˚ for 360˚revolution, to create a full view of the object.
5) Repeat 3) and 4) twice, first with the object facing flat, and then with the object placed on its back. (This allows top side reference with full view of the object during the alignment.)

Alignment and Fusion

To align the 2D scans and fuse them for a full 3D scan, the following steps are followed:

1) Use a texture reference from one scan to the next to align successive scans (computationally intensive but necessary for fusion)
2) Use HP 3D scanning software after alignment for fusion. (This process compares textures of the aligned scans and allows the user to fill in any existing gaps).

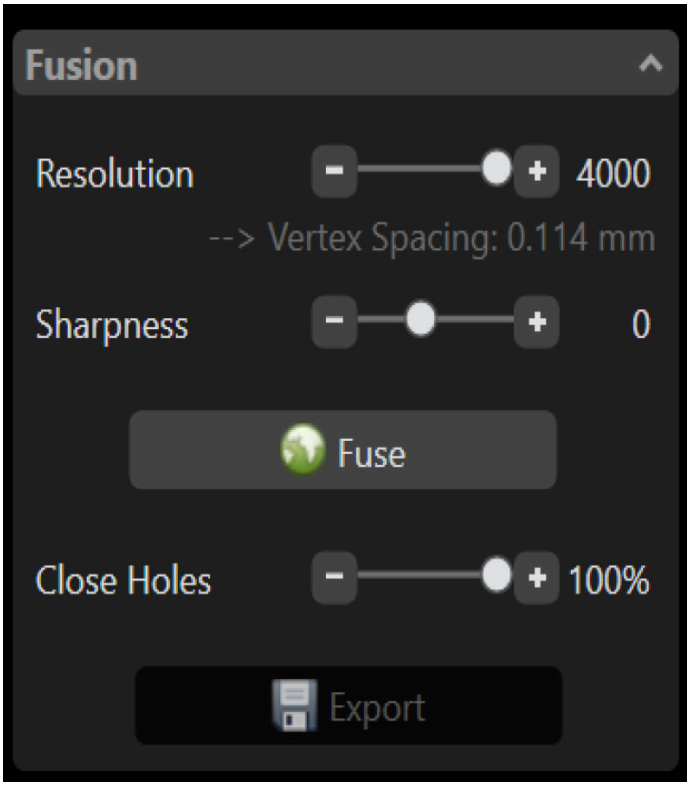

Figure 4. Software's fusing options.

3) Mitigate gaps by including additional scans in the alignment process, whennecessary.

Exporting data to and Calibration in MATLAB:

To begin attribute measurements, data is exported to MATLAB software tool and calibrated using the following procedure:

1) After image fusion, create a fusionmodel.
2) Export the 3D scan data from scanning software to Autodesk Meshmixer(version 3.5.474) for reorienting the shellusing Stereolithography (STL) fileformat. (Figure 5 shows the model view in Autodesk Meshmixer.)

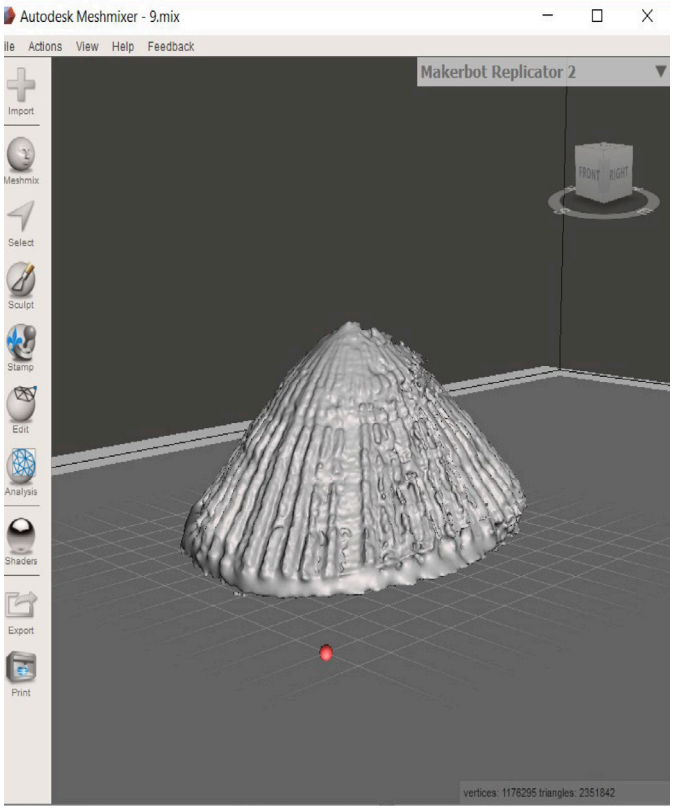

Figure 5. Model view in Autodesk Meshmixer.

3) Export 3D scan data to MATLAB(version R2019b) for other 3D modellingand volume computations usingStereolithography (STL) file format.

Initial MATLAB dimensions are verified by physically measuring the shell axes with a ruler for calibration purposes. Figure 6 shows a 3D limpet shell model in MATLAB.

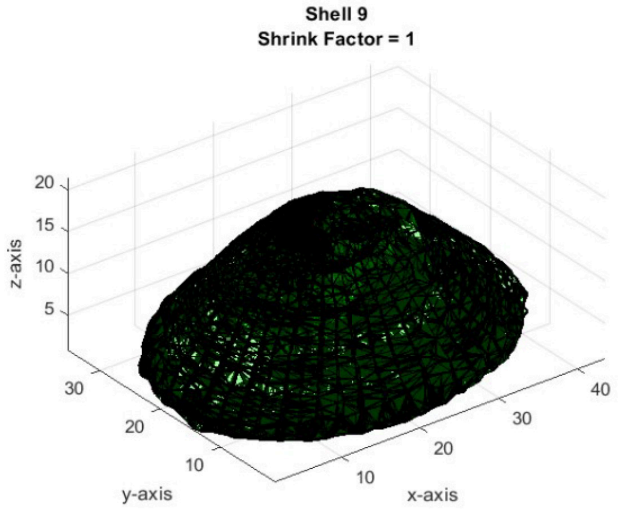

Figure 6. MATLAB 3D model example.

4. Utilize surface features, such as location of vertices and length of vertices, inherent in STL file, to determine volumetric characteristics of objects.

Naming Convention:

The batch of shells collected in Hawaii were previously numbered during collection for archiving from P1 to P30. In this research, nine shells were selected from this batch, three from each test size of large, medium and small. The samples were renumbered from 1 to 9 to represent those used in this research, and correlates to the original naming convention as shown in Table 1.

Table 1. Numbering the shells.

Sample Number (Tested Shells)	Shell Number (original)	Size
1	P 9	Large
2	P 16	Large
3	P 15	Large
4	P 7	Medium
5	P 22	Medium
6	P 8	Medium
7	P 6	Small
8	P 12	Small
9	P 23	Small

Results and Analysis

Each scan took approximately one hour to complete, and the alignment and fusion process took anywhere from one to two hours.

Figure 7 contains 2D color images of three out of the nine shells, one from each sample size. This is a visual representation of the three size differences.

Figure 7. 2D color photographs of shells samples: (a) P 16 (b) P 22 (c) P 23.

Figure 8 displays a 2D image of the same three shells after they have been scanned and fused using the 3D scanner and software.

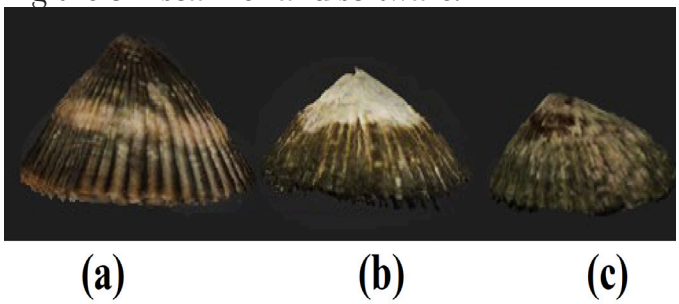

Figure 8. 3D scan - 2D image fusion results: (a) P 16 (b) P 22 (c) P 23.

Figure 9 depicts the 3D stereolithography models for the same three shells.

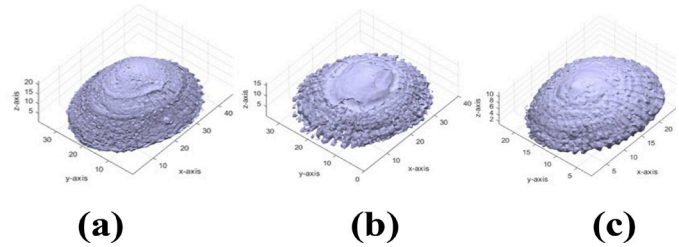

Figure 9. 3D Stereolithography Models (units in mm): (a) P 16 (b) P 22 (c) P 23.

Figure 10 demonstrates the 2D views obtained from the 3D scan model to compute the major and minor axes of the shell as well as height and peak shift. For these attributes, the shells are rotated to align the 2D view with the measurable 1D attribute (major axis, minor axis, height.)

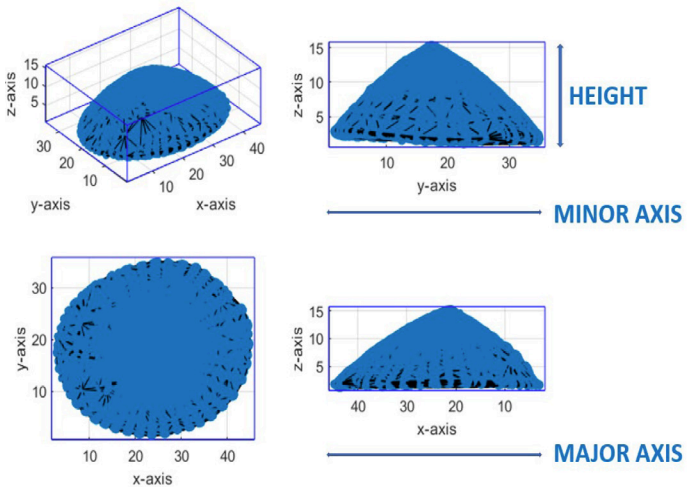

Figure 10. Determining major axis, minor axis and height of a limpet shell.

After all the measurements for all shells were collected, mean, standard deviation and variance was calculated for all shells together as well as for the large, medium and small sized shells. The results of these statistical measurements are presented in Tables 2 to 8.

Table 2. Inner shell volume mean, standard deviation and variance.

Inner Shell Volume	Mean (cm^3)	Standard Deviation (cm^3)	Variance (cm^6)
Large (n = 3)	7.551	0.896	0.802
Medium (n = 3)	5.475	0.246	0.061
Small (n = 3)	2.063	0.112	0.013
All Shells (N = 9)	5.030	2.326	5.410

Table 3. Outer volume mean, standard deviation and variance.

Outer Shell Volume	Mean (cm^3)	Standard Deviation (cm^3)	Variance (cm^6)
Large (n = 3)	11.012	1.546	2.390
Medium (n = 3)	7.790	0.488	0.238
Small (n = 3)	2.981	0.287	0.083
All Shells (N = 9)	7.261	3.434	11.792

Table 4. Solid shell volume mean, standard deviation, and variance.

Solid Shell Volume	Mean (cm^3)	Standard Deviation (cm^3)	Variance (cm^6)
Large (n = 3)	3.46	0.73	0.54
Medium (n = 3)	2.31	0.39	0.15
Small (n = 3)	0.92	0.20	0.04
All Shells (N = 9)	2.23	1.15	1.32

Table 5. Major axis mean, standard deviation and variance.

Major Axis	Mean (cm)	Standard Deviation (cm)	Variance (cm^2)
Large (n = 3)	4.312	0.195	0.038
Medium (n = 3)	4.057	0.133	0.018
Small (n = 3)	2.958	0.082	0.007
All Shells (N = 9)	3.776	0.605	0.366

Table 6. Minor axis mean, standard deviation and variance.

Minor Axis	Mean (cm)	Standard Deviation (cm)	Variance (cm^2)
Large (n = 3)	3.492	0.099	0.009
Medium (n = 3)	3.406	0.045	0.002
Small (n = 3)	2.326	0.116	0.013
All Shells (N = 9)	3.075	1.445	0.290

Table 7. Height mean, standard deviation and variance.

Height	Mean (cm)	Standard Deviation (cm)	Variance (cm^2)
Large (n = 3)	2.014	0.122	0.015
Medium (n = 3)	1.563	0.070	0.005
Small (n = 3)	1.113	0.073	0.005
All Shells (N = 9)	1.563	0.379	0.144

Table 8. Peak shift mean, standard deviation and variance.

Peak Shift	Mean (cm)	Standard Deviation (cm)	Variance (cm^2)
Large (n = 3)	0.160	0.108	0.012
Medium (n = 3)	0.116	0.073	0.005
Small (n = 3)	0.241	0.083	0.007
All Shells (N = 9)	0.173	0.103	0.011

All measurements show higher variance with large shells compared to medium and small shells with the exception of minor axis, which shows higher variance with small shells compared to medium and large shells. With 3D attributes, the highest variance occurs with solid shell volume. With the 1D attributes, variance was highest for major axis among all shells, and minimum for peak shift.

Figures 11 through 16 show the linear relationship and correlation of inner shell volume with all other attributes. Inner shell volume was taken as the measurement to compare to since this is where the animal resides.

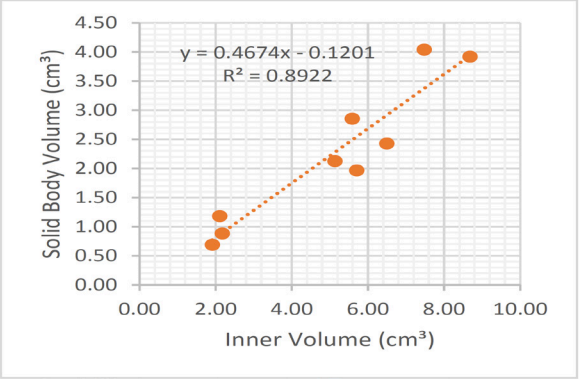

Figure 11. Inner Shell Volume vs Solid Shell Volume.

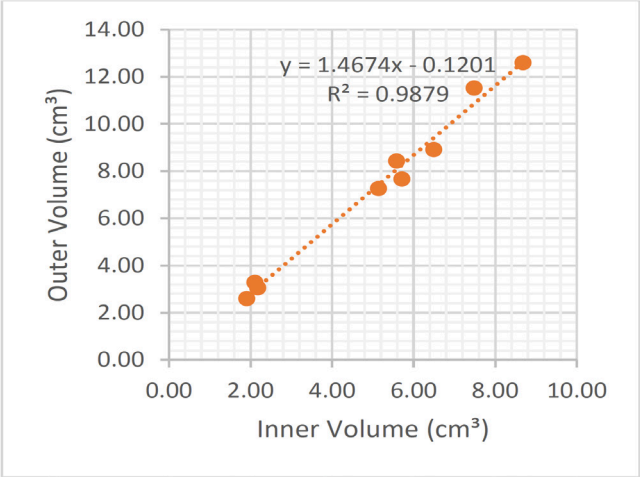

Figure 12. Inner Shell Volume vs Outer Shell Volume.

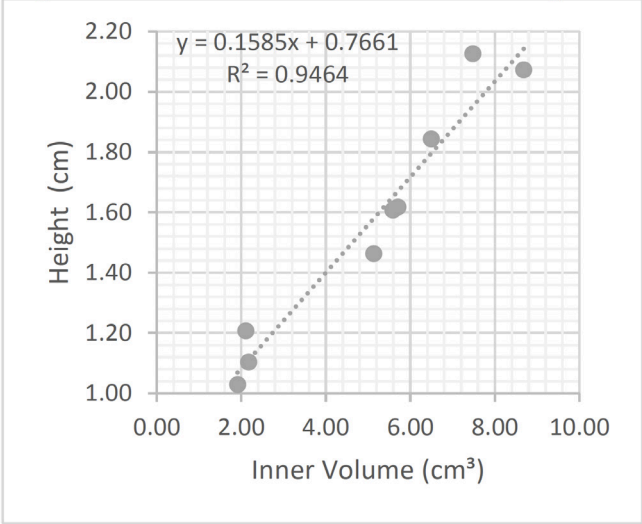

Figure 13. Inner Shell Volume vs Height.

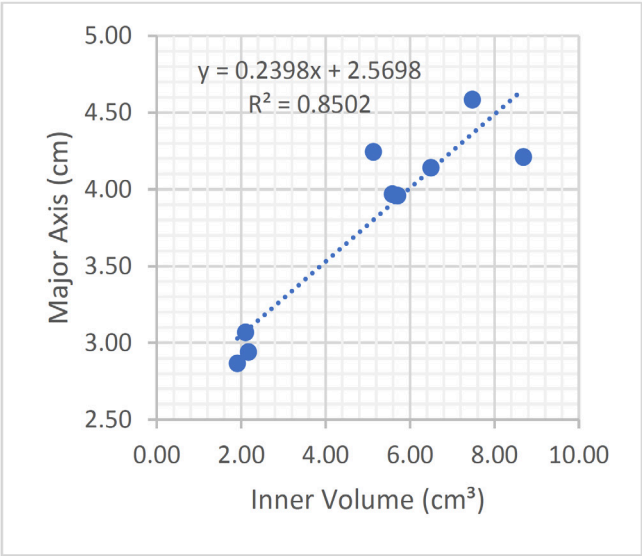

Figure 14. Inner Shell Volume vs Major Axis.

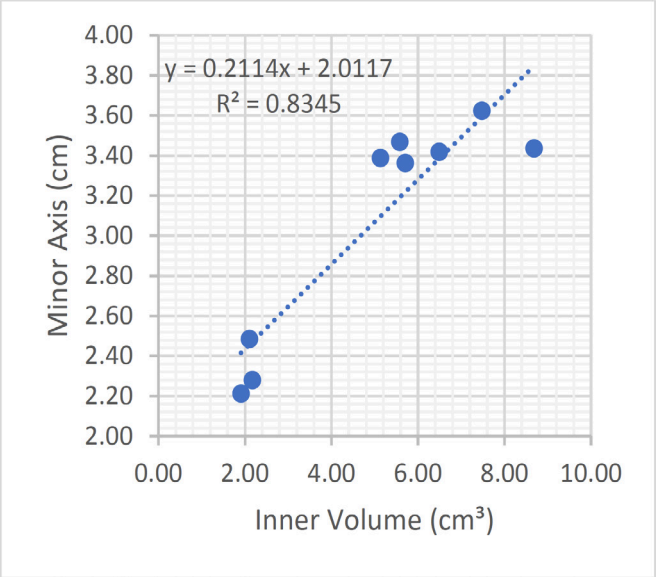

Figure 15. Inner Shell Volume vs Minor Axis.

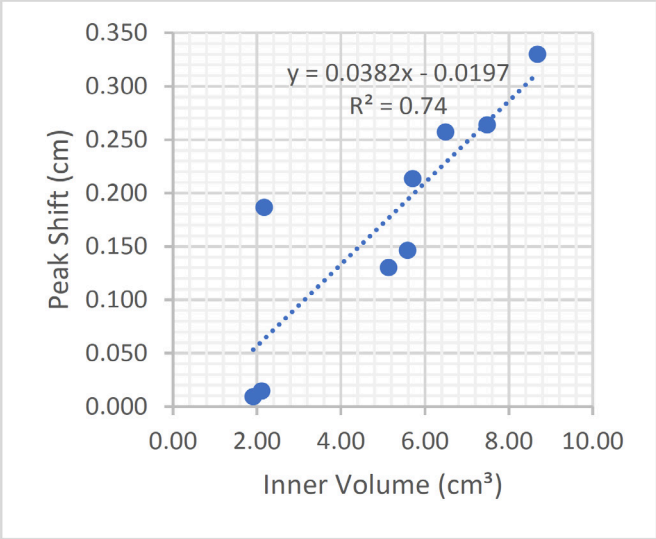

Figure 16. Inner Shell Volume vs Peak Shift.

As can be seen from Figures 11-16, all attributes show a linear and positive correlation with inner shell volume. Inner shell volume was best correlated with outer shell volume, with minimum variance in the data, and r2 of 0.99. This was followed by the next highest correlation of inner shell volume with shell height with r2 of 0.94. The lowest correlation value was obtained for the plot of inner shell volume vs. peak shift.

Conclusion

In this research, 3D and 1D shell attributes were measured for nine limpet shells. First the shells were scanned using 3D structured light scanning. After 3D scanning, the 3D scan data were exported into Autodesk Meshmixer and MATLAB software tools for modeling and computations. This paper presented the measurements, statistics, and correlation among seven limpet shell attributes that would be of interest to scientists.

As more shells are scanned and measured, it will be possible to obtain statistically significant data, compare shell characteristics, and establish trends across different locations and environmental conditions. This work represents the first step in achieving this final goal with very promising results.

Acknowledgements

The research team thanks Kim Morishige, Pelika Andrade, and "Na Maka Onaona" from Hawaii for providing the limped shells used in this research.

References

Adamczak, L. (2018). The use of 3d scanning to determine the weight of the chicken breast. *Computers and Electronics in Agriculture, 155*, 394–399. https://doi.org/10.1016/j.compag.2018.10.039

Dang, H. S. & Guo, C. J. (2014). Volume measurement method for irregular objects based on shape from shading. *Applied Mechanics and Materials*, 494–495, 789–792.

Harford, N., O'Connor, N., and Taylor, D. (2020). Impact resistance of limpet shells: a study of local adaptations. *Applied Physics A, 126*, 757.

Hennad, A., Cockett, P., McLauchlan, L, and Mehrubeoglu, M. (2019). Characterization of Irregularly-Shaped Objects Using 3D Structured Light Scanning. Proc. 2019 International Conference on Computational Science and Computational Intelligence (CSCI), Las Vegas, NV, USA. 600-605, https://doi.org/10.1109/CSCI49370.2019.00113.

Igathinathane, C. (2010). Application of 3d scanned imaging methodology for volume, surface area, and envelope density evaluation of densified biomass. *Bioresource Technology, 101* (11), 4220–4227. https://doi.org/10.1016/j.biortech.2009.12.140

Le Cozler, Y. (2019). Volume and surface area of holstein dairy cows calculated from complete 3d shapes acquired using a high-precision scanning system: Interest for body weight estimation. *Computers and Electronics in Agriculture.* www.sciencedirect.com/science/article/pii/S0168169919313456

Li, B. (2018). A comparative analysis of two point cloud volume calculation methods. International *Journal of Remote Sensing, 40* (8), 3227–3246.

Pang, X. (2014). A tool-free calibration method for turntable-based 3d scanning systems. *IEEE Computer Graphics and Applications, 36* (1), 52–61.

Reichert, J. (2016). 3d scanning as a highly precise, reproducible, and minimally invasive method for surface area and volume measurements of scleractinian corals. *Limnology and Oceanography: Methods, 14* (8), 518–526. https://doi.org/10.1002/lom3.10109

Shanks, A. L. and Wright, W. G. (1986). Adding teeth to wave action: the destructive effect of wave-borne rocks on intertidal organisms. *Oecologia, 69*, 420-428.

Shariff, S. M. (2019). Development of new shoe-sizing system for malaysian women using 3d foot scanning technology. *Measurement, 140*, 182–184. https://doi.org/10.1016/j.measurement.2019.03.057

Sholts, S. B. (2010). Variation in the measurement of cranial volume and surface area using 3d laser scanning technology. *Journal of Forensic Sciences, 55* (4), 871–876. https://doi.org/10.1111/j.1556-4029.2010.01380.x

Siswantoro, J. (2013). Volume measurement of food product with irregular shape using computer vision and monte carlo method: *A framework. Procedia Technology, 11*, 764–770.

Spelitz, S. (2019). Automatic geometry, metrology, and visualisation techniques for 3d scanned vessels. *Digital Applications in Archaeology and Cultural Heritage.* https://doi.org/10.1016/j.daach.2019.e00105

Stewart, A. (2015). Body size and ability to pass through a restricted space: Observations from 3d scanning of 210 male uk offshore workers. *Applied Ergonomics, 51*, 358–362. https://doi.org/10.1016/j.apergo.2015.06.017

Tello, J. (2016). Application of 2D and 3D image technologies to characterise morphological attributes of grapevine clusters. *Journal of the Science of Food and Agriculture, 96* (13).

Treleaven, P. & Wells, J. (2007). 3d body scanning and healthcare applications. *Computer, 40* (7), 28–34.

Xu, J. (2017). Digital reproduction of historical building ornamental components: From 3d scanning to 3d printing. *Automation in Construction, 76*, 85–96.

Predation Results in Reproductive Trade-Offs in *Gambusia affinis* in Texas Coastal Bend Streams

by: Sayge Flores

Abstract

Animal populations often respond to extrinsic factors such as an increase in predation by changing their reproductive investment like altering the number or size of offspring produced. A previous study of stream fish communities in the Texas coastal bend showed a high degree of variation in the abundance of predatory fishes among streams. We test the hypothesis that higher predation leads to predictable trade-offs in offspring number and size using a wide-spread prey species Gambusia affinis. We predicted that female G. affinis would produce more but smaller embryos when predators were in greater abundances. G. affinis samples were collected via electrofishing from 7 Texas streams along the coastal bend. The samples collected were measured using calipers and female G. affinis were dissected and the embryos were extracted. The developmental stage of each embryo was determined visually using a compound microscope. Embryos were categorized into three stages: stage-1 (egg), stage-2 (early eye development), and stage-3 (late eye development). The average abundance of embryos of each stage from each stream was compared with the predator abundances at each site. The results showed that the number of stage-3 embryos produced was highly, positively correlated with the mean abundance of predators. These results support our hypothesis that G. affinis females may adjust their reproductive investment in response to predation.

Mentor

Dr. James Hogan

Associate Professor

Department of Life Sciences

Introduction

Animal populations often respond to extrinsic factors such as an increase in predation by changing their reproductive investment like altering the number or size of offspring produced. For example, nesting birds increase the size of their eggs when predators are removed from their environment (Fontaine & Martin 2006). Such changes in the reproductive investment can result in reproductive trade-offs.

One of the most common types of reproductive trade-offs observed in egg producing animals (birds, fish, etc.) is the size vs. weight of offspring produced, because females have a limited amount of energy to invest in offspring. Selection pressure from predators can shift the balance of the trade-off to increase the fitness of the mother. In relatively long-lived animals like voles, increased predator abundances result in reduced reproductive investment, individuals produce fewer offspring in high predator abundances in hopes of surviving to reproduce later (Korpimaki et al. 1994).

For short lived species that cannot delay reproductive investment, the opposite has been observed. For example, in short-lived live-bearing fishes like guppies, females will produce smaller less well developed embryos when predator density is high, but the abundance of embryos will be high. Inversely when the predator abundance is low females will produce fewer embryos, but each individual embryo will be larger and more developed (Reznik 1981). In a study conducted by David Reznick embryos from a species of guppies (*Poecilia reticulata*) were collected and weighed from various locations then compared to the predator abundance in the areas where the guppies were collected. The outcome of the study showed the trade-off prediction to be true in guppies (Reznik 1981).

Texas's coastal streams are an excellent study system to study the reproductive trade-offs associated with predation. The coastline is the meeting point of two distinct biogeographic regions the Tamaulipan fauna in the west and Texan fishes in the east. These two regions contain very different sets of predatory species with Rio Grande cichlids and killifishes dominant in the west, and bass, sunfishes, and catfish dominant in the east (Hubbs 1957). Fish densities also vary across the coast (JD Hogan, *pers. comm.*).

One species, the Western Mosquitofish (*Gambusia affinis*) is widespread across the Texas coast. A close relative of the Trinidadian guppies in Reznik's study, this species was chosen as the study species to determine how predator densities in Texas streams influences reproductive investment of prey species.

The hypothesis we tested was that the number and size of embryos in pregnant *Gambusia affinis* would be correlated with predator density. I expect that as predator densities increase, *G. affinis* females will invest in more but smaller embryos, matching the pattern observed in predation environments ensures that at least one offspring survives to reproduce.

Methods

Study Species

Gambusia affinis (the Western Mosquitofish) is a small freshwater fish that specializes in eating small insects such as mosquito larvae. *G. affinis* can be found in many states along the Gulf Coast and prefer shallow heavily vegetated streams with minimal current. *G. affinis* are live-bearing and carry their young inside the females until birth. They have many potential predators in Texas streams including sunfish, bass, killifish, cichlids, and catfishes.

Sample Collection

For this study samples were collected via electrofishing from 7 Texas streams along the coastal bend. From west to east, the streams were San Fernando Creek (SFC), Aransas River (AR), Mission River (MR), Perdido Creek (PDC), Garcitas Creek (GC), West Mustang Creek (WMC), and East Mustang Creek (EMC) (Figure 1). Electrofishing is the method of collection in which an electric current is transmitted through the water temporarily stunning all organisms that are within range of the electrical current.

Before sample collection could begin at each of the sites a 75-meter stretch of the stream was measured out and a seine net was placed at each end of the 75-meter stretch. The seine nets separate the sampling area from the rest of the stream while also maximizing the number of samples collected by trapping organisms within the sampling area. A multi-pass fishing method was used which ensures that we collected all of the fish in the 75-meter reach. This allows for precise abundances of all species to be measured in each stream. Field researchers collected all *Gambusia affinis* individuals that were caught during electrofishing. These specimens were then placed in a vial containing 95% ethanol labelled with the site and date of collection. The ethanol was changed periodically throughout the project to ensure the samples were properly preserved.

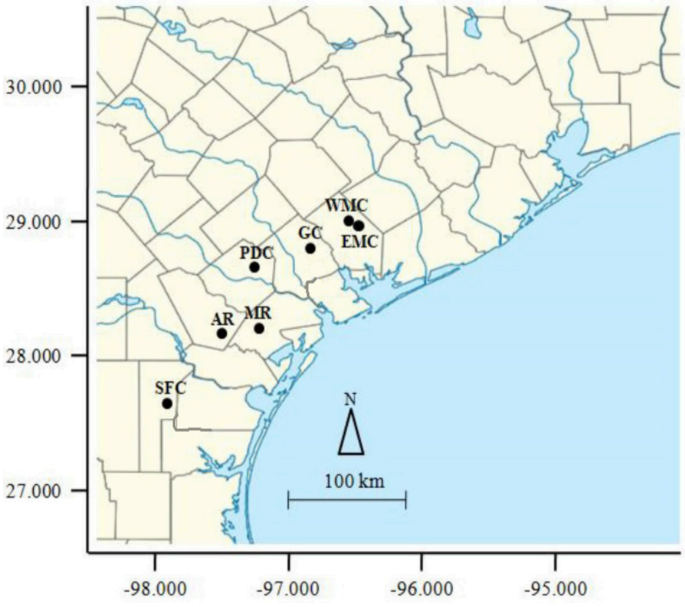

Figure 1. Map showing the locations of seven study streams in Texas' Coastal Bend.

SFC = San Fernando Creek;
AR =Aransas River;
MR = Mission River;
PDC = Perdido Creek;
GC = Garcitas Creek;
WMC = West Mustang Creek;
EMC =East Mustang Creek.

Quantification of Embryos

The samples from each of the sites were measured using calipers and the standard length (mm) was recorded. Next the samples were sexed, and a small incision was made on the female samples from which the embryos were extracted using forceps. Each female and her embryos were then placed in individual vials labeled with date collected, site collected as well as assigned a sample number. Next the embryos from each of the females were viewed using a microscope. While being viewed under the microscopes pictures of each embryo were recorded. The pictures were used to determine the developmental stage of each embryo. The embryos were categorized into three stages: stage 1 (egg), stage 2 (early eye development), and stage 3 (late eye development). The stage development classifications were taken and modified from Reznik (1981). For each of the sample locations the number of embryos in each of the three developmental stages were recorded.

Statistical Analysis

The average abundance of embryos of each stage from each stream was compared with the predator abundances at each site. Species of fish were categorized as potential predators of *G. affinis* based on known presence in the diet and based on expert opinion (JD Hogan pers. comm.). The average abundance of predatory species was calculated for each stream. Linear correlation analysis was used to determine if predator abundance (log10 transformed) was correlated with the mean abundance of each stage of embryos.

Results

Eighty-two *Gambusia affinis* were collect from 7 streams across the Texas coastal bend. Fifty-three of these specimens were female from which the embryos were extracted.

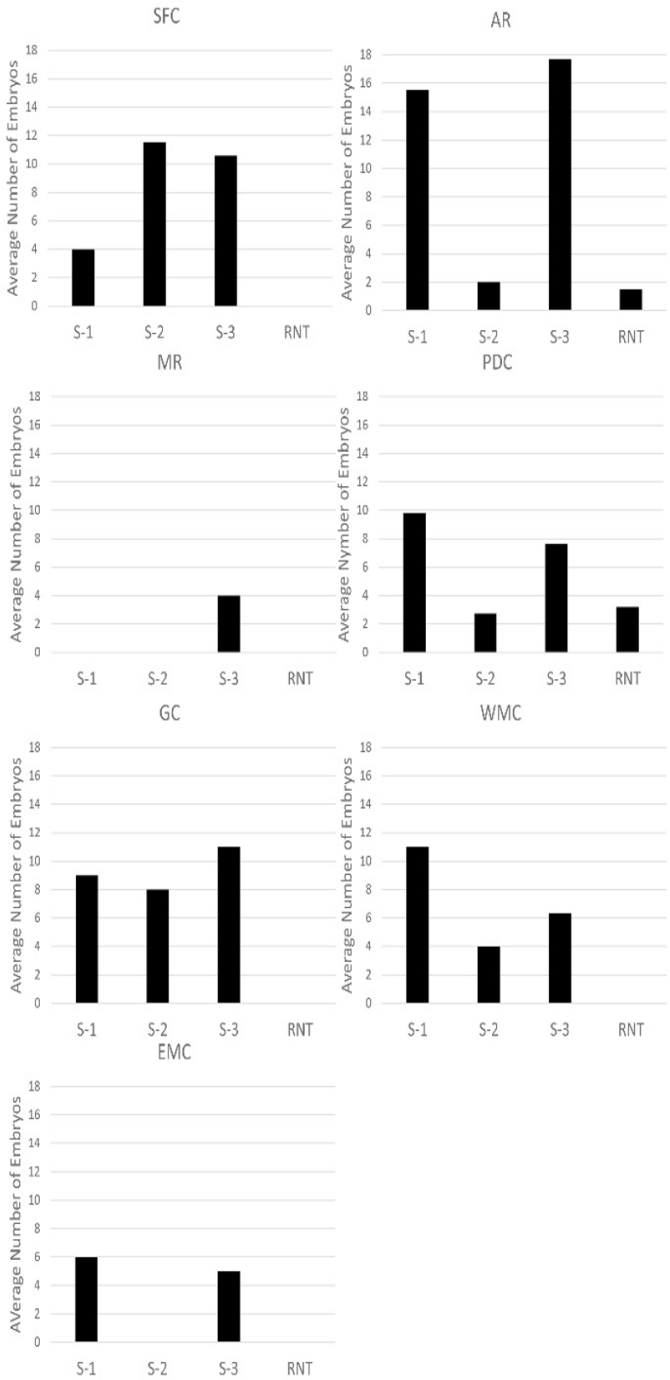

Figure 2. Average number of embryos of each developmental stage per stream.
S-1 = stage 1;
S-2 = stage 2;
S-3 = stage 3;
RNT = "runt".

Stream abbreviations are above each figure. Streams are organized from west-most (upper left) to east most bottom left).

The result of the categorization of embryos showed that there was a total of 152 stage 1, 63 stage 2, and 256 stage 3 embryos in addition to 19 embryo samples that were considered underdeveloped or "runts".

Runts were characterized as any misshapen eggs or embryos that did not clearly fit into any of the morphological descriptions of embryo stages from Reznik (1981).

The average number of embryos collected from each of the three developmental stages varied among the 7 streams (Figure 2). MR had smallest mean number of embryos (mean = 4 per female) while AR had the highest average (mean = 12 per female). We observed that GC had the most even distribution of the three stages while stream (MR) was the least diverse only having stage 3 embryos being collected (Figure 2).

The mean abundance of Stage-3 embryos was strongly correlated with log10 predator abundances ($R2 = 0.47$). Greater mean abundances were found in streams with greater log10 predator abundances (Figure 3). The other two stages were not correlated with log10 predator abundances (S-1 $R2 = 0.02$; S-2 $R2 = 0.007$; Figure 3).

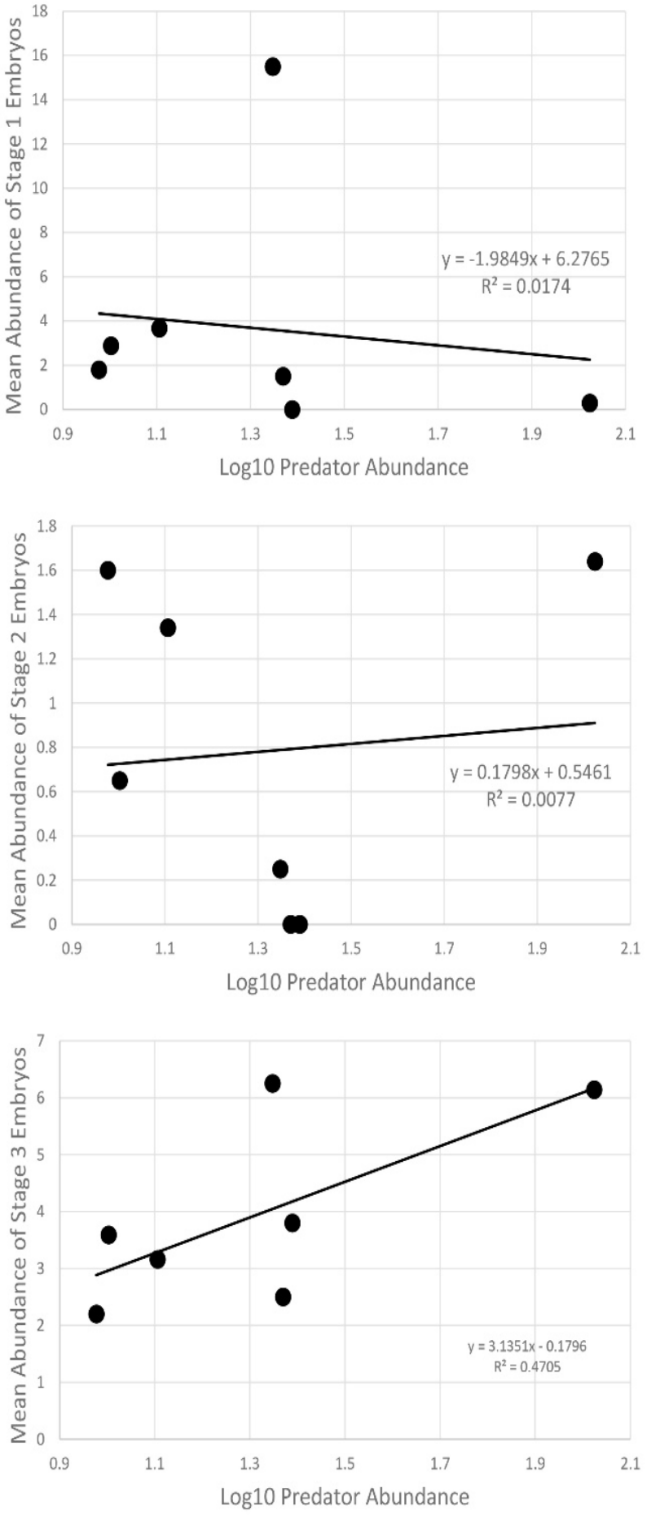

Figure 3. Linear correlations between log10 predator densities and the mean abundance of each of the three stages of embryo development. Stage-1 (top), Stage-2 (middle), Stage-3 (bottom).

Discussion

We hypothesized that if predator density in a stream is high female Gambusia affinis will produce smaller embryos and increase the amount of embryos that are produced. Our data show that there was a high degree of variance in the mean number of embryos produced across our seven study streams. In addition, the number of Stage-3 embryos produced was highly correlated with the mean abundance of predators. The correlation shows that as predator density moves from low to high across a gradient the number of Stage-3 embryos increased thus supporting our hypothesis.

In this study we were only able to quantify the abundance of embryos in various developmental stages. However, to fully test whether there is a trade-off happening between the number and size of embryos being produced, we must conduct an additional study in which the dry weights of each individual embryo are measured and recorded for each developmental stage. Then using this data compare the embryonic dry weights per stage against the same predator density gradient. If the trade-off hypothesis is correct, then we would expect to see a negative correlation between embryo weight and predator abundance, as well as a negative correlation between mean embryo weight and mean embryo abundance for each female. Future studies should focus on measuring the embryos weights.

In this study the only variable we compared with embryo number is the abundance of predators. We hypothesized that predation is thought to be the factor encouraged the change in the reproductive investment in G. affinis. However, in order to know if predation is the only factor that results in the alteration of the reproductive investment a study must be conducted in which G. affinis are exposed to a variety of different environmental factors to observe if these additional factors alter the reproductive investment.

It is known that some environmental variables can alter reproductive investment in G. affinis and the related G. holbrooki. G. affinis are known to produce fewer embryos in streams when exposed to heavy metal toxins (Franssen 2009). Also, G. holbrooki females produce fewer embryos as water temperatures increase, a two degree increase in temperature led to a reduction in embryo number by half (Edwards et al. 2006). In addition, females produced smaller embryos as nitrate levels in the water increased (Edwards et al. 2006). In Texas coastal bend streams, the mean annual water temperatures do vary by as much as 2 degrees, with warmer temperatures in the west, and cooler temperatures in the east (unpubl. data). We don't believe this affected our results here, because the number of embryos was correlated with predator abundance, and those predator abundances were not higher in the cooler sites and lower in the warmer sites. There may be an effect of temperature, but we believe our conclusion that predator abundances affect reproductive investment is supported by the data.

Acknowledgements

We would like to thank Dr. Chris Patrick and Dr. Brandi Reese for providing funds for this research in a collaborative NSF grant with Dr. Hogan. We thank Jennifer Whitt, Sean Kinard, Madison Hightower, Alex Solis, Chris Groff, Roy Roberts, Colton Muller, Victoria Jenkings, Don Youngblood, and Fernando Carvallo for assistance with specimen collections, and electrofishing. This research was funded by NSF Award #1761677.

References

Edwards, T. M., Miller, H. D., & Guillette Jr, L. J. (2006). Water quality influences reproduction in female mosquitofish (Gambusia holbrooki) from eight Florida springs. *Environmental Health Perspectives, 114*(Suppl 1), 69-75.

Fontaine, J. J., & Martin, T. E. (2006). Habitat selection responses of parents to offspring predation risk: an experimental test. *The American Naturalist, 168*(6), 811-818.

Franssen, C. M. (2009). The effects of heavy metal mine drainage on population size structure, reproduction, and condition of western mosquitofish, Gambusia affinis. *Archives of environmental contamination and toxicology, 57*(1), 145-156.

Hubbs, C. (1957). Distributional patterns of Texas fresh-water fishes. *The Southwestern Naturalist*, 89-104.

Korpimäki, E. (1994). Rapid or delayed tracking of multi-annual vole cycles by avian predators? *Journal of Animal Ecology*, 619-628.

Reznick, D. (1981). Grandfather Effects: The Genetics of Interpopulation Differences in Offspring Size in the Mosquito Fish. *Evolution, 35*(5), 941-953. doi:10.2307/2407865

Visual Search: Do You Believe What You Are Told

by: Gabriella Garcia

Abstract

The use of an automated aid has increased over the past few years. Automated aid is used in everyday life as well as in professional settings. The accuracy of automation has shown to influence trust and decision-making process. The experiment aimed to analyze the influence of an automated system on a visual search task. Thirty-one students performed a visual search task for a described a target among a letter array with the assistance of an automated aid. Before the letter array a recommendation was given by the automated aid stating: "a target was detected" or "the target was not detected", the participant had 5 seconds to review the array and then were instructed to identify if the target was present or not present. Experimental trials differed in automation accuracy at either 75% or 95%. Those in the 95% automation accuracy condition had a higher hit rate and sensitivity, on average, compared to the 75% condition. Overall, the trials with categorical targets were found less frequently (hit rate) than featural and specific, especially in the 75% condition. There was increased compliance and reliance when the condition was 95% accurate. Most importantly, our results show that use of automated aids was most beneficial when a task was difficult. This research is a foundation to further examine the impact of automation accuracy in real-life situations.

Keywords: [Automated aid, Target templates, Decision making]

Mentors

Dr. Miguel Moreno

Associate Professor of Psychology
Department of Psychology and Sociology

Dr. Collin Scarince

Associate Professor of Psychology
Department of Psychology and Sociology

The use of automation has increased drastically over the years. Day-to-day we use automated devices like voice-to-text or uploading a resume onto LinkedIn. Other automated systems that we use every day are air conditioning systems, text autofill, and smart coffee makers. These automated systems alleviate tasks that could be tedious or time-consuming, while these tasks were once performed by humans manually, the automated systems have helped substantially.

The proliferation of automation technology has made data gathering via unmanned autonomous vehicles (UAVs) a useful practice across industries. For example, farmers can use UAVs to collect aerial images of their crops in a fraction of the time it would take to cover the same area manually. Farmers can use the collected data to search for blight, pests, or other problems more efficiently (Zhang et al., 2018). Since UAVs can cover a large amount of space in a short time, the farmer can locate the problem and proceed to fix the problem much faster than them walking the entire field.

Most automated systems, from calendar reminders on smartphones to image recognition software, are not entirely perfect or are limited to specific tasks and, thus, require some oversight and interaction from a human operator. So, it becomes important to understand how humans change their behavior as a result of the reliability of the automated tools they use. As the reliability of the automated system increases people will develop trust (Pop et al., 2014) and can move through a task more quickly and not have to reverify a task that has been completed (Rice, 2009). If the automated system is not programmed correctly this can cause an inconvenience, leading to the person doing double work, fixing the machine and, doing the task the machine was supposed to perform. In the current study, we investigated how the reliability of an automated aid affected performance in a visual search task of varying difficulty.

Generally, automation is the use of technology and machines to complete tasks or subtasks on their own without direct human control. Automation is primarily used for jobs that are either dull, dirty, or dangerous ("How robots are taking on the dirty, dangerous, and dull jobs," 2019). The level of involvement from the automation can vary depending on the sophistication of the task. A boring and repetitive task that requires a lot of simple calculations or constant monitoring might be best left to a computer to perform, whereas tasks that require flexibility or contextual judgments might rely more on human decision making. Because the levels of automation between tasks vary from fully autonomous to fully operator run (Parasuraman, Sheridan, & Wickens, 2000), it is important to understand how operators learn to interact and trust the automated system they work with.

For example, there are systems in place that monitor the pressure in valves at chemical plants, these systems alert the operator if the pressure is too high or too low. If there is a malfunction, the operator is to find the issue and resolve it, if the pressure system monitor states that the pressure in the valve is low or off and the operator goes to open it when in fact the pressure is high, this could cause serious harm to those in the facility and the equipment. A well-designed automated system can reallocate the operator's attention from boring, repetitive tasks to other tasks better suited for human cognition. If a system is not designed well, however, the human operator might experience a cost to their attention.

Meyer (2001) examined the adaptive changes participants used in response to warning signals. In this study, participants categorized bars of different lengths into one of two categories based on length, short or long (similar to identifying a system malfunction in a pressure-monitoring system).

The bar lengths were drawn from two different distributions that had some overlap, so correctly sorting the bars required some level of guessing. An automated "warning" system helped the participants make their decision by making a recommendation of which distribution the target line was drawn from. A continuous, lengthed bar was displayed at the top of the display screen that was correlated with the state of the system. The participant was to use the combination of the length of the presented bar and warning signal to make a decision. The warning system was imperfect, in that its recommendations were sometimes wrong, and the patterns of when the participants agreed or disagreed with the warning system revealed two types of agreement based on which "recommendation" the assistant gave. The results showed that the participants' sensitivity or, how their behavior changed based on the aid's recommendation, was lower when the warning system was not valid than when it was valid and as the experimental trials went on the sensitivity increased, as expected reliance. The levels of bias changed depending on the type of warning indicator, when the indicator was red, meaning the length of the bar did not match the bar above, and when the indicator was green, meaning no malfunction the bar was the same length as above. The operator heavily relied on the aid and agreed with it and when the warning gave a red indication, the operator was more likely to agree with the aid and investigate the problem compliance. Based on distinct patterns of agreement with warning and non-warning signals, Meyer proposed that automation trust can be broken down into two types: compliance and reliance. Compliance refers to the rate at which the operator agrees with an automated system when it reports a target event. Reliance, on the other hand, refers to the rate at which the operator agrees with an automated system when no signal is detected. Compliance and reliance can vary independently depending on the behavior of the automated system.

Rice (2009) conducted an experiment that specifically investigated how automation error-type and rate affects compliance and reliance. A simulated "combat task" was performed where participants were to examine the aerial photographs and search for an enemy target (e.g., a tank). A "diagnostic aid" was provided to assist in recommendations during each trial. The aid reported "The automation has detected a tank!" or "The automation has determined that there is no tank!" before the scene the participant was to search appeared. The reliability and response bias of the aid were manipulated between participants to have varying miss and false-alarm errors ranging from 95%-55%. Rice found that performance increased as the reliability of the automated aid increased. More importantly, though, he found that compliance and reliance rates changed based on the type of bias of the diagnostic aid. When the aid was false-alarm-prone, compliance was reduced, and when the aid was miss-prone, reliance decreased. The results showed that in designing automation it is beneficial to use a reliable automation when possible because less reliable tends to harm human-automation performance negatively. The different types of errors like miss-prone and false-alarm prone affect the trust or compliance and reliance of the automated aid. People will either adjust to the types of errors or stray away from using the automation altogether.

Visual Search

Visual search is the process of using perception and attention to locate visual targets amongst non-target distractors. "I Spy" puzzles and looking for a car in a parking lot are common examples of visual search tasks. People use visual search every day and some professions rely on it, like TSA baggage screeners and radiologists.

Target Templates

When someone is performing a visual search task, they usually aren't randomly directing their attention in the visual field (Treisman & Gelade, 1980; Wolfe, 1998), they use a mental representation, called a target template (Malcolm & Henderson, 2010). Sometimes a target template can be very specific and precise or vague which has a higher variety of potential features to search for. More precise the template, the more efficient the search, generally. For example, if you and a friend walk to a parking garage your friend says, "Help me find my Jeep," the kind of template you use to guide your attention will depend on your mental representation of Jeeps. You might think of a black Jeep Cherokee, a white Wrangler, or a bright green Jeep from the movie Jurassic Park. The features for the target template will be based on your individual expectations and might not match the model and color of your friend's actual car, resulting in poor attentional guidance. If your friend were to ask, "Help me find by Jeep, it's a blue Cherokee," your target template will be less broad, and your attention will be directed to cars that match that target description.

In a series of experiments done by Hout and Goldinger (2015), the precision of participants' target templates was manipulated based on how targets were presented. For example, in one condition a participant might be shown a blue teddy bear and be asked "Find this object." This is a case of a precise template because the features of the target are clear and exact. In another condition, a participant might be shown a blue teddy bear and a brown teddy bear with a hat and be asked "Find one of these objects." In this condition, the target template is "wider" because more features need to be incorporated into the guiding template.

Schmidt and Zelinsky (2009) investigated template precision by manipulating the words used to describe a target (compared to an image cue control group).

Targets were either described abstractly or precisely and with a color or without a color. For example, if an upcoming target was a pair of brown, tall hiking boots, the target could be described as boots (precise), footwear (abstract), brown boots (precise and color), or brown footwear (abstract and color). Schmidt and Zelinsky found that participants were more likely to direct their first eye movement toward the target as the precision of the target description increased. The prior research suggests that the more accurate a target description is, the easier the search becomes.

Automated Aids in Visual Search Tasks

Visual search tasks are not always as simple as finding your keys on your desk. Sometimes the target is very similar to non-targets or the target might show up in a variety of ways, which makes search more difficult. Automated systems can be used to help people complete searches more accurately (e.g., highlighting an area that is likely abnormal tissue on a CT scan).

Helbren et al. (2015) conducted a visual search experiment that involved an automated aid. The authors recruited inexperienced and experienced colonography readers to search for polyps in a prerecorded video of a CT colonography with the use of computer-aided detection (CAD). Half of the participants (in both groups) watched the colonography with a CAD system and the other half watched the without the aid. The authors were primarily interested in pursuit time, which was measured as the response time from when the searcher's eye movements were directed towards a polyp until the manual response. The group of participants that used CAD had a red dot or marker indicating high-potential abnormalities. Pursuit time, identification time, and CAD location pursuit time were analyzed with the use of the eye tracker. Identification time was the amount of time it took the searcher to identify the polyp without CAD and CAD location pursuit time was a similar analysis with CAD.

The CAD drew experienced and inexperienced readers' attention to polyps faster than without the CAD leading to a reduction in time in identifying polyps. Inexperienced readers relied and complied with the CAD, the overreliance on the CAD influenced the readers to miss polyps when the CAD did not identify it.

Current Investigation

In our current investigation, we want to examine how automation influences the participant's decision making in a visual search task when targets vary in specificity. Participants performed a visual search task for targets of varying description precision with an "automated aid." The aid's accuracy was manipulated between participants to be either reliable (95% accuracy) or unreliable (75% accuracy) to investigate how the participants' trust in the aid would vary with the aid's accuracy and the difficulty of the search task. First, we hypothesized that search performance (hit rate, sensitivity, and reaction time) would be superior in conditions where the target is well defined, as opposed to categorically, and when the automation aid was accurate. We also predicted that the aid would be most beneficial when searching for a categorically defined target (due to the increased difficulty of the task). Second, we hypothesized that agreement (compliance and reliance) would be higher when the aid was reliable compared to unreliable, and an agreement would be highest when the aid was accurate and the search task was difficult.

Methods

Participants completed a visual search task that involved looking for a target letter amongst distractors. The target was different on each trial and was described with varying degrees of precision. An automated aid provided a warning about the presence or absence of a target before each trial.

Participants

Participants were 31 undergraduate students enrolled at Texas A&M University-Corpus Christi. Participants were 18 years old or older and reported normal or corrected-to-normal vision.

Apparatus

Data were collected on Dell desktop computers with 18-inch monitors with a refresh rate of 60 Hz. The experiment was run using E-Prime 2.0.

Stimuli

Stimuli were arrays of 100 letters distributed across the computer screen. There were 180 letter arrays, 90 arrays had target present and 90 arrays had target absent. Letters were black capital letters in Arial font at 18 font size. The letters were rotated such that they were never perfectly horizontally or vertically oriented and were never placed in the same location. The letters were evenly distributed across the display with "jitter" to prevent the array from creating a noticeable grid pattern. No letters overlapped with each other and were presented against a light-gray background.

Automated Aid

The automated aid was part of the experimental program and was set to give correct target warnings in pre-determined amounts equal to the accuracy described to the participant. In one condition, the aid was 75% accuracy and it was 95% accuracy in a second condition. Errors from the aid were evenly distributed between target-present trials (misses) and target-absent trials (false alarms).

Procedure

The experiment began with participants reading the instructions for the experiment, including the information about the automated aid. Each trial sequence began with a description of the target for the upcoming trial.

Three target types were used to manipulate the precision of the target template participants used to guide their attention: specific, featural, and categorical. The trial began with instructions that stated the specific description directly naming the letter the participant was to search for (e.g., "find the letter F"). The featural description instructed participants to search for a "curvy" letter. Finally, the categorical description asked participants to search for a vowel. Next, the information from the automated aid was presented, which informed the participants if it had "detected" a target or not. Participants then self-initiated the search trial. The letter array appeared on the screen for five seconds or until the participants pressed the spacebar to make a final response. The array of letters was then replaced with a mask (randomly placed "@" and "#") and participants were instructed to press the "J" key if the target was present and the "F" key if the was not present. Finally, they were given feedback on whether their decision was correct or not. Participants completed six practice trials and 180 experimental trials.

Design

A 2(automation accuracy: 95% vs 75% accuracy) x 3(target type: specific vs featural vs category) x 2(trial type: target-present vs target-absent) was used. Automation accuracy was a between-subjects variable, while target type and trial type were within-subjects variables. We collected responses regarding target presence and absence as well as response time (the elapsed time from the onset of the search array until the termination of the search array).

Results

Accuracy

We analyzed accuracy of the search task with two different measures. First, we analyzed the hit rate, the proportion of correct target-present responses. Second, we calculated the signal detection metric for sensitivity, d' (Macmillan & Creelman, 2004), to account for both how successful participants were at correctly responding to targets but also not making false-positive responses. Higher values of d' indicate better target-distractor discriminability than lower scores.

Hit rate

We used a mixed analysis of variance to analyze hit rate with automation accuracy as a between-subjects factor and target type and trial type were within-subject factors. The analysis revealed a main effect of target type, $F(2,120)= 60.49, p< .001, \eta_p^2 = .502$. Vowel targets (52.5%) were found less frequently than feature (69.5%) or specific (70.7%) targets. The difference between featural and specific targets was not significant ($p = .048$). There was also a main effect of automation accuracy, $F(1,60) = 4.09, p = .048, \eta_p^2 = .064$. Hit rate was higher in the 95% automation accuracy condition (66.7%) compared to the 75% condition (61.7%).

There was a significant two-way interaction between target type and automation accuracy, $F(2,120) = 7.52, p = .001, \eta_p^2 = .107$ (see Figure 1). There were no significant differences between the automation accuracy conditions for feature and specific targets, but there was a significant difference between the automation accuracy conditions for categorical targets ($p = .001$).

Sensitivity

Similar to hit rate, we used a mixed analysis of variance to analyze sensitivity. The analysis revealed a main effect of target type, $F(2,120) = 44.08, p< .001, \eta_p^2 = .424$. Sensitivity was significantly higher for specific targets ($d'= 2.07$) compared to featural ($d'= 1.80$) and categorical targets ($d'= 1.14$). Sensitivity for featural targets was also significantly different from categorical targets. There was no main effect of automation accuracy, $F(1,60)= 3.75, p= .057$.

There was a significant interaction between target type and automation accuracy, $F(2,120) = 3.30$, $p = .014$, $\eta_p^2 = .052$ (see Figure 2). There were no significant differences between automation accuracy conditions for the feature and specific targets, but there was a significant difference between the automation accuracy conditions for categorical targets ($p = .002$).

Agreement

We assessed trust in automation by calculating the agreement rate for each of the two recommendations from the automated aid. Compliance rates were the proportion of trials the automation made a target-present warning, and the participant gave a target-present response. Likewise, reliance rates were the proportion of trials the automation made a target-absent warning, and the participant gave a target-absent response. Higher compliance or reliance rates indicate more agreement with the aid. Simple means for compliance and reliance rates are presented in Figure 3.

Compliance

We used a mixed analysis of variance to analyze compliance rates with automation accuracy as a between-subjects variable and target type and trial type were within-subject factors (similar to the analyses of accuracy). The analysis revealed a main effect of target type, $F(2,120)= 21.70$, $p < .001$, $\eta_p^2 = .266$. There was less agreement between when the target was categorical (56.3%) compared to specific (65.4%) and featural (66%). There was also a main effect of automation accuracy, $F(1, 60) = 13.82$, $p < .001$, $\eta_p^2 = .187$. There was more agreement when the automation was 95% (67.2%) accurate compared to 75% accurate (57.9%). The interaction between target type and automation accuracy was not significant, $F(2,120) = 1.90$, $p = .153$.

Reliance

We used the same analysis as compliance to analyze reliance rates. The analysis revealed a main effect of target type, $F(2,120) = 3.70$, $p = .028$, $\eta_p^2 = .058$. Reliance for featural targets was slightly higher (79.1%) than for specific (76.1%) and categorical (75.3%). There was also a main effect of automation accuracy, $F(1,60) = 35.86$, $p<.001$, $\eta_p^2= .374$. There was more reliance in the 95% (85.3%) compared to 75% (68.4%). There was no interaction between target type and automation accuracy $F(2,120)= 0.90$, $p = .914$.

Response Time

We used a mixed analysis of variance to analyze response time with automation accuracy as a between-subjects variable, and trial type and target type as within-subjects variables. Only response times from correct responses were analyzed. The analysis revealed a main effect of target type, $F(2,120) = 13.27$, $p < .001$, $\eta_p^2 = .181$. Response times were significantly shorter for specific targets (3,730 ms) compared to featural (3,798 ms) and categorical (3,961 ms). Unsurprisingly, there was also a main effect of trial type, $F(1,60) = 102.23$, $p < .001$, $\eta_p^2 = .630$. Response times for target-present trials were shorter (3,379 ms) than target-absent response times (4,280 ms). There was no significant effect of automation accuracy, $F(1,60) = 1.22$, $p = .274$.

There was a significant two-way interaction between target type and trial type, $F(2,120)= 6.85$, $p=.002$, $\eta_p^2 = .102$. Specifically, the difference between target-present and target-absent response times for the categorical targets was smaller than for feature or specific targets (see Figure 4). There was no significant two-way interaction between trial type and automation accuracy, $F(1,60) = 3.61$, $p= .062$ or target type and automation accuracy, $F(2,120) = 0.46$, $p = .630$. The three-way interaction was also not significant, $F(2,120) = 0.24$, $p = .788$.

Discussion

In this experiment, we examined the effect of automation on decision making when searching for a target in a visual search task. We found a higher hit rate and sensitivity for specific and featural target types compared to categorical targets. Search was also more accurate with the help of the reliable automated aid, especially when the target was categorical—the most difficult of the three target types to find quickly. Compliance and reliance were higher when the automation aid was at 95% accuracy compared to 75% accurate. Reliance on the aid was also increased with featural target types, compared to categorical and specific. Finally, specific targets were found more quickly compared to the other two target types.

Visual Search with Automated Aids

Past research (Helbren et al., 2015; Rice, 2009) and our current investigation shows how the accuracy of an automated aid affects the human decision-making process, especially in the context of task difficulty. We manipulated the difficulty of the visual search task by the specificity of the target template our participants used for different search trials. A target template is a mental representation that will help guide us to search and identify a target. As the template becomes more precise, search becomes more efficient (fewer errors and shorter search times). If the description for a target is vague, only a broad set of features can be used as a template, and the amount of time to locate the target increases. In both groups, 75% and 95%, the participant was given a vague description like "find a curvy letter", our results showed an increase in reliability and compliance. When asked to "find a vowel" the letters A, E, I, O, U, and Y there are few, if any, shared features amongst potential targets. This limits the construction of a template that can guide attention to features of potential targets. On the other hand, when asked "find a curvy letter" the target template becomes more precise, letters like S, P, and O fall into this category. Curvy letters share a distinctive feature that separates themselves from other letters like X or T, while vowels do not have a specific feature, they are described in a semantic category. During the search for a categorical target, the target template has little if any guiding information and the results reflected that response times were longer compared to other target types like featural or specific. As revealed by the interaction between the aid accuracy and types of targets, performance for finding featural and specific targets was not heavily impacted by the aid, while search for the categorical targets benefited substantially from the accurate aid. Since finding a specific letter like X or a featural letter like "find a curvy letter" is easier for participants to search for by themselves, the aid's recommendations were not needed as much. As to the categorical target type, the more accurate aid benefited the participants in the search since there was little to no template.

Radiologists, as well as TSA agents, go through extensive training to identify abnormal objects with the help of an automated aid. As more tools are designed to aid professionals, like radiologists or farmers surveying images of crops, the difficulty of the task for the professional should be kept in mind because the accuracy of the aid could potentially increase target or abnormal identifications. Similar to our investigation, participants were asked to identify an object given a description with the help of an automated assistant and as the difficulty of the task increased so did the sensitivity to the automation.

Limitations and Future Directions

Our study had some limitations. The participants were limited to 5 seconds when asked to search for the target, which could have led to them blindly relying on the automated aid falsely reflecting increased use of compliance and reliance in results. Another limitation was that there was only one type of featural description used during the entire experiment.

As the trials proceeded the participant could have experienced fatigue and again blindly rely on the automated aid, further increasing the compliance and reliance results. In a future study, longer search time and a variation of categorical descriptions could perhaps give more accurate results. Moving this type of investigation into a more realistic setting could help increase efficiency and productivity in other areas. The stimuli in our experiment would never be used in a realistic scenario, with that being said, transferring our concept to a realistic scenario would look like the use of railroad track aerial images. These images could assist railroad engineers in finding breaks on the ties or debris on the tracks. If programmed correctly, the automated assistant would help the engineers identify these hazards, allowing them to repair them quickly and safely.

Conclusions

In summary, our results show how accuracy of an automated aid affects performance in a visual search task with varying degrees of difficulty. Our results showed that an increase in automation accuracy led to an increase in correctly identifying a target in a visual search task. Most importantly, automated aid use increased as the target description was vague. These findings highlight the importance of understanding which tasks are difficult for human operators and designing systems to alleviate those potential shortcomings.

References

Helbren, E., Fanshawe, T. R., Phillips, P., Mallett, S., Boone, D., Gale, A., Altman, D. G., Taylor, S. A., Manning, D., & Halligan, S. (2015). The effect of computer-aided detection markers on visual search and reader performance during concurrent reading of CT colonography. *European Radiology, 25*(6), 1570-1578. https://doi.org/10.1007/s00330-014-3569-z

Hout, M. C., & Goldinger, S. D. (2015). Target templates: The precision of mental representations affects attentional guidance and decision-making in visual search. *Attention, Perception, & Psychophysics, 77*(1), 128-149.https://doi.org/10.3758/s13414-014-0764-6

Macmillan, N. A., & Creelman, C. D. (2004). Detection theory: A user's guide. Psychology press.

Malcolm, G. L., & Henderson, J. M. (2010). Combining top-down processes to guide eye movements during real-world scene search. *Journal of Vision, 10*(2), 4-4.

Meyer, J. (2001). Effects of warning validity and proximity on responses to warnings. Human Factors: *The Journal of the Human Factors and Ergonomics Society, 43*(4), 563-572. https://doi.org/10.1518/001872001775870395

Parasuraman, R., Sheridan, T. B., & Wickens, C. D. (2000). A model for types and levels of human interaction with automation. IEEE Transactions on systems, man, and cybernetics-Part A: *Systems and Humans, 30*(3), 286-297.

Rice, S. (2009). Examining single- and multiple-process theories of trust in automation. The *Journal of General Psychology, 136*(3), 303-322. https://doi.org/10.3200/genp.136.3.303-322

Robotics Online Marketing Team. (2019, October 15). How robots are taking on the dirty, dangerous, and dull jobs. *Robotics Online.* https://www.robotics.org/blog-article.cfm/How-Robots-Are-Taking-on-the-Dirty-Dangerous-and-Dull-Jobs/209

Schmidt, J., & Zelinsky, G. J. (2009). Short article: Search guidance is proportional to the categorical specificity of a target cue. *Quarterly Journal of Experimental Psychology, 62*(10), 1904-1914. https://doi.org/10.1080/17470210902853530

Treisman, A. M., & Gelade, G. (1980). A feature-integration theory of attention. *Cognitive Psychology, 12*(1), 97-136.

Wolfe, J. M. (1998). What can 1 million trials tell us about visual search? *Psychological Science, 9*(1), 33-39. https://doi.org/10.1111/1467-9280.00006

Zhang, D., Zhou, X., Zhang, J., Lan, Y., Xu, C., & Liang, D. (2018). Detection of rice sheath blight using an unmanned aerial system with high-resolution color and multispectral imaging. PLOS ONE, 13(5), e0187470. https://doi.org/10.1371/journal.pone.0187470

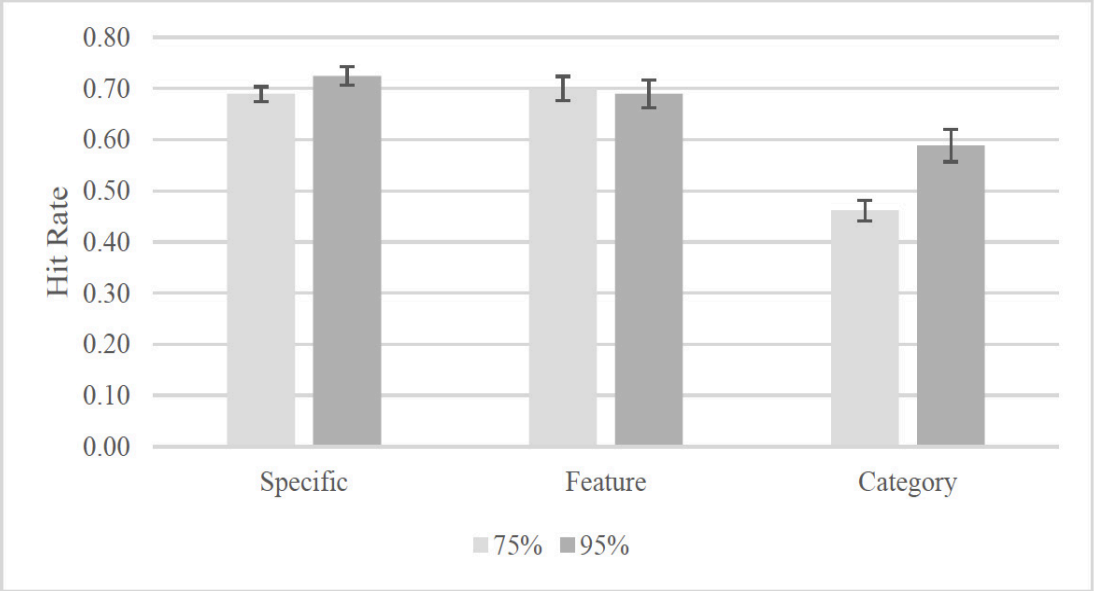

Figure 1. Mean correct hits for each target type by automation accuracy. Bars represent one standard error around the mean. Categorical target descriptions were found less frequently compared to specific and featural.

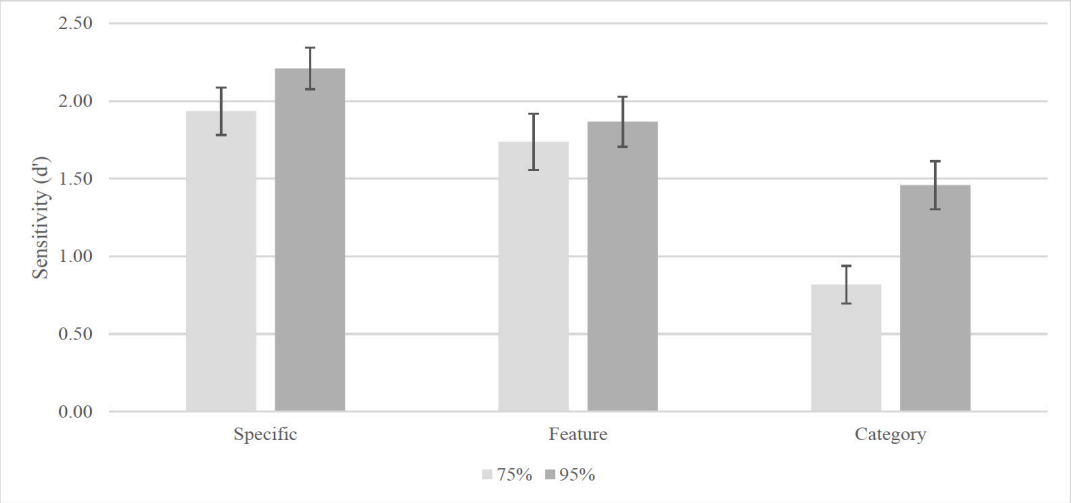

Figure 2. Mean sensitivity (measured by d') by target type and automation accuracy conditions. Light bars are means for when the automation was 75% accurate, and dark bars are for when the automation was 95% accurate. Sensitivity was higher for specific than categorical and featural.

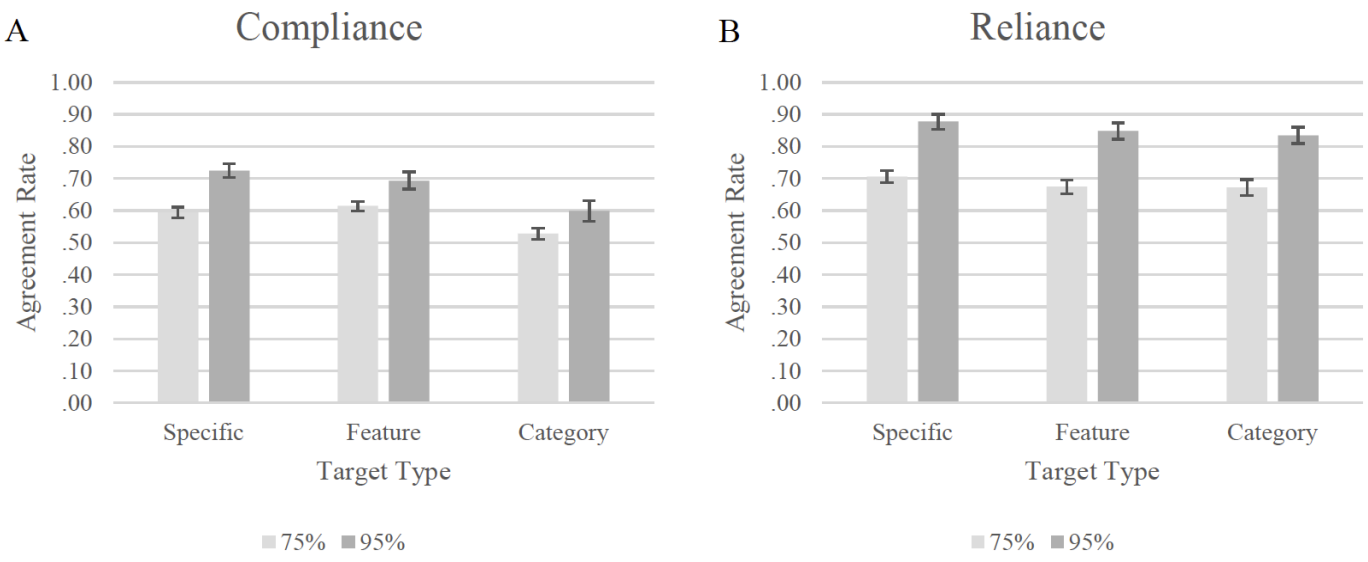

Figure 3. Compliance (A) mean agreement rate by target type and condition type. Reliance (B) mean agreement rate by target type and condition type. Error bars represent one standard error around the mean.

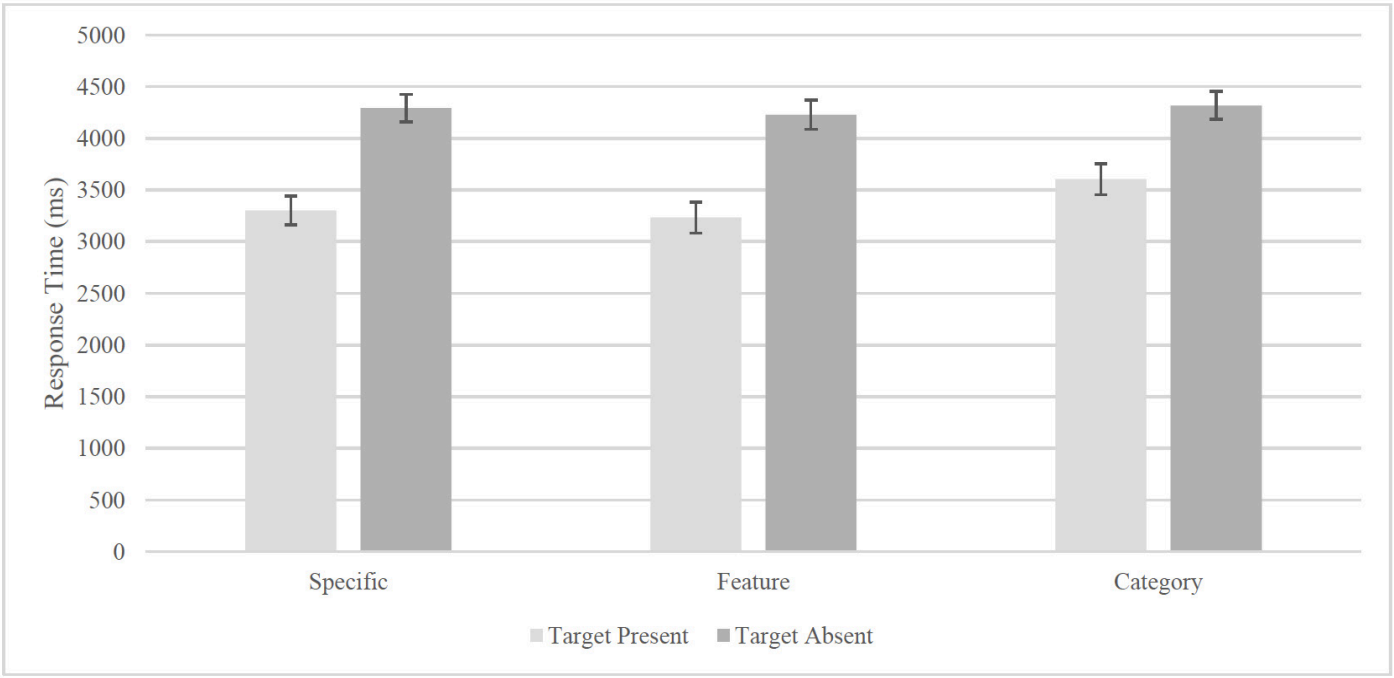

Figure 4. Mean response time in milliseconds by target type and target presence. Light bar represents means of target present. Dark bar represents means of target absent. Error bars represents one standard error around the mean. Reaction time was shorter in featural description for both target present and absent.

Estuarine DOM composition response to Hurricane Harvey: lessons learned

by: Megan Greige

Abstract

Recent studies characterizing dissolved organic matter (DOM) inputs and biogeochemical processes in coastal regions following storm events have focused on riverine and marine environments and overlooked estuarine systems. Bay surface-water samples (n=16) were collected from nearshore in Corpus Christi Bay, Texas, two days before Hurricane Harvey made landfall until two months after. PPL-solid phase extraction and UPLC Orbitrap Fusion Tribrid mass spectrometry, in positive mode, was utilized to molecularly characterize surface-water DOM. Analysis revealed input of carbon-rich compounds during landfall, followed by an increase of nitrogenous DOM that decreased over time. In the area, Hurricane Harvey brought trace amounts of precipitation but strong northwesterly winds that caused a significant drop in bay water level. It is believed that this caused a sudden and significant steepening of bayward aquifer hydraulic gradients that enhanced input of groundwater and flushing of porewater DOM to temporarily exposed sediments and shallow waters. These changes in DOM composition could significantly influence the ecological health of estuaries.

Mentor

Dr. Dorina Murgulet

Associate Professor of Hydrogeology

Department of Physical and Environmental Sciences

1. Introduction

Estuaries are one of the world's most important environmental resources (Costanza et al., 1997; Savage, Thrush, Lohrer, & Hewitt, 2012). They provide habitat, nursery, and food sources for many ecologically and economically important marine organisms (Beck et al., 2001). They also provide other ecosystem services, such as the filtration of sediment and pollutants (Teuchies et al., 2013). In recent years, these environments have been subjected to an increasing amount of anthropogenic and natural perturbations that may alter or even compromise the productivity of estuarine ecosystems. Among these are extreme hydroclimatic events, such as hurricanes, droughts, and flood events (Shelton, 2009), which have all been predicted to increase in frequency and intensity due to climate change (Webster et al., 2005). Extreme hydroclimatic events greatly influence the delivery of freshwater to estuaries. Freshwater inflows provide nutrients, sediments, and organic matter important to biogeochemical cycling and ecological productivity in the estuary.

Thus, any changes in freshwater inflow can greatly impact biogeochemical cycling in these habitats and nutrient exports to the open ocean (Palmer et al., 2012; Riera et al., 2000). A number of studies have identified changes in water quality and ecosystem functioning after, and in relation to, storm events, like hurricanes. (Mallin et al., 1999; Paerl et al., 1998). However, only in recent years has the impact of storm events on organic matter cycling and composition become of focus of research in riverine (Raymond & Saiers, 2010; Lu & Liu, 2019) and estuarine systems (Letourneau & Medeiros, 2019).

Dissolved organic matter (DOM) is shown to be an important source of carbon (C) and carbon-bound nutrients, such as nitrogen (N), phosphorus (P), and sulfur (S), in estuaries and plays an important role in the biogeochemistry and ecological functioning of these environments (Findlay et al., 2002; Hansell & Carlson, 2014). Studies indicate that DOM affects the solubility (Chiou et al., 1986), bioavailability (Akkanen et al., 2004; Ksionzek et al., 2018), and reactivity (Opsahl & Benner, 1998) of nutrients, trace metals, and contaminants in aquatic environments. Reactions of DOM at land-ocean boundaries, like estuaries, play a key role in the biochemical transformations of these nutrients, thus further studies are necessary.

There are several sources for DOM in the estuarine environment, with freshwater inputs and in-situ marine inputs among the primary. Terrestrial DOM sources dominate in estuaries with significant freshwater inputs. This DOM is produced as precipitation percolates though the soil and dissolves atmospheric dusts and gases, root exudate, leaf and root litter, and metabolites of microorganisms (Findlay et al., 2002). Humic substances, a broad class of organic acids containing aromatic rings, represent a main fraction of terrestrially sourced DOM (Thurman, 1985). Much of these substances originate in plant detritus, specifically lignin, a heterogeneous phenylpropanoid polymer found in the cell walls of vascular plants, and tannin, a polyphenolic compound most commonly found in the bark and leaves of plants (Findlay et al., 2002). As plants decay, this detritus can be transported directly into rivers or be leached into groundwater from where it can directly discharge to rivers or estuaries, ultimately to be exported towards coastal margins and the open ocean (Findlay et al., 2002; Sleighter & Hatcher, 2008).

Estuarine-derived DOM inputs could be signifcant in coastal environments when freshwater inputs are limited. Phytoplankton, N2 fixers, bacteria, zooplankton, and viruses produce DOM within the water column via excretion, fecal pellet dissolution, passive and active diffusion, exoenzymes, and lysis (Sipler & Bronk, 2015). In shallower environments, direct release from microalgae and sediments via diagenesis are also sources of DOM (Sipler & Bronk, 2015).

The source of DOM reflects on its composition and degree of biodegradation in estuarine and marine environments. For instance, terrestrial DOM is characterized by more aromatic compounds and a greater CHO composition, due to the nature of terrestrial plant detritus described (Bianchi & Bauer, 2011). When compared to terrestrial sources, marine DOM is characterized by higher weighted averages of phosphorous and nitrogen heteroatoms and aliphatic compounds (Bianchi & Bauer, 2011). The source and quantity of DOM has been shown to influence estuarine ecology through changes in microbial community composition (D'Andrilli et al., 2019; Traving et al., 2017). This has implications for marine primary production, especially when seasonal effects on marine primary production are considered.

DOM is a vital nutrient source for estuaries, and coastal seas rely on the exports of organic matter from these environments to stimulate beneficial ecological activity and support diversity within the ecosystem (Savage et al., 2012). Conversely, excess inputs can stimulate harmful algal blooms, especially during warm months and increased runoff from storms (Boyer et al., 2006).

Perturbations that alter the source and flow of water to estuaries, such as extreme hydroclimatic events, can influence the quantity of DOM inputs, composition, and degradation pathways in estuarine waters. Given the different sources and sinks for DOM converging in estuaries, including riverine inputs, flanking marshes, groundwater, and benthic fluxes, atmospheric deposition, and oceanic waters (Hedges & Keil, 1999), these types of investigations are scarce and have proven challenging. For instance, river discharge and ocean tides experience daily and seasonal variations and can be altered by extreme hydroclimatic events (Wetz & Yoskowitz, 2013). These physical processes induce changes in temperature, pH, salinity, dissolved oxygen (DO), and turbidity, which in turn, have the ability influence DOM bioavailability and transformations in estuaries (Liu et al., 2019). Molecular characterization of DOM can aid in our understanding of biogeochemical cycling in estuaries after extreme hydroclimatic events, like hurricanes, that are expected to increase in frequency and intensity.

Studies have begun to assess changes in DOM after storm events but have focused on freshwater discharge, such as stream flow and surface runoff (Lu & Liu, 2019; Chen et al., 2019; Dennis et al., 2017). This study investigates the changes in DOM composition in an estuarine environment after a hurricane event using Ultrahigh Performance Liquid Chromatography (UPLC) coupled with mass spectrometry and uses statistical analysis of DOM composition to determine potential sources of these changes.

2. Methods

2.1 STUDY AREA AND SAMPLING SITE

Samples were collected on the southern shore of Corpus Christi Bay at University Beach on Ward Island, originally predicted to be within the landfall path of Hurricane Harvey (Figure 1). Corpus Christi Bay is a shallow embayment comprised of fine sand and silt along the shoreline and mud towards the middle of the bay (Morton & Winker, 1980). The bay formed by the backfilling of an incised valley during a quaternary sea level transgression sequence when sea level rise exceeded the rate of sediment supply from local rivers (Morton & Winker, 1980). Ward Island is a remnant of the Nueces River/Oso Creek deltaic complex discharging into the bay. University Beach was constructed in 2001 to restore the beach that once extended along the entire shoreline fronting the island. Terminal groins stabilize 366 meters of beach and three detached breakwaters protect the beach from forces exerted towards the shore (Williams, 2002). Water samples were collected from surface water, within ten meters of the shore. Two samples were collected daily prior to landfall. Post-landfall, ten samples were collected daily between days four and fourteen. Two more samples were collected weekly after this date, and one last sample was collected on September 30.

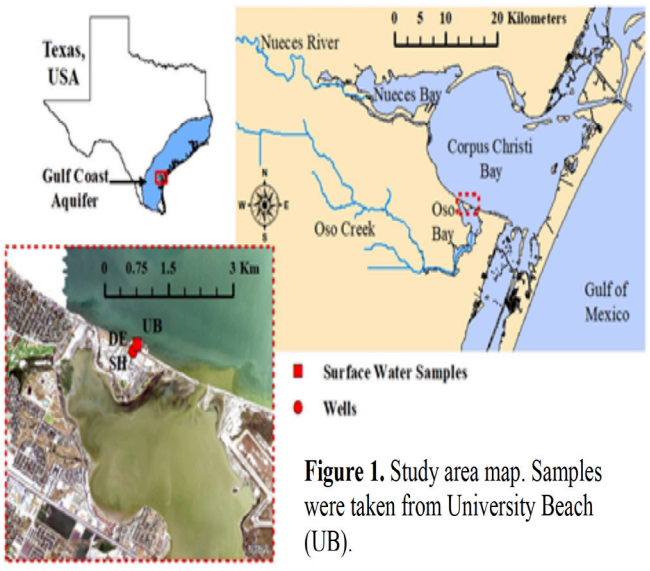

Figure 1. Study area map. Samples were taken from University Beach (UB).

2.2 HYDROCLIMATIC CONDITIONS

Hurricane Harvey originated in the Atlantic and rapidly intensified as it approached the Texas coast, reaching a maximum windspeed of 115 knots—category 4 status on the Saffir-Simpson scale—before making landfall (National Hurricane Center, 2018). It made landfall on August 26 on the northern end of San Jose Island, a barrier island approximately 58 kilometers (36 miles) north of Ward Island. Landfall on the Texas mainland occurred approximately three hours later with an estimated windspeed of 105 knots (National Hurricane Center, 2018). After stalling near the Houston, Texas, area, the storm drifted offshore three days later before making another final landfall in southwestern Louisiana on September 30 (Figure 2). The study area received input from both Corpus Christi Bay to the north, which is separated from the Gulf of Mexico by barrier islands, and Oso Bay (Figure 1).

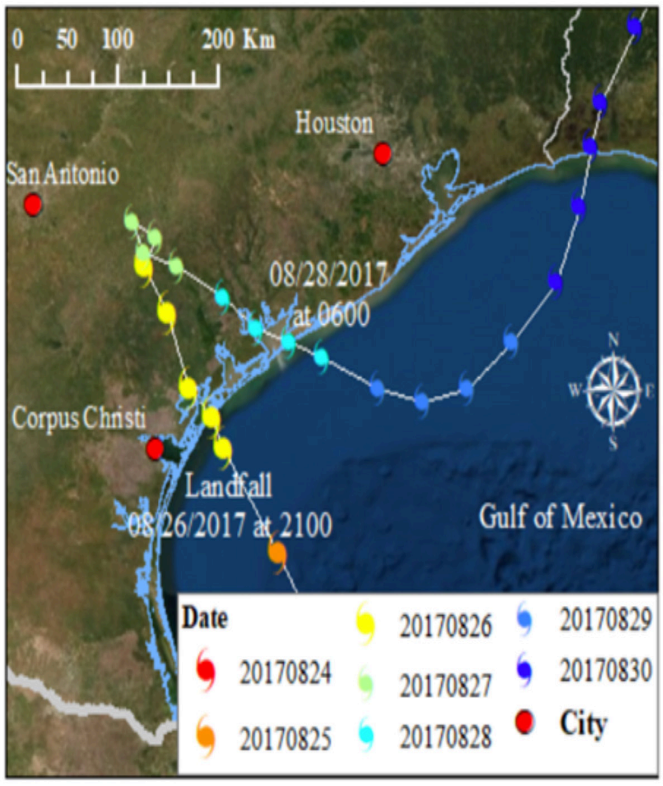

Figure 2. Movement of Hurricane Harvey colored by day.

2.3 DATA COLLECTION AND ANALYSES

2.3.1 Solid Phase Extraction

Immediately after collection, samples were passed through 0.2 µm polyesthersulfone filters to remove particulates. Prior to extraction, 100 mL of each sample was acidified to pH 2 with HCl to increase extraction efficiency for organic acids and phenols. DOM samples were then prepared for mass spectrometric analysis using Bond Elut PPL solid phase extraction (SPE) cartridges following the procedure recommended by Dittmar et al (2008). Prior to elution of the DOM from the cartridges, two cartridge volumes of 0.01 HCl were passed through the cartridge to completely remove salts and then dried. The samples were eluted with 6 mL Optima LC/MS grade methanol. The methanol eluents were dried in a Centrivap benchtop concentrator and reconstituted with 1 mL with of 95:5 water to acetonitrile.

2.3.2UPLC-Orbitrap Fusion Tribrid Mass Spectrometry

Analyses of DOM were conducted using UPLC with mass spectrometry using the Orbitrap Fusion Tribrid mass spectrometer (UPLC-OT-FTMS). An auto sampler injected the samples into the LC C18 column before heated electrospray ionization (H-ESI) of 3500 V for analysis in positive mode by the mass spec. Compound Discoverer software 3.0 (Thermo Fisher) was used to identify the DOM compounds according to the following criteria: 1) it has a signal-to-noise ratio above 3; 2) a minimum of 5 mass scans per chromatographic peak, 3) a minimum peak intensity of 50,000, and 4) at least one isotope peak detected. A molecular formula calculator (Molecular Formula Calc version 1.0 NHMFL, 1998) was used to determine empirical formula matches with the following parameters:$C_{4-100}H_{4-200}O_{0-50}N_{0-10}S_{0-3}P_{0-3}$. Coupled UPLC8 OT-FTMS is also able to reveal compound structure, allowing separate isomers to be identified that reduced the number of "duplicate" compounds.

Remaining duplicates were reduced using MatLab with a set of conservative rules, which helped eliminate any remaining compounds not known to exist in nature or below detection limit, among others, as described in detail in Abdulla, et al. (2013).

2.3.3 DOM Molecular Data Statistical analysis

Principal Component Analysis

Using Compound Discoverer (Thermofisher Scientific), a principal component analysis (PCA) was employed to detect temporal changes in molecular composition. This approach takes into account the molecular composition and the normalized signal intensities for all samples. Briefly, PCA is a data reduction procedure that analyzes the thousands of compounds and associated data in compound discoverer and calculates new synthetic variables (principal components), that account for as much of the variance as possible, which can be represented in a coordinate system (Ramette, 2007). This allows not only to identify if and how DOM composition in samples vary with time based on spatial variance in the coordinate plane, but also determine which compounds are significant to this variance.

van Kevelen Diagrams

Organic compounds from PCA were also classified into major compound classes based on their O/C and H/C ratios. These characteristic O/C and H/C ratios are correlated to the major classes in van Krevelen Diagrams, with certain classes clustering in different areas of the plot based on Koch and Dittmar's findings (Dittmar et al., 2008). Classifying compounds in this way aids in identifying the source and transformation of compounds in the time series as well as potential environmental drivers.

2.3.4 Nutrition Method

Inorganic nutrients (nitrate (NO_3^-), nitrite (NO_2^-), ammonium (NH_4^+), orthophosphate (HPO_4^{2-}), silicate ($HSiO_3^-$)) were determined from the filtrate using a Seal QuAAtro autoanalyzer. The method detection limit was determined for each analyte and matrix by the EPA method detailed in 40 CFR Part 136, Appendix B.

The method detection limit (MDL) is defined as the Student's t for 99% confidence level times the standard deviation of seven replicate measurements of the same low-level sample or spiked sample. If the sample concentration exceeds the linear range, the sample was diluted and reanalyzed. The method detection limit (MDL) in µm for the nutrients are: 0.11 for NO_3^-, 0.012 for NO_2^-, 0.057 for NH_4^+, 0.025 for HPO_4^{2-}, 0.14 for HSiO3-. DOC and TDN measurements were conducted using a Shimadzu TOC-V analyzer with nitrogen module. Dissolved organic nitrogen (DON) was estimated as the difference between TDN and dissolved inorganic nitrogen ($DIN=NO_2^-+NO_3^-+NH_4^+$). The method detection limit is approximately 1 $mg \cdot L^{-1}$.

3. Results

3.1 HYDROLOGIC CONDITIONS

Although there was a considerable amount of precipitation and surface runoff north of the study area as a result of Hurricane Harvey, stream flow discharge to the study area (i.e., from Oso Creek) and precipitation were relatively low compared to other events that year (Figure 3A). Water levels in Corpus Christi Bay, on the other hand, changed significantly during and after hurricane landfall, falling approximately 0.1 meters below the Mean Lower Low Water Level (MLLW) during landfall, hovering around the MLLW for a time, and falling again to 0.2 meters below the MLLW on September 30, the day of the first post-hurricane sample (Figure 3A). Water level eventually recovered to Average Sea Level (ASL) but dropped again (not as severely) before recovering.

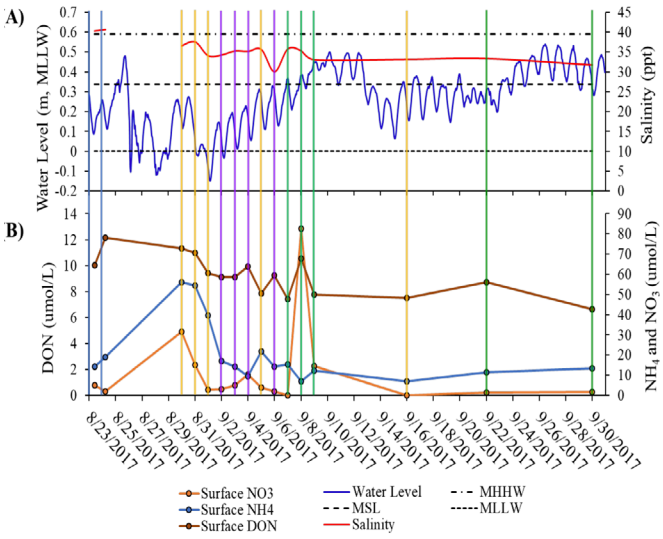

Figure 3. (A) Water level and salinity and (B) nitrogen nutrients (ammonium, nitrate, and dissolved organic nitrogen) over time. Vertical bars correspond to Hurricane Harvey prelandfall (blue) and PCA clusters (see Figure 5): yellow bars are hydrologic pull, purple bars are benthic, green bars normal conditions.

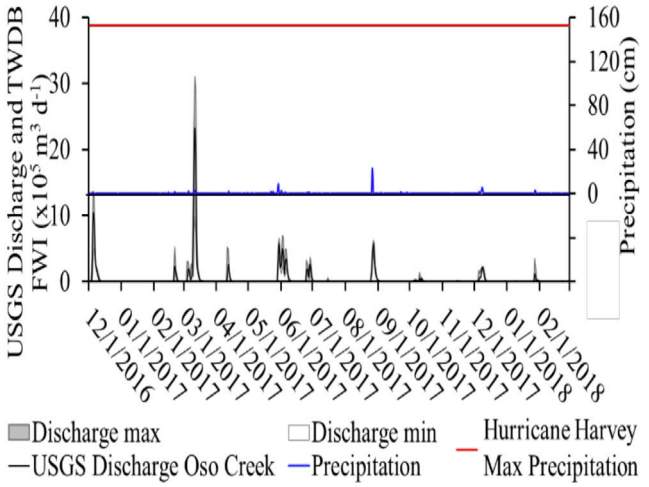

Figure 4. Oso Creek water discharge and precipitation at study area along with maximum precipitation recorded for Hurricane Harvey (152 cm near Nederland, Texas) (National Hurricane Center).

3.2 NUTRIENT CONCENTRATIONS

DON concentrations initially decreased as Hurricane Harvey made landfall and dropped further when the water level decreased again, while NO_3 levels initially rose immediately after landfall (Figure 3B). However, both NO_3 and DON fluctuated in a similar manner up to 10 days after the landfall and remain at the lowest end for the following 3 weeks. A reduced form of nitrogen, NH_4, initially rose with NO_3 as Hurricane Harvey made landfall and water levels decreased by ~0.5 m.NH_4 was observed to decrease again with other observed drops in water levels, like DON and NO_3. However, daily fluctuations in NH4 showed a reverse trend to those of NO_3 and DON (Figure 3B).

An evaluation of the relationship between nutrient concentration and hydrologic parameters indicates that an increase in water levels leads to higher NH_4 and DON levels (Table 1). In addition, DON levels increase with salinity.

Table 1. Correlation coefficients (r) and significance levels (p-values) between nutrients and hydrologic parameters, water level (wl) and salinity (sal)

Sign	NO_3 vs sal	NO_3 vs wl	NH_4 vs sal	NH_4 vs wl	DON vs sal	DON vs wl
r	0.1025	0.2689	0.2829	0.6139	0.6958	0.4584
p-value	0.7056	0.3139	0.2884	0.0114	0.002757	0.0742

3.3 DOM MOLECULAR CHARACTERIZATION

For the samples, a total of 1,649 unique compounds were detected by the UPLC-OTFTMS, of which 1249 (75.9%) were assigned formulas. The assigned formulas were primarily CHO (38.7%), CHON (38.6%), and CHOS (7.7%) with the remaining being N- and Scontaining heteroatoms (7.0%) and CHOP (3.3%). From these, the PCA identified significant variance amongst the days of sampling. PCA analysis revealed a significant difference in the DOM composition between samples collected before and after hurricane landfall, as well as throughout post-Harvey time series (days 4-14 after landfall). Variation analyses reveal a separation of pre- and post-hurricane samples based on their molecular characteristics. Samples days 4-14, after hurricane landfall, clustered in three groups: cluster 1: days 4, 5, 6, 10, and 22, cluster 2: days 7, 8, 9, and 11, and cluster 3: days 12, 13, 14, 28, and 35.

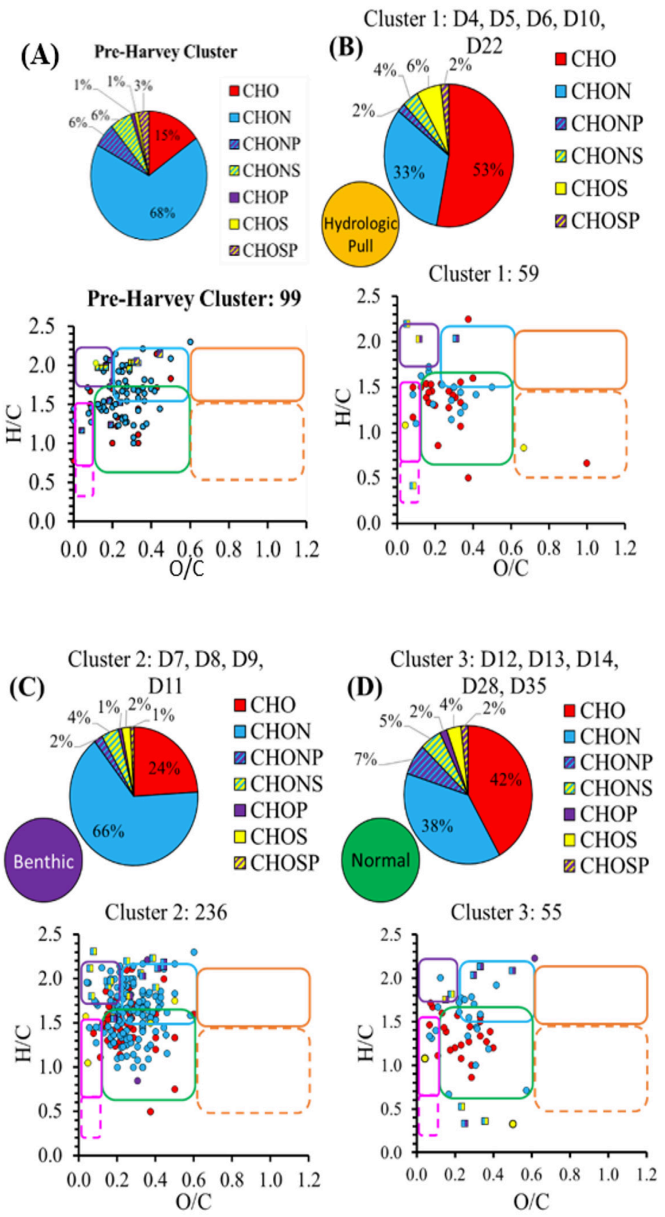

Figure 5. DOM compound classifications by pie chart and van Krevelen diagram (O/C vs H/C elemental ratios) for each PCA cluster (A, B, C, and D). Generalized compound class regions for van Krevelen diagrams are defined by the boxes: CRAM/lignin (black), lipids (green), protein (solid blue), amino sugars (dashed blue), carbohydrate (orange), tannins (dark red), condensed hydrocarbons (solid pink), unsaturated carbon (dashed pink).

The PCA scores for the pre-hurricane samples and each cluster of the post-hurricane samples were correlated to the specific DOM formulas that contributed to the clustering. The prehurricane cluster was highly characterized by organic compounds containing nitrogen (80%), which is typical of marine environments (Figure 5A). Cluster 1 was especially dominated by CHO (53%) and depleted of nitrogen compounds in comparison to the other clusters of samples (Figure 5B). Additionally, plotting on the van Krevelen Diagram revealed lower H/C ratios and higher proportions of lignins and tannins. Tannins were present only in thiscluster. Terrestrial DOM, which includes tannins and lignins, is characterized by more aromatic compounds and a greater CHO composition. Cluster 2 was highly characterized by nitrogen containing organic compounds (72%), including compounds with higher H/C ratios (Figure 5C), while cluster 3 was characterized by a mix of nitrogen containing compounds and CHO (50% and 42%, respectively) (Figure 5D). Cluster 2 shared a similar DOM composition with the prehurricane samples. While a larger number of compounds were found pre-hurricane, cluster 2 had more than twice the number (Figure 5 A, B).

4. Discussion

Results of PCA analysis and correlation with DOM composition indicate significant mobilization of terrestrial DOM during Hurricane Harvey. Studies have found similar results showing that hurricanes and storms mobilize and export terrigenous DOM towards coasts; however, for many of these studies, stream flow was found to be the major source of terrestrial DOM to marine waters during storm events, normally as a result of increased precipitation and run-off (Chen et al., 2019; Inamdar et al., 2011; Lu & Liu, 2019). For instance, Lu and Liu (2019) examined rivers not far north of Corpus Christi Bay and identified results consistent with these expectations.

Although Hurricane Harvey brought significant amounts of precipitation over coastal Texas, stream flow discharge was relatively low compared to other events that year (Figure 3A). However, water levels in the bay changed significantly. Cross-referencing of samples with water level data revealed that cluster 1, the most samples with the greatest terrestrial signature, correlated with decreases in water level, while cluster 2, the more nitrogenous samples, correlated with overall rising water level. Cluster 3, the more mixedncompound set of samples, correlated with the return to average mean sea level (MSL). The decreases in sea level are accounted for by the hurricane path. Hurricane Harvey made landfall north of the study area, placing the study area on the south western side of the hurricane, where winds pushing offshore pulled water bayward and drove sea level down. This is resulted in a rare phenomenon often known as negative or, reverse, storm surge. The unique path of Hurricane Harvey, with its stalling near Houston and returning to the Gulf of Mexico before making an additional final landfall, led to further impacts on local sea level (Figures 2, 3A). Although no groundwater level measurements are available during this time, the DOM molecular characterization and nutrient concentration data suggest that an expected increase in the hydraulic gradient between the marine environment and terrestrial groundwater, driven by sudden drops in sea level, may be
responsible for influx of groundwater and terrestrial (CHO) compounds to the marineenvironment (Figure 6). There are a large number of studies that have shown sea level and tidal changes have the ability to influence submarine groundwater discharge on both short-term and long-term scales, causing tidal pumping of groundwater into sea water (Kim & Hwang, 2002; Taniguchi & Iwakawa, 2004). Ongoing studies confirm rapid responses in groundwater levels to tidal changes near the sampling site of this study.

The progressive rise in sea level poststorm allowed recirculation of nearshore sediments, which resulted in a benthic flux of trapped nitrogenous organic compounds in porewater, similar to pre-storm conditions (Figure 6.). Recall the similarity in terms of compositions of significant compounds for both the prestorm and cluster 2 samples (Figure 5). Similarly, Dixon et al. (2014) identified evidence of benthic resuspension events of degraded, planktonic organic matter in an estuary during increased windspeed and shifts in wind direction.

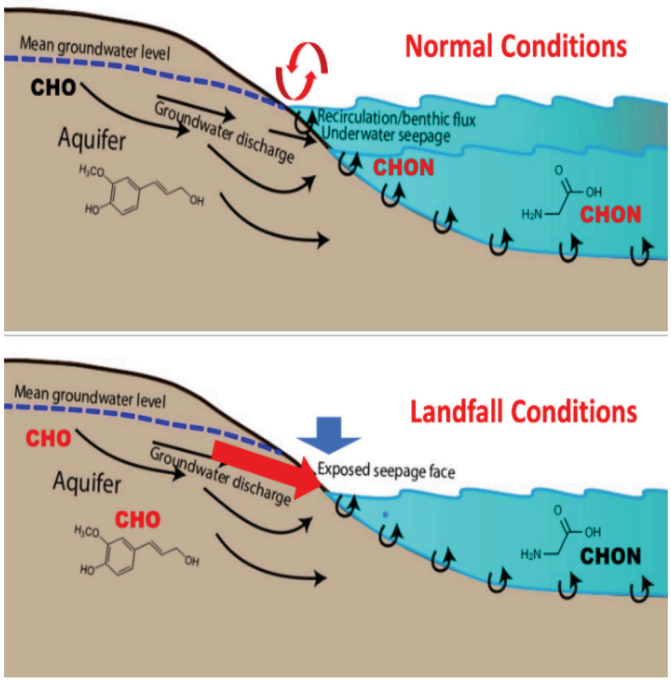

Figure 6. Conceptual model of changes in DOM and hydrologic system during and outside of Hurricane Harvey.

Nutrient concentration also supports this interpretation of the DOM inputs. Nitrogen nutrients overall decreased after day 4, with the greatest drop (including all forms of nitrogen measured) being associated with Cluster 1. The decrease in salinity on day 8 (September 6) with an increase in DON, followed by an increase of NH_4 the following day, could have potentially been caused by photooxidation of DON, which releases NH_4 (Mesfioui et al., 2015).

This occurred during the gradual resuspension of nearshore sediments reflected in Cluster 2 as tides recovered to normal levels. A large peak in NO_3 concentrations on day 10 (September 8) following a salinity spike indicates possible discharge of saline groundwater (common found in the surrounding area). Although, generally, the water level was recovering to mean sea level, some fluctuation occurred during this time, with smaller drops and a prolonged return to higher diurnal water levels. Statistical correlation analysis supports this, with NH_4 concentrations being significantly correlated to average daily wate levels and DON being significantly correlated to salinity.

5. Conclusion

This study identified a change in DOM composition due to hydrologic disturbance caused by Hurricane Harvey. Molecular composition and nutrient data varied both according to pre- and post-storm event and in correlation with changing water levels. Hurricane Harvey enhanced the tidal pumping mechanism through drops in sea level and steepening of the hydraulic gradient between the water table and marine system. This led to an influx of more terrestrial CHO-rich compounds into the marine system, and release of sediment-trapped CHON compounds through recirculation caused by wind-driven turbulence. These results add to the growing number of studies that have found tidal forcing significant to groundwater discharge and nutrient transport and transformation. Extreme events, including hurricanes, have the ability to impact biogeochemical cycles in estuarine areas in a number of ways, including changes of DOM sources and transformations. The expected increase in occurrence and intensity of storms and hurricanes as well as changes in local hydrology is expected to become a significant driver of DOM dynamics and thus, estuarine biogeochemistry.

Acknowledgments

The Center for Water Supply Studies and Texas A&M University-Corpus Christi and the McNair Scholars Program financially supported this research. I would like to thank Dr. Joseph D. Felix for help with sample collection and Dr. Hussain Abdulla for providing lab equipment, instruction, and expertise for the mass spectrometry analysis used in this project. A special thank you to Dr. Audrey R. Douglas for providing aid with all aspects of the project and to Dr. Dorina Murgulet for her guidance, aid, and oversight of the entirety of this project. Finally, I would like to thank the McNair Scholars Program for providing me with this opportunity to complete a research project as an undergraduate student at Texas A&M University—Corpus Christi and the TAMU-CC Center for Water Supply Studies for providing equipment and additional resources and data used in this project.

Sources Cited

Abdulla, H. A. N., Minor, E. C., Dias, R. F., & Hatcher, P. G. (2013). Transformations of the chemical compositions of high molecular weight DOM along a salinity transect: Using two dimensional correlation spectroscopy and principal component analysis approaches. *Geochimica et Cosmochimica Acta, 118,* 231–246. https://doi.org/10.1016/j.gca.2013.03.036

Akkanen, J., Vogt, R. D., Kukkonen, J. V., & K. (2004). Essential characteristics of natural dissolved organic matter affecting the sorption of hydrophobic organic contaminants. *Aquatic Sciences, 66*(2), 171–177. http://dx.doi.org/10.1007/s00027-004-0705-x

Beck, M. W., Heck, K. L., Able, K. W., Childers, D. L., Eggleston, D. B., Gillanders, B. M., Halpern, B., Hays, C. G., Hoshino, K., Minello, T. J., Orth, R. J., Sheridan, P. F., & Weinstein, M. P.(2001).The Identification, Conservation, and Management of Estuarine and Marine Nurseries for Fish and Invertebrates. *BioScience, 51*(8), 633–641. https://doi.org/10.1641/0006 3568(2001)051[0633:ticamo]2.0.co;2

Bianchi, T. S., & Bauer, J. E. (2011). Particulate Organic Carbon Cycling and Transformation. In Treatise on Estuarine and Coastal Science (pp. 69–117). Elsevier. https://doi.org/10.1016/B978-0-12-374711-2.00503-9

Blake, E. S., & Zelinsky, D. A. (2018). *Tropical Cyclone Report: Hurricane Harvey*. National Hurricane Center.

Boyer, J. N., Dailey, S. K., Gibson, P. J., Rogers, M. T., & Mir-gonzalez, D. (2006). The role of dissolved organic matter bioavailability in promoting phytoplankton blooms in Florida Bay. *Hydrobiologia, 569*(1), 71–85. http://dx.doi.org/10.1007/s10750-006-0123-2

Chen, S., Lu, Y., Dash, P., Das, P., Li, J., Capps, K., Majidzadeh, H., & Elliott, M. (2019). Hurricane pulses: Small watershed exports of dissolved nutrients and organic matter during large storms in the Southeastern USA. *Science of The Total Environment, 689*, 232–244. https://doi.org/10.1016/j.scitotenv.2019.06.351

Chiou, C. T., Malcolm, R. L., Brinton, T. I., & Kile, D. E. (1986). Water solubility enhancement of some organic pollutants and pesticides by dissolved humic and fulvic acids. *Environmental Science & Technology, 20*(5), 502–508. https://doi.org/10.1021/es00147a010

Costanza, R., d'Arge, R., de Groot, R., Farber, S., Grasso, M., Hannon, B., Limburg, K., Naeem, S., O'Neill, R. V., Paruelo, J., Raskin, R. G., Sutton, P., & van den Belt, M. (1997). The value of the world's ecosystem services and natural capital. Nature, 387(6630), 253–260. https://doi.org/10.1038/387253a0

D'Andrilli, J., Junker, J. R., Smith, H. J., Scholl, E. A., & Foreman, C. M. (2019). DOM composition alters ecosystem function during microbial processing of isolated sources. Biogeochemistry, 142(2), 281–298. http://dx.doi.org/10.1007/s10533-018-00534-5

Denis, M., Jeanneau, L., Petitjean, P., Murzeau, A., Liotaud, M., Yonnet, L., & Gruau, G. (2017). New molecular evidence for surface and sub-surface soil erosion controls on the composition of stream DOM during storm events. *Biogeosciences, 14*(22), 5039–5051. http://dx.doi.org/10.5194/bg-14-5039-2017

Dittmar, T., Koch, B., Hertkorn, N., & Kattner, G. (2008). A simple and efficient method for the solid-phase extraction of dissolved organic matter (SPE-DOM) from seawater. *Limnology and Oceanography: Methods, 6*(6), 230–235. https://doi.org/10.4319/lom.2008.6.230

Denis, M., Jeanneau, L., Petitjean, P., Murzeau, A., Liotaud, M., Yonnet, L., & Gruau, G. (2017).New molecular evidence for surface and sub-surface soil erosion controls on the composition of stream DOM during storm events. *Biogeosciences, 14*(22),5039–5051.http://dx.doi.org/10.5194/bg-14-5039-2017

Dixon, J. L., Osburn, C. L., Paerl, H. W., & Peierls, B. L. (2014). Seasonal changes in estuarine dissolved organic matter due to variable flushing time and wind-driven mixing events. Estuarine, *Coastal and Shelf Science, 151*, 210–220. https://doi.org/10.1016/j.ecss.2014.10.013

Findlay, S., Sinsabaugh, R. L., & Findlay, S. (2002). Aquatic Ecosystems: Interactivity of Dissolved Organic Matter. *Elsevier Science & Technology.* http://ebookcentral.proquest.com/lib/tamucc/detail.action?docID=344634

Hansell, D. A., & Carlson, C. A. (2014). Biogeochemistry of Marine Dissolved Organic Matter. *Elsevier Science & Technology.* http://ebookcentral.proquest.com/lib/tamucc/detail.action?docID=1813981

Hedges, J. I., & Keil, R. G. (1999). Organic geochemical perspectives on estuarine processes: Sorption reactions and consequences. *Marine Chemistry, 65*(1), 55–65. https://doi.org/10.1016/S0304-4203(99)00010-9.

Inamdar, S., Singh, S., Dutta, S., Levia, D., Mitchell, M., Scott, D., Bais, H., & McHale, P. (2011). Fluorescence characteristics and sources of dissolved organic matter for stream water during storm events in a forested mid-Atlantic watershed. *Journal of Geophysical Research. Biogeosciences, 116*(3). http://dx.doi.org/10.1029/2011JG001735

Kim, G., & Hwang, D.-W. (2002). Tidal pumping of groundwater into the coastal ocean revealed from submarine 222Rn and CH4 monitoring. *Geophysical Research Letters*, *29*(14), 23 1-23–24. https://doi.org/10.1029/2002GL015093

Ksionzek, K. B., Jing Zhang, Kai-Uwe Ludwichowski, Wilhelms-Dick, D., Trimborn, S., Jendrossek, T., Kattner, G., & Koch, B. P. (2018). Stoichiometry, polarity, and organometallics in solid-phase extracted dissolved organic matter of the Elbe-Weser estuary. *PLoS One, 13*(9). ProQuest Central; SciTech Premium Collection. https://doi.org/10.1371/journal.pone.0203260

Letourneau, M. L., & Medeiros, P. M. (2019). Dissolved Organic Matter Composition in a Marsh- Dominated Estuary: Response to Seasonal Forcing and to the Passage of a Hurricane. *Journal of Geophysical Research: Biogeosciences, 124*(6), 1545–1559. https://doi.org/10.1029/2018JG004982

Liu, M., Chen, J., Sun, X., Hu, Z., & Fan, D. (2019). Accumulation and transformation of heavy metals in surface sediments from the Yangtze River estuary to the East China Sea shelf. *Environmental Pollution, 245*, 111–121. https://doi.org/10.1016/j.envpol.2018.10.128

Lu, K., & Liu, Z. (2019). Molecular Level Analysis Reveals Changes in Chemical Composition of Dissolved Organic Matter From South Texas Rivers After High Flow Events. Frontiers in Marine Science. ProQuest Central; *SciTech Premium Collection.* https://doi.org/10.3389/fmars.2019.00673

Mallin, M. A., Posey, M. H., Shank, G. C., McIver, M. R., Ensign, S. H., & Alphin, T. D. (1999). Hurricane Effects on Water Quality and Benthos in the Cape Fear Watershed: Natural and Anthropogenic Impacts. *Ecological Applications, 9*(1), 350–362. JSTOR. https://doi.org/10.2307/2641190

Mesfioui, R., Abdulla, H. A. N., & Hatcher, P. G. (2015). Photochemical Alterations of Natural and Anthropogenic Dissolved Organic Nitrogen in the York River. *Environmental Science & Technology, 49*(1), 159–167. https://doi.org/10.1021/es504095c

Morton, R. A., & Winker, C. D. (1980). Distribution and significance of coarse biogenic and clastic deposits on the Texas inner shelf. Bureau of Economic Geology, The University of Texas at Austin.

Opsahl, S., & Benner, R. (1998). Photochemical Reactivity of Dissolved Lignin in River and Ocean Waters. *Limnology and Oceanography, 43*(6), 1297–1304. JSTOR.

Paerl, H. W., Pinckney, J. L., Fear, J. M., & Peierls, B. L. (1998). Ecosystem responses to internal and watershed organic matter loading: Consequences for hypoxia in the eutrophying Neuse River Estuary, North Carolina, USA. *Marine Ecology Progress Series*, 166, 17–25. JSTOR.

Palmer, T. A., Montagna, P., & Beseres Pollack, J. (2012). *Hydrological Changes and Estuarine Dynamics*. Springer New York. http://ebookcentral.proquest.com/lib/tamucc/detail.action?docID=1082013

Ramette, A. (2007). Multivariate analyses in microbial ecology. F*EMS Microbiology Ecology, 62*(2), 142–160. ProQuest Central; SciTech Premium Collection. https://doi.org/10.1111/j.1574-6941.2007.00375.x

Raymond, P. A., & Saiers, J. E. (2010). Event controlled DOC export from forested watersheds. *Biogeochemistry, 100*(1/3), 197–209. JSTOR.

Riera, P., Montagna, P. A., Kalke, R. D., & Richard, P. (2000). Utilization of estuarine organic matter during growth and migration by juvenile brown shrimp Penaeus aztecus in a South Texas estuary. *Marine Ecology Progress Series, 199*, 205–216. JSTOR.

Savage, C., Thrush, S. F., Lohrer, A. M., & Hewitt, J. E. (2012). Ecosystem Services Transcend Boundaries: Estuaries Provide Resource Subsidies and Influence Functional Diversity in Coastal Benthic Communities. *PLoS ONE, 7*(8), e42708. Gale OneFile: Health and Medicine.

Shelton, M. L. (2009). *Hydroclimatology perspectives and applications*. Cambridge University Press.

Sipler, R. E., & Bronk, D. A. (2015). Chapter 4—Dynamics of Dissolved Organic Nitrogen. In D. A. Hansell & C. A. Carlson (Eds.), Biogeochemistry of Marine Dissolved Organic Matter (Second Edition) (pp. 127–232). Academic Press. https://doi.org/10.1016/B978-012-405940-5.00004-2

Sleighter, R. L., & Hatcher, P. G. (2008). Molecular characterization of dissolved organic matter (DOM) along a river to ocean transect of the lower Chesapeake Bay by ultrahigh resolution electrospray ionization Fourier transform ion cyclotron resonance mass spectrometry. *Marine Chemistry, 110*(3), 140–152. https://doi.org/10.1016/j.marchem.2008.04.008

Taniguchi, M., & Iwakawa, H. (2004). Submarine groundwater discharge in Osaka Bay, Japan. *Limnology, 5*(1), 25–32. ProQuest Central; SciTech Premium Collection. https://doi.org/10.1007/s10201-003-0112-3

Thurman, E. M. (1985). *Organic geochemistry of natural waters*. Springer Netherlands. https://doi.org/10.1007/978-94-009-5095-5

Traving, S. J., Rowe, O., Jakobsen, N. M., Sorensen, H., Dinasquet, J., Stedmon, C. A., Andersson, A., & Riemann, L. (2017). The Effect of Increased Loads of Dissolved Organic Matter on Estuarine Microbial Community Composition and Function. *Frontiers in Microbiology*. Gale OneFile: Health and Medicine. https://link.gale.com/apps/doc/A484729180/HRCA?u=txshracd2566&sid=HRCA&xid=b6b677f

Webster, P. J., Holland, G. J., Curry, J. A., & Chang, H.-R. (2005). Changes in tropical cyclone number, duration, and intensity in a warming environment. *Science, 309*(5742), 1844+. Gale In Context: Science.

Wetz, M. S., & Yoskowitz, D. W. (2013). An 'extreme' future for estuaries? Effects of extreme climatic events on estuarine water quality and ecology. *Marine Pollution Bulletin, 69*(1), 7–18. https://doi.org/10.1016/j.marpolbul.2013.01.020

Williams, D. D. (2002). Monitoring, analysis and interpretation of the post-construction evolution of a restored beach at TAMU-CC. *Corpus 5*(31):2003.

Farmer's Walk Electromyographical Data and its Relation to Muscular Soreness

By: Eduardo A. Luna

Abstract

Currently, no studies have been done to examine if a relationship exists between Electromyography (EMG) amplitudes and perceived muscular soreness. ***PURPOSE:*** *The purpose of this study is to investigate if a correlational relationship between EMG amplitudes measured during Farmer's Walk (FW) bouts and perceived muscular soreness exists.* ***METHODS:*** *Five participants (mean age 23.72 ± 0.85) were tested to obtain both EMG amplitudes and visually perceived muscle soreness (VPMS) measures while completing a normal walk and FW exercise. For both variations, the participants were asked to complete ten repetitions of 20-meter walks while EMG amplitudes were recorded and VPMS questionnaires were completed prior to experimental procedures, immediately post, and 24-, 48-, and 72-hours post exercise. Pearson product correlations and linear regression models were used to investigate the possible relationship between peak EMG amplitudes and perceived muscular soreness.* ***RESULTS:*** *There was a difference between FW and NW (Control) peak EMG muscle amplitude (465. 4 ± 83.5 vs 134.8 ± 11.91; p = <.0001). No difference was found between the mean peak EMG amplitude in the muscle groups recorded during the FW condition (p = .5). No differences were found between VPMS measures between FW and NW conditions (p = > .05). No correlational relationship was found between any of local VPMS muscle soreness measures (IP-72 h) and peak EMG muscle amplitude (p = >.05) during the FW and were also found to be the sorest but were still reported averagely as only minimally sore (2.75 ± 1.1).* ***CONCLUSION:*** *The results of this study suggest that EMG peak amplitudes recorded during a FW bout do not relate to reported post-exercise delayed onset muscle soreness (DOMS) and would not be a good predictor of perceived muscular soreness post-FW.*

Mentors

Dr. Daniel Newmire

Assistant Professor
Department of Kinesiology

Dr. Heather E. Webb

Associate Professor
Department of Kinesiology

Introduction

Electromyography (EMG) has been proven as a scientifically valid way of quantifying the amount of muscular activation at a given time. However, despite its validity and growing use, there have been no studies that have examined if the amount of muscular activation determined by EMG analysis correlates with perceived muscular soreness or delayed onset muscle soreness (DOMS). This study will aim to examine if there is any potential relationship.

In recent years, investigations of strongman training have been on the rise. This type of training has been noted for its unique demand that it places on the body to complete the given task. Some of the unique demands that this type of training requires is the stabilization of heavy loads while walking, force production in the horizontal plane, and short intense bouts of physical exertion (Keogh et al., 2010; McGill at al., 2009; Winwood et al., 2014; Winwood et al. 2015; Woulfe et al., 2014; Zemke & Wright, 2011). Most of these studies were examining this style of training because it showed promise of developing better training adaptations that are thought to also be more transferable to sport-specific settings. These findings made strongman training and more specifically the Farmer's Walk (FW) appear to be well suited to create an optimal testing situation for use in this study. However, it is unknown if this typical strongman exercise could be utilized by the general population due to its multifactorial demands.

EMG is an instrument that has been used to assess neuromuscular electrical activity, and is an experimental technique that focuses on the development, recording and analysis of muscle "electric signals" or myoelectricity. Myoelectric signals are formed by physiological variations in the state of muscle fiber membranes. Additionally, EMG directly assesses the myoelectrical activity of muscles during postural tasks, functional movements, work conditions and exercise training protocols (Konrad, 2006).

It has been reported that EMG myoelectrical activity and force values approach a "quasi-linear" relationship, yet there is much variability between populations. Untrained individuals may express higher levels of EMG activity while exerting the same amount of force exerted by someone who is trained (Lawrence & DeLuca, 1983). Additionally, there is variability between muscle groups and there inherent myoelectrical activity and force potential. Essentially, muscle groups with mainly one fiber type tend to have a more linear relationship between force exerted and myoelectrical activity. In muscles of a mixed muscle fiber type (Type I and Type II fibers), the relationship appears to be more curvilinear (Criswell, 2010). Currently, there is limited research assessing myoelectrical activity during the FW and the peak myoelectrical activity. The combination of its uncommon strength demands and high intensity may produce high EMG amplitudes and lead to muscular soreness, which may dissuade the use of this mode of exercise by the general population.

Delayed onset muscle soreness (DOMS) has been described and classified as a type I muscle strain that is often accompanied by stiffness or tenderness with touch or movement (Cheung et al., 2003). DOMS has been known to be caused by unfamiliar and high-force muscular work and more specifically eccentric forces (Cheung et al., 2003). The FW may produce all these factors that are attributed to the development of DOMS due to its unique demands such as force production in the horizontal direction, muscle recruitment patterns, and stabilization requirements (Keogh et al., 2010; McGill at al., 2009; Winwood et al., 2014; Winwood et al. 2015; Woulfe et al., 2014; Zemke & Wright, 2011). The purpose of this study is to investigate if a relationship exists between peak EMG amplitudes recorded during FW bouts and perceived muscle soreness.

Methodology

Participants

The participant population consisted of five subjects (n=5), two of whom were males and the remaining three were females. The average age was 23.72 ± 0.85 years, average height was 168.6 ± 6.21 cm, the average weight was 88.74 ± 14.68 kg. All participants were self-reported as healthy and not having any conditions that could hinder their performance. Additionally, the participants were unaccustomed to the FW exercise.

Instrumentation

This study utilized Surface EMG (DTS EMG, Noraxon U.S.A. Inc., Scottsdale, AZ) to record the myoelectrical activity of the muscles under examination. Disposable, self-adhesive Ag–AgCl pre-gelled disc electrodes (HEX Dual Electrodes, Noraxon U.S.A. Inc., Scottsdale, AZ) were placed on the muscles selected for examination. Signals obtained from these electrodes were sampled at 1500 Hz then filtered and normalized to have peak and mean amplitudes calculated by myoMUSCLE software (myoMUSCLE, Noraxon U.S.A. Inc., Scottsdale, AZ). This study also utilized a visually perceived muscle soreness (VPMS) questionnaire that uses a visual analog scale (VAS) to select a response. The VAS was formatted as a left-to-right slide bar that only allowed whole number answers. The VAS was numbered 0 (no soreness) to 10 (maximal soreness) (Fitzgerald et al., 1991; Lau et al., 2013; Yakut et al., 2003).

Procedures

Initial session

All methods and procedures were approved by the Texas A&M University-Corpus Christi Institutional Review Board (IRB) prior to initial sessions and any data collection. Qualified participants started with the initial session where they were provided with detailed information about the study and what their commitment would be if they decide to continue participating in the study. Once informed consent was obtained, the participant completed a health history questionnaire which was reviewed for any information that would have made it unsafe for the participant to continue in the study. If there were no issues with the provided information, then the participant proceeded to have height, weight, and body composition measures recorded. The height and weight were recorded via a stadiometer and digital scale (SECA model 769, Hamburg, Germany), and their body composition was recorded via dual X-ray absorptiometry (General Electric iDXA). After these measures, the participant then performed a five-minute warm-up on a treadmill before their deadlift one repetition maximum (1RM) testing. The 1RM deadlift testing was performed with a high-handled hex-bar. After the 1RM deadlift was collected, the data collection days were scheduled for the following two weeks. The second data collection day was to be at least one week after the initial session to ensure proper rest and recovery.

Experimental Procedures

Both session two and three occurred within two consecutive weeks to ensure proper rest and recovery was achieved between sessions. In these two sessions, the participants either performed a FW or an unloaded walk. This was determined randomly for each participant on the day of their second session. During both protocols, the participants started by answering a visually perceived muscle soreness (VPMS) questionnaire related to the involved musculature. The questions were answered using a visual analog scale (VAS) which consisted of a left-to-right slide bar in single increments from 0 (no soreness) to 10 (maximal soreness) (Yakut et al., 2003).

Next, the protocol for surface electromyography (sEMG) (DTS EMG, Noraxon U.S.A. Inc., Scottsdale, AZ) began. The participant had disposable, self-adhesive Ag–AgCl pre-gelled disc electrodes (HEX Dual Electrodes, Noraxon U.S.A. Inc., Scottsdale, AZ) placed on the following locations: erector spinae (ES), biceps brachii (BB), upper trapezius (UT), lower trapezius (LT), and the C7 bony prominence (C). Once all the sensors were in place and verified to be transmitting signals, the participant was taken through the maximal voluntary isometric contraction (MVIC) protocol. The MVIC protocol consisted of three sets of contractions for each specific muscle group against an immovable force (Bigland-Ritchie, 1981). The EMG signals were recorded only while contractions were occurring and paused in between each effort. Once this was completed, the participant then performed a five-minute dynamic warm-up on a treadmill. Upon completion of their warm-up, they began either the FW protocol or the unloaded walk protocol.

The FW protocol consisted of ten walks of 20-meters (Winwood et al., 2014) while carrying a high-handled hex-bar loaded with 75% of the participant's 1RM deadlift (ACSM, 2009). The unloaded walk protocol also consisted of ten walks of 20-meters; however, this did not involve any load for the participant to carry. For both protocols, the participant was asked to sit in a chair and rest for 30 seconds after the odd repetitions (e.g. 1,3,5,7,9) and 120 seconds on the even repetitions (e.g. 2,4,6,8,10). EMG data was only recorded during the walking bouts and was started after the participant lifted the load and was stable for the loaded walks. The EMG recording was also stopped as the participants crossed the 20-meter mark for each walk. After the tenth walk for both protocols, the participant was asked to fill out another VPMS questionnaire.

Then the participant had the EMG sensors removed and then completed the final VPMS questionnaire for the session. Once the questionnaire was completed, the session was also completed. The end-time of the session was noted, and the participant was asked to attend recovery sessions for the next three days (24-, 48-, 72-h) at the noted time. Each of the three recovery sessions consisted of the participant completing the VPMS questionnaire.

Electromyography

The placement of these electrodes was determined by the standardized process that follows. The ES location protocol was to place it two finger widths laterally from the spinous process of the first lumbar vertebra. The BB location protocol was to measure the distance from the acromion process to the fossa cubital and placed the electrode 1/3 the distance from the fossa cubital. The UT location protocol was to place the electrode at the 50% point between the C7 bony prominence and the acromion process. The LT placement protocol was to place the electrode at 2/3 the distance from the trigonum spinae to the eighth thoracic vertebra. The protocol for the C7 electrode placement was to place it directly on the bony prominence of the seventh cervical vertebra. Each electrode was placed in the most inline direction with individual muscle fibers. The skin on and around the placement sites was shaved if the participant had any excess hair, abraded using a towel, and cleaned using isopropyl alcohol and allowed to dry prior to any sensor placement. (Konrad, 2006). All raw EMG signals were sampled at 1500Hz then filtered. This was done to ensure that peak and mean amplitudes were obtained while utilizing myoMUSCLE software (myoMUSCLE, Noraxon U.S.A. Inc., Scottsdale, AZ) during MVIC recording and recording of experimental bouts.

Experimental Design and Statistics

SPSS (v26) was used for statistical analyses, with an alpha level of p= < 0.05 used for all statistical tests. Data are presented within the results as Mean ± SEM. A 2 (condition) x 6 (time) RMANOVA was used to evaluate changes in reported muscular soreness (VPMS) across time between the two conditions and between peak EMG amplitude. A one-way ANOVA was used to assess differences between peak EMG amplitude between muscle groups assessed. Finally, a Pearson Product correlation coefficient analysis was performed to examine relationships between EMG peak values for the UT, LT, ES, and BB and reported VPMS values. Figures were fabricated using GraphPad Prism (version 8.0.0 for Mac, GraphPad Software, San Diego, California USA, www.graphpad.com).

Results

Participant Information

The participants in this study had an absolute 1RM deadlift of 120.9 ± 14.70 kg and a 75% 1RM of 90.82 ± 10.98. Other characteristics of the participants are below in Table 1.

Table 1: Participant Characteristics

Variable	Mean ± SEM
Age (y)	23.72 ± 0.85
Height (cm)	168.6 ± 6.21
Weight (kg)	88.74 ± 14.68
Lean Body Mass (kg)	55.56 ± 7.48
Body Fat (%)	32.48 ± 3.57
Absolute 1RM (kg)	120.9 ± 14.70
Relative 1RM (kg/LBM)	2.20 ± 0.09
Actual 75% 1RM (kg)	90.82 ± 10.98

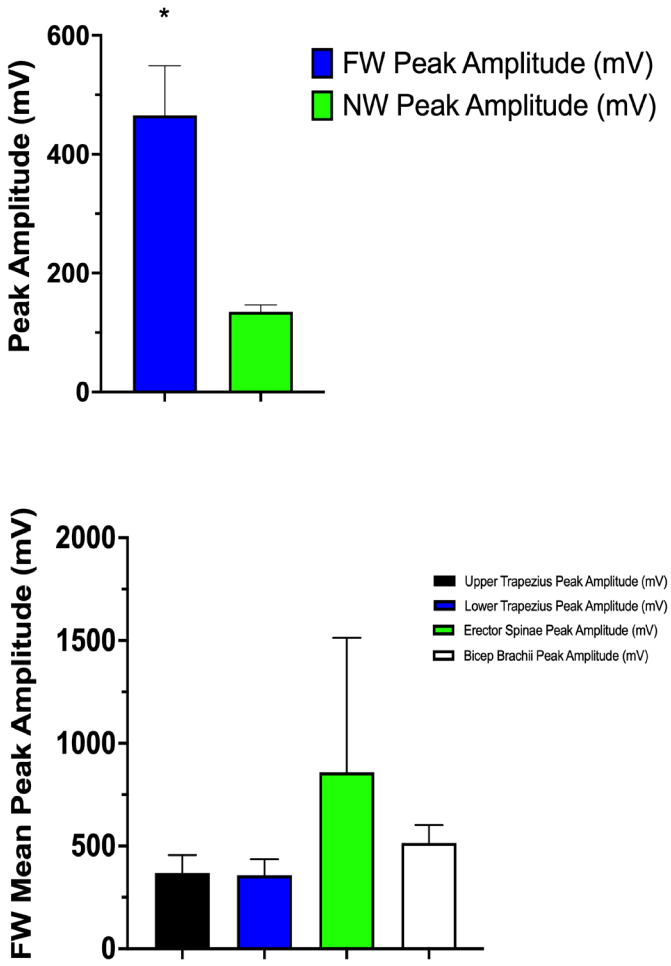

Figure 1: (Mean ± SEM) sEMG Peak Amplitude: A. The mean peak amplitude during the FW was assessed and showed had a greater average mV (465.4 ± 83.5) compared to the NW (134.8 ± 11.91) condition (p = <.0001). **B**. During the FW, no differences were found between mean peak amplitudes and muscle groups (p = .54).

Peak EMG amplitude

Average peak muscle amplitude was used over percent MVIC amplitude because percent MVIC measures in this study were found to be questionable. This was thought to be due to an ineffective MVIC protocol that resulted in poor MVIC measures. It was found that all the examined muscles had higher average peak muscle amplitudes during the FW bouts when compared to the unloaded walking bouts. The muscles with the highest average peak amplitudes during the FW bouts were the ES and BB. For more information on the average peak muscle amplitude see Table 2 below.

	Muscles							
	UT n = 5		LT n = 5		ES n = 5		BB n =5	
Rep	FW	NW	FW	NW	FW	NW	FW	NW
1	0.49 ± 0.09	0.06 ± 0.01	0.28 ± 0.05	0.06 ± 0.02	0.97 ± 0.83	0.36 ± 0.16	0.29 ± 0.05	0.05 ± 0.03
2	0.43 ± 0.07	0.06 ± 0.01	0.32 ± 0.07	0.07 ± 0.01	0.13 ± 0.05	0.41 ± 0.26	0.50 ± 0.10	0.06 ± 0.03
3	0.47 ± 0.09	0.07 ± 0.01	0.35 ± 0.07	0.06 ± 0.02	1.25 ± 1.13	0.52 ± 0.34	0.53 ± 0.07	0.05 ± 0.02
4	0.44 ± 0.08	0.06 ± 0.01	0.35 ± 0.08	0.06 ± 0.01	1.41 ± 1.25	0.34 ± 0.21	0.63 ± 0.17	0.02 ± 0.00
5	0.40 ± 0.07	0.07 ± 0.01	0.31 ± 0.07	0.07 ± 0.01	1.24 ± 1.04	0.54 ± 0.40	0.45 ± 0.08	0.05 ± 0.02
6	0.38 ± 0.06	0.06 ± 0.01	0.37 ± 0.09	0.06 ± 0.01	1.33 ± 1.18	0.24 ± 0.09	0.51 ± 0.06	0.04 ± 0.01
7	0.44 ± 0.07	0.06 ± 0.01	0.38 ± 0.10	0.07 ± 0.02	1.05 ± 0.82	0.50 ± 0.34	0.51 ± 0.08	0.03 ± 0.00
8	0.42 ± 0.07	0.05 ± 0.01	0.41 ± 0.09	0.06 ± 0.02	1.23 ± 0.84	0.21 ± 0.09	0.54 ± 0.14	0.04 ± 0.01
9	0.44 ± 0.07	0.05 ± 0.01	0.35 ± 0.08	0.07 ± 0.02	0.89 ± 0.39	0.12 ± 0.03	0.56 ± 0.10	0.04 ± 0.01
10	0.38 ± 0.06	0.05 ± 0.01	0.40 ± 0.08	0.05 ± 0.01	0.68 ± 0.34	0.21 ± 0.08	0.58 ± 0.12	0.04 ± 0.01

Values represent average peak amplitudes in mV and are presented as Mean ± SEM. FW = Farmer's Walk; NW = Normal Walk; ES = Erector Spinea; BB = Biceps Brachii.

VPMS

The VPMS findings were lower than expected for the FW bouts and this means that the 75% 1RM load for the FW was not enough to cause significant muscular soreness in the participants. The soreness that was indicated by the VPMS data indicated that the participants primarily experienced the most soreness 24 hours after the FW bout but this was only mild soreness. It was also found that the participants found their arms and lower back to be the most sore and these areas peaked in soreness 24 hours after the FW bout. For a graphical representation of the VPMS data see Figure 2.

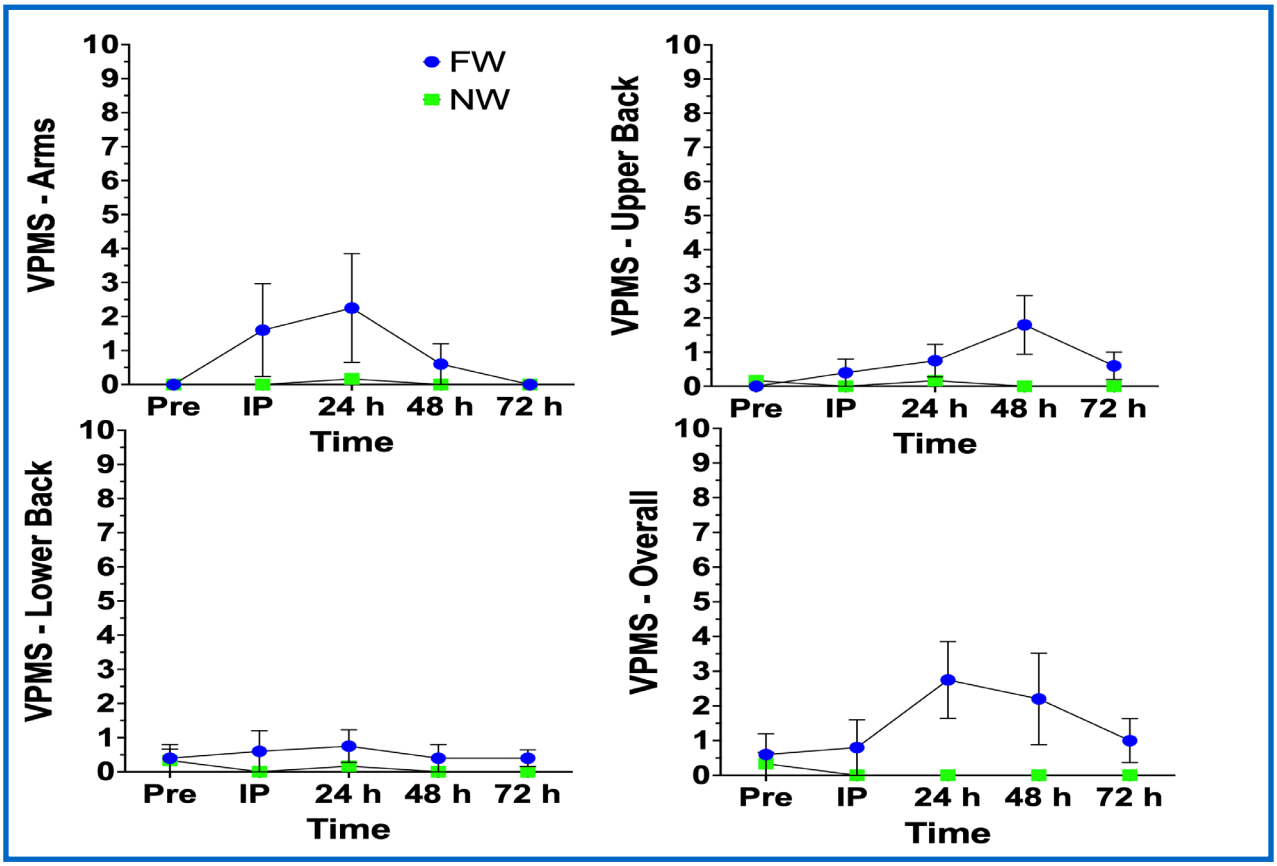

Figure 2 (Mean ± SEM) VPMS Measures: Assessing the effect of the FW on VPMS measures no differences were found (conidition x time). **A.** Arms, no difference found (p = .18); **B.** Upper Back, there was an interaction (p = .004); no differences between condition (p = .06); **C.** Lower Back no differences found (p = .29); **D.** Overall, a interation was found (p = .02); no differences were found between condition (p = .06). Prior to experimental sessions (Pre); Immidiatly post-experimental session (IP); 24-hour recovery session (24-h); 48-hour recovery session (48-h; 72-hour recovery session (72-h).

Peak EMG Amplitude & VPMS

Pearson r correlation coefficient was conducted using the peak amplitude for all repetitions of the FW by the VPMS data for IP, 24-, 48-, and 72-h post-FW bouts. There was no correlation found between peak EMG amplitude and VPMS measures IP, 24-, 48-, and 72-h post-FW in any muscle group assessed (See Figure 2).

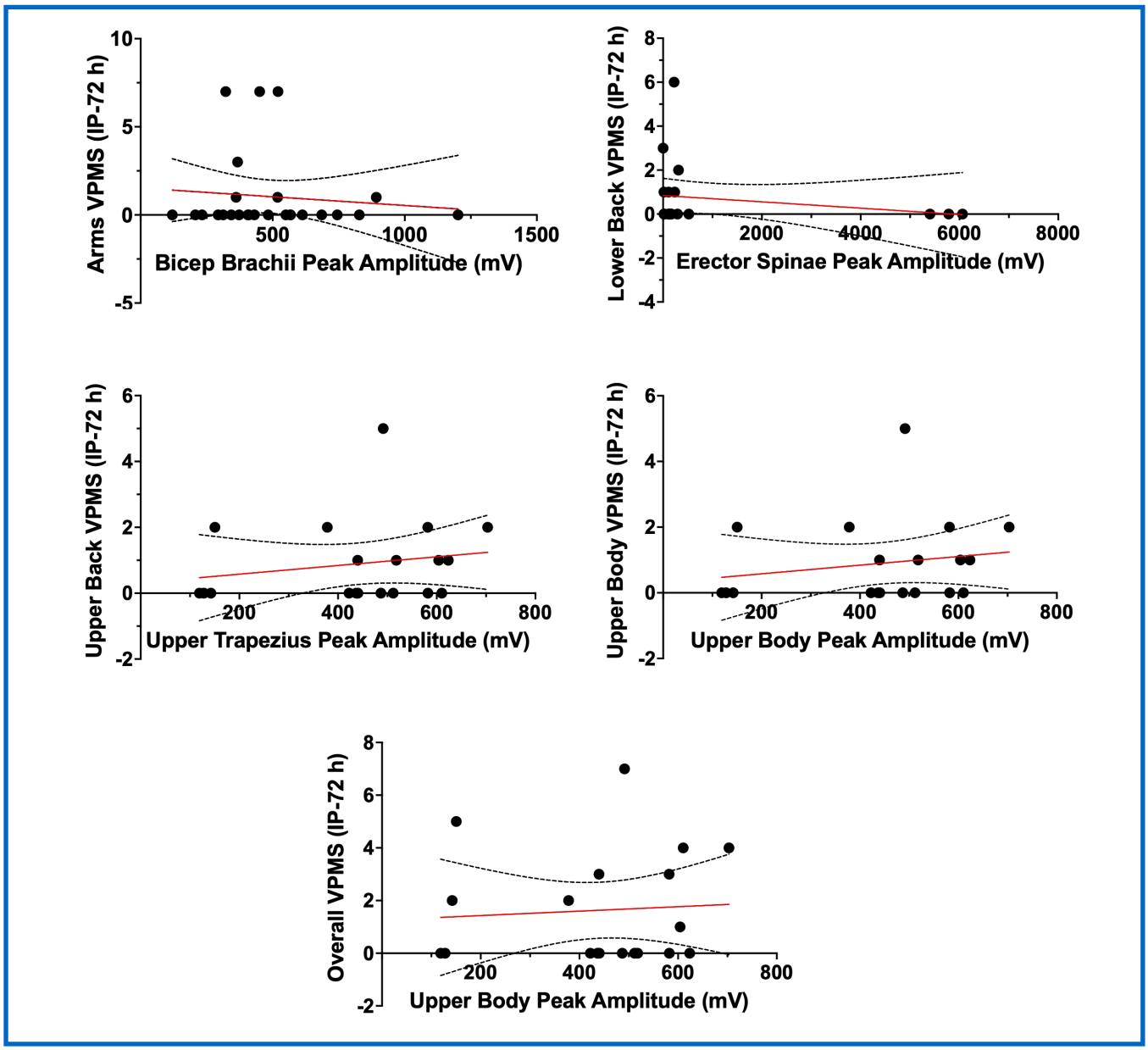

Figure 2: EMG & VPMS Pearson Correlation Coefficient: Comparing local muscular soreness (VPMS) IP-72 h FW exercise. No correlation was found between A. Arms VPMS and Bicep Brachii Peak Ampltiude (r = .01; p = .62); B. Lower Back VPMS and Erector Spinae Peak Amplitude (r = .03; p = .40), C. Upper Body VPMS and Upper Body Peak Amplitude (all four Upper Body EMG locations) (r = .03; p = .4), D. Upper Back VPMS and Upper Trapezius Peak Amplitude (r = .03; p = .4), and E. Overall VPMS (whole body) and Upper Body Peak Amplitude (all four Upper Body EMG locations) (r = .005; p = .7). Prior to experimental sessions (Pre); Immidiatly post-experimental session (IP); 24 hour recovery session (24-h); 48-hour recovery session (48-h; 72-hour recovery session (72 h).

Discussion

The finding for the primary focus of this study was that no correlation was found between peak EMG amplitude and muscular soreness after the FW exercise. This implies that peak EMG amplitude during a FW may not be a good indicator of levels of muscular soreness after the exercise bouts.

Peak EMG amplitudes were found to be highest in the BB and ES muscles during the FW bouts, these muscles were also found to be the "most sore" but this was still deemed minimally sore by the VPMS questionnaire. The highest average score for VPMS was found 24 h post-FW in the overall category (2.75 ± 1.1 out of 10). This may be due to the overestimation of muscle force production due to the influence of fatigue Dideriksen et al. (2010) found that surface EMG amplitude may overestimate muscle force when fatigue was present. So, this refutes the idea that EMG amplitudes may be good predictors of muscular soreness especially when fatigue may be present and thus also refutes the idea that EMG amplitudes may be good predictors of perceived muscular soreness.

It must be noted that there are several limitations to this study that could have influenced the outcomes of this study. First, the low number of participants, which was due to closure of the laboratory following new university policies because of the presence of a global COVID-19 pandemic limited the ability to obtain a greater sample size. Another limitation could have been the difference in training levels of the participants which could have affected their susceptibility to fatigue during the FW bouts. Another notable issue is that the peak muscle amplitude may be variable between participants and a more accurate representation would be normalized peak amplitude to peak maximal voluntary isometric contraction (MVIC) (Bigland-Ritchie, 1981; Konrad, 2006). However, we found error (i.e. ~2000 % of MVIC) in our MVIC protocol where the assumed peak muscle amplitude during MVIC testing may not have been a true representation of the maximal amplitude the participant may have been able to produce. Due to the lack of normalization, our peak amplitude data may be further influenced by variability. It has been suggested that variability may be ~25% from the mean (Criswell, 2010). Further research on this topic should incorporate a way to measure muscular force alongside the use of EMG technology and should utilize a larger sample size. Additionally, other methods should be used to properly assess MVIC to normalize EMG amplitude data to properly express and compare.

Conclusion

In conclusion, this investigation produced results indicating that there was a difference between FW and NW (Control) peak EMG muscle amplitude. But there was no correlational relationship found between any local VPMS muscle soreness measures (IP-72 h) and peak EMG muscle amplitude. This suggests that peak EMG amplitudes do not relate to post-exercise muscle soreness and would not be a good predictor of perceived muscular soreness post FW. These results may have been influenced by the limitations to the study referred to previously, due to these limitations further investigation may be warranted to better investigate this topic.

References

1. American College of Sports Medicine (ACSM). (2009). Progression Models in Resistance Training for Healthy Adults. *Medicine & Science in Sports & Exercise, 41,* 687–708.

2. Bigland-Ritchie, B. (1981). EMG/force Relations and Fatigue of Human Voluntary Contractions. *Exercise and Sport Sciences Reviews, 9*, 75–117.

3. Cheung, K., Hume, P. A., & Maxwell, L. (2003). Delayed Onset Muscle Soreness. *Sports Medicine, 33,* 145–164.

4. Criswell, E. (2010). Cram's Introduction to Surface Electromyography. Jones & Bartlett Publishers.

5. Dideriksen, J. L., Farina, D., & Enoka, R. M. (2010). Influence of Fatigue on the Simulated Relation Between the Amplitude of the Surface Electromyogram and Muscle Force. Philosophical Transactions of the Royal Society A: Mathematical, *Physical and Engineering Sciences, 368*(1920), 2765-2781.

6. Fitzgerald, G. K., Rothstein, J. M., Mayhew, T. P., & Lamb, R. L. (1991). Exercise-induced Muscle Soreness After Concentric and Eccentric Isokinetic Contractions. *Physical therapy, 71*, 505-513.

7. Keogh, J. W. L., Payne, A. L., Anderson, B. B., & Atkins, P. J. (2010). A Brief Description of the Biomechanics and Physiology of a Strongman Event: The Tire Flip. *Journal of Strength and Conditioning Research, 24*, 1223–1228.

8. Konrad , P. (2006). Abc of Emg – A Practical Introduction to Kinesiological Electromyography . Noraxon INC. USA.

9. Lawrence, J. H., & De Luca, C. J. (1983). Myoelectric Signal Versus Force Relationship in Different Human Muscles. *Journal of applied physiology: respiratory, environmental and exercise physiology, 54*(6), 1653–1659. https://doi.org/10.1152/jappl.1983.54.6.1653

10. Lau, W. Y., Muthalib, M., & Nosaka, K. (2013). Visual Analog Scale and Pressure Pain Threshold for Delayed Onset Muscle Soreness Assessment. *Journal of Musculoskeletal Pain, 21*, 320-326.

11. McGill, S. M., Mcdermott, A., & Fenwick, C. M. (2009). Comparison of Different Strongman Events: Trunk Muscle Activation and Lumbar Spine Motion, Load, and Stiffness. *Journal of Strength and Conditioning Research, 23*, 1148–1161.

12. Winwood, P. W., Cronin, J. B., Brown, S. R., & Keogh, J. W. L. (2014). A Biomechanical Analysis of the Farmers Walk, and Comparison with the Deadlift and Unloaded Walk. *International Journal of Sports Science & Coaching, 9*, 1127–1143.

13. Winwood, P. W., Cronin, J. B., Posthumus, L. R., Finlayson, S. J., Gill, N. D., & Keogh, J. W. (2015). Strongman vs. Traditional Resistance Training Effects on Muscular Function and Performance. *Journal of Strength and Conditioning Research, 29*, 429–439.

14. Woulfe, C., Harris, N., Keogh, J., & Wood, M. (2014). The Physiology of Strongman Training. *Strength and Conditioning Journal, 36*, 84–95.

15. Yakut, E., Bayar, B., Meriç, A., Bayar, K., & Yakut, Y. (2003). Reliability and Validity of Reverse Visual Analog Scale (Right to Left) in Different Intensity of Pain. *The Pain Clinic, 15*, 1–6.

16. Zemke, B., & Wright, G. (2011). The Use of Strongman Type Implements and Training to Increase Sport Performance in Collegiate Athletes. *Strength and Conditioning Journal, 33*, 1–7.

Temporal Changes in the Radiogenic Signature of Shallow Groundwater and its Potential Implications in the SGD Estimates in a Semiarid Area

by: Loren Walker

Abstract

Interactions between groundwater and surface water occur at a range of spatial and temporal scales and are highly variable depending on meteorological, fluvial, geological, and anthropogenic processes. Submarine groundwater discharge (SGD) may constitute an ecologically significant source of nutrients, heavy metals, radionuclides, and organic compounds originating from aquifers or bottom sediment which contribute to surface water quality degradation. Thus, an improved understanding of SGD rates into coastal systems and corresponding groundwater solute fluxes is necessary to develop comprehensive biogeochemical budgets and management practices. Quantification of groundwater fluxes is difficult due to the inherent logistical complications of measuring a dispersed flux of water and the significant spatial and temporal heterogeneity of groundwater inputs. Commonly used geochemical tracer mass balances, like those of radium (Ra) and radon (Rn), have varying spatial and temporal integration scales and large estimation errors associated with endmember selection to consider in the final SGD estimates. This study seeks to evaluate the temporal changes in the radiogenic signature of shallow groundwater that will help inform SGD mass balance estimates. This study indicates that radioactive isotope signatures vary by 1 to 3 orders of magnitude and are not always correlated with changes in salinity. The most significant radioactive isotope activities response to changes in salinity radium were found in the marine island environment in the deeper formation which is in direct hydrogeologic connection with Corpus Christi Bay. In the river flood plain environment, radioactive tracer activities show different responses to climatic conditions and relationship to surface water bodies for the two locations. Thus, since groundwater characteristics of tracer isotopes are observed to change monthly with magnitudes that differ among environments, SGD mass balances should carefully consider a variable groundwater endmember.

Mentor

Dr. Dorina Murgulet

Associate Professor of Hydrogeology

Department of Physical and Environmental Sciences

Introduction

The discharge of groundwaters to coastal waters is of significant environmental importance. Groundwater supplies much of the water used for human consumption in the U.S. (Dieter et al., 2015), and it is now identified as a significant source of nutrient to surface waters. Excess nutrient inputs from groundwater could result in ecological impacts such as harmful algal blooms, which lead to anoxic waters that harm aquatic life. Although, changes in the chemistry of surface waters such as decreasing salinity due to fresh groundwater inputs have positive effects on the ecosystem health like oyster reefs, the timing and location of some nutrient-reach inputs may have adverse impacts on the health of estuaries.

Fluxes of nutrients and other solutes from submarine groundwater discharge (SGD) have been studied extensively to determine their importance within that nutrient/tracer's inventory and the overall effect on ecosystem health (Burnett, et al., 2008; Buesseler, et al., 1999; Cho, et al., 2016). To estimate SGD, studies have employed a variety of techniques among which are the use of radiogenic isotopes like radon and radium. For geochemical tracer studies, to determine the advective fluxes of groundwater and the associated solute inputs, a groundwater endmember must be identified. The location of the endmember is usually evaluated based on the direction/path of groundwater flow in relation to the surface water body. However, near the coast, interactions between surface water and groundwater become more convoluted and selection of an appropriate endmember becomes difficult. For instance, subsurface heterogeneity can cause spatial differences in aquifer recharge, seawater recirculation, and SGD rates. In addition, tidal pumping induced exchange between groundwater and surface water with no net loss/gain of water may cause changes in the water chemistry within the nearby aquifer, subterranean estuary and porewater. As a result of changes in salinity or redox conditions, activities of radium and nutrients could vary both spatially and temporally. For instance, saline waters entering fresh aquifers are expected to cause significant radium desorption and increase in activities and may induce biogeochemical changes (Burnett and Dulaiova, 2003). Thus, the assumption of a constant endmember could misrepresent the true flux of SGD and associated solute fluxes.

This study is the first to our knowledge to monitor monthly changes in geochemical characteristics of shallow groundwater for over a year. Hydrologic parameters and water samples have been collected monthly from two locations: Ward Island, by the University Beach and along downstream Nueces River. Hydroparameters included groundwater levels, salinity, dissolved oxygen, and pH. Samples were analyzed for radon (222Rn) and radium (223Ra, 224Ra, and 226Ra). The results of this study may serve as a starting point for constraining temporal changes of groundwater endmembers and implications on estimates of SGD and solute fluxes.

Background

Groundwater, which collects in the subsurface within the pore spaces and fractures of soil, sediments or rock materials, is a major source of freshwater around the world. (U.S. Geological Survey, n.d. -a). Groundwater levels, in particular in unconfined shallow aquifers, fluctuate both seasonally and annually as a result of hydroclimatic conditions (e.g., precipitation and aquifer recharge) and human activity (e.g., pumping, channels, etc.) (Yan et al., 2015). Wherever there is a hydrologic connection between an aquifer, or the water producing geologic formation, and surface water bodies, groundwater-surface water interaction occurs. For instance, unconfined or water table aquifers are generally in direct connection with rivers and streams, yet estuaries and groundwater discharge occur at different rates.

Human activities may halt, increase, or decrease the flow of groundwater to the sea by altering the hydrologic gradient, the change in water level between groundwater and surface water. Locally, natural hydraulic gradients can also be altered by heterogenous subsurface sediments and structural differences (U.S. Geological Survey, 2016).

Naturally occurring geochemical tracers are used as indicators of groundwater movement and for quantification of groundwater discharge rates to surface water bodies. Radioactive elements of uranium and thorium, for instance, are naturally occurring in some rocks and soils, and are eventually introduced into groundwater through water-rock interaction reactions. Within their decay chains are the unstable, metallic isotopes 224Ra, 223Ra, 226Ra, in order of least to greatest half-life (3.6 and 11.4 days and 1,600 years), as well as the short-lived, gaseous isotope 222Rn (3.8 days). These daughter products enter surface waters generally via groundwater discharge, thus enable observation of changes in subterranean terrestrial and recirculated (seawater) inputs. When using radium tracers to observe groundwater movement, other parameters such as salinity, pH, and redox characteristics have to be observed, as these greatly affect radium solubility in water and desorption from sediments. For instance, salinities of approximately 20 ppm (parts per million – 1 milligram of TDS per liter of water) result in the highest levels of radium desorption from sediments, increasing their activities in the water. At salinities less than 10 ppm, radium tends to bind to sediments because of chemical bonding, decreasing water activities (Webster et al., 1995). Higher pH values (indicating alkaline waters) are associated with lower radium activities and vice versa, thus high salinities and more acidic conditions are ideal for radium desorption (Vienna: International Atomic Energy Agency, 2014).

Groundwater in general has low salinities and moderate pH (5.5 to 9) while rivers and lakes typically have neutral pH levels and low salinities and estuaries have neutral pH and higher salinities (USGS.gov). While more saline waters such as seawater, bays, and estuaries are likely to have higher rates of desorption, they are depleted in radium unless groundwater inputs exist (The Water Quality Association, 2013).

Methods

Study Area

Water samples were collected on a monthly basis beginning with June 2018 until December 2019 at three locations from piezometer pairs consisting of one shallow and one deeper monitoring well. Sampling locations are within the Beaumont Formation, a Quaternary alluvial deposit composed of silty clay. The Beaumont Formation is characterized by alluvial and marine sediments deposited under fluctuating sea levels. The area is low relief and soils are well developed (National Cooperative Soil Survey, 2010). Predominant are clayey soils, which experience significant shrink and swell associated with changes in water saturation (precipitation) and climate conditions (Ito, 2010).

Two of the three locations are within the Nueces River flood plain, Hazel Bazemore Park (Figure 1), just to the east side of Nueces River and in proximity to Corpus Christi Bay. The Nueces River Basin encompasses approximately 4.4 x 1010 square meters within the southern part of Texas and drains into the Gulf of Mexico. One of the piezometer pairs is meters inland of the riverbank (W3 and W4) and the other is further inland in proximity to an evaporation pond (W1 and W2).

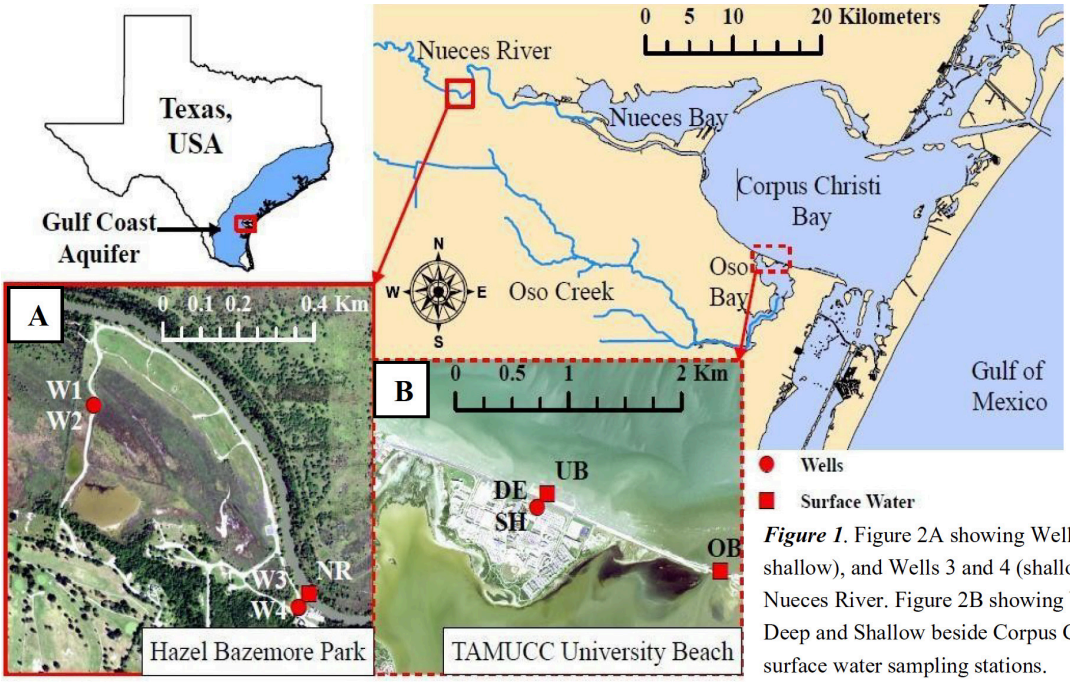

Figure 1. Figure 2A showing Wells 1 and 2 (deep, shallow), and Wells 3 and 4 (shallow, deep), beside Nueces River. Figure 2B showing Ward Island, Wells Deep and Shallow beside Corpus Christi Bay. Adjacent surface water sampling stations.

The former area is frequently inundated during wet periods and subsequently experiences periods of extreme drying evidenced by the presence of deep mud cracks. Piezometers W1 and W2 are 6.7 and 2.6 meters deep, respectively, while W3 and W4 are 3 and 7 m, respectively. These wells represent a fresh, riverine environment. The third pair of piezometers is located ~61 m from the Corpus Christi Bay shoreline, on University Beach, Ward Island. Denoted as DE for the deep well and SH for the shallow, these two wells reach a depth of 5.8 and 12.8 meters respectively and represent a marine or island environment.

Data Collection and Processing

Groundwater depth was measured at each well using a pre-labeled "steel tape". A Yellow Springs Instrument (YSI), a commonly used professional grade water quality meter, was used to measure field parameters such as pH, temperature, pressure, dissolved oxygen and oxidation reduction potential, specific conductance, and salinity before sample collection. Water was pumped through a flow-through cell connected to the YSI until readings stabilized. All sampling containers were previously sterilized using standard lab procedures and rinsed three times with the sample water prior to collection. Bottles were overfilled with groundwater pumped through sterile tubing, capped, and placed on ice to prevent biogechemical changes or degassing.

Approximately 8 L of sample was collected from each well for radium measurements. In the laboratory, filtered samples were processed through ~15g fluffed manganese dioxide, MnO2, impregnated acrylic fibers twice at a rate of <1 L/min (Dimova et al., 2007; Kim et al., 2001). Mn-fibers were than rinsed with Ra-free water, to eliminate salts or particulates, and then pressed to a water to fiber ratio of 0.3-1g (i.e., 20-30 g wet weight) (Sun and Torgersen, 1998). The fibers were placed in gas-tight cartridges and tested for ^{223}Ra and ^{224}Ra on a Radium Delayed Coincidence Counter (RaDeCC), which were done within three days of collection (Moore, 2006).

For ^{226}Ra measurements, fibers were flushed with nitrogen gas and sealed for >21days to reach secular equilibrium before they were run on a RAD-7 with measurements corrected to a calibration curve determined from 5 standards.

Radon water samples are collected in 250 mL glass bottles and measured using a Durridge RAD-7 radon-in-air monitor and the RAD AQUA accessory. The RAD AQUA is used to bring the radon concentration in a closed air loop into equilibrium with the radon concentration in a flow-through water supply. A detailed description of RAD-7 capabilities and measurement principles can be found in (Burnett and Dulaiova, 2003).

Data analyses was conducted using cross plots and time series graphs in addition to correlation analyses.

Results and Discussion

Overall salinities in the riverbank and nearby evaporation pond wells ranged from 2 to 27 ppt, with a mean of 9 ppt. Riverbank well salinities (Wells 3 and 4) did not exceed 10, while the evaporation pond well (Wells 1 and 2) salinities were greater than 10, except for in January 2019 when salinities were ~3. Well 2, shallow, consistently had much higher salinities than all other wells. Values for pH ranged from 5.6 to 8.9 with a mean of 6.95. No conclusive seasonal (monthly) trends were observed for pH in relation to precipitation volumes or elevations.

Groundwater elevations ranged from 0.69 meters to 3.35 meters overall. Water levels in the evaporation pond wells were more related than in the riverside wells, with correlation factors of 0.40 and 0.27 respectively. Evaporation pond wells (1 and 2) averaged a groundwater elevation of 1.61, while the shallow riverbank well (3) averaged 2.68 and its deep counterpart (4) averaged 2.91 meters.

Groundwater levels in the deeper riverbank well are mostly consistent when compared to other three riverside wells. Water levels for all wells decreased following the heaviest precipitation event of the sampling period except for Well 4.

Changes in water level do not appear to be solely affected by local watershed precipitation nor did there appear to be a seasonal trend associated with changes in groundwater elevation (Figure 2). Activities of 223Ra ranged from 89.5 disintegrations per minute per cubic meter (dpm/m3) to an 2,072 dpm/m3, with a mean of 484 dpm/m3. Activities of 224Ra ranged from 1,789 to 26,281 dpm/m3, with a mean of 6,645 dpm/m3 (Figure 3). Radon ranged from 370 to 511,470 dpm/m3 with a mean of 99,507 dpm/m3 and a few outliers in the hundreds. Radon decreased signifantly from the previous year in all wells to an all time low at the end of the sampling period for Wells 1, 2, and 4; these were the outliers in the hundreds, while Well 3 had ~12,000 dpm/m3 in the same time period.

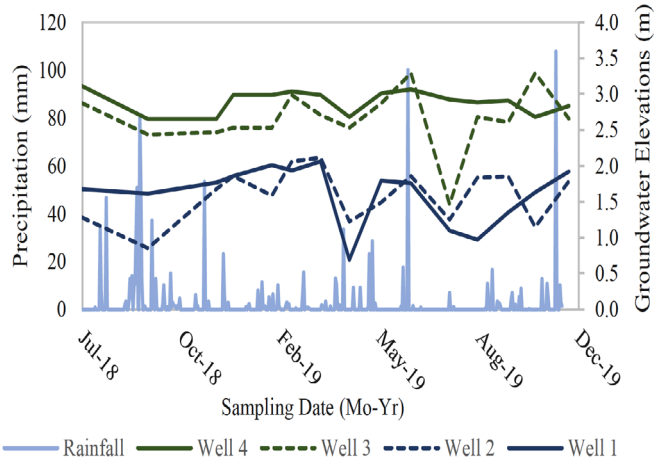

Figure 2. Precipitation depths for the Nueces estuary from April 2018 to October 2019 (USC00417677), plotted with groundwater elevations (m above mean sea level) for the four riverside wells.

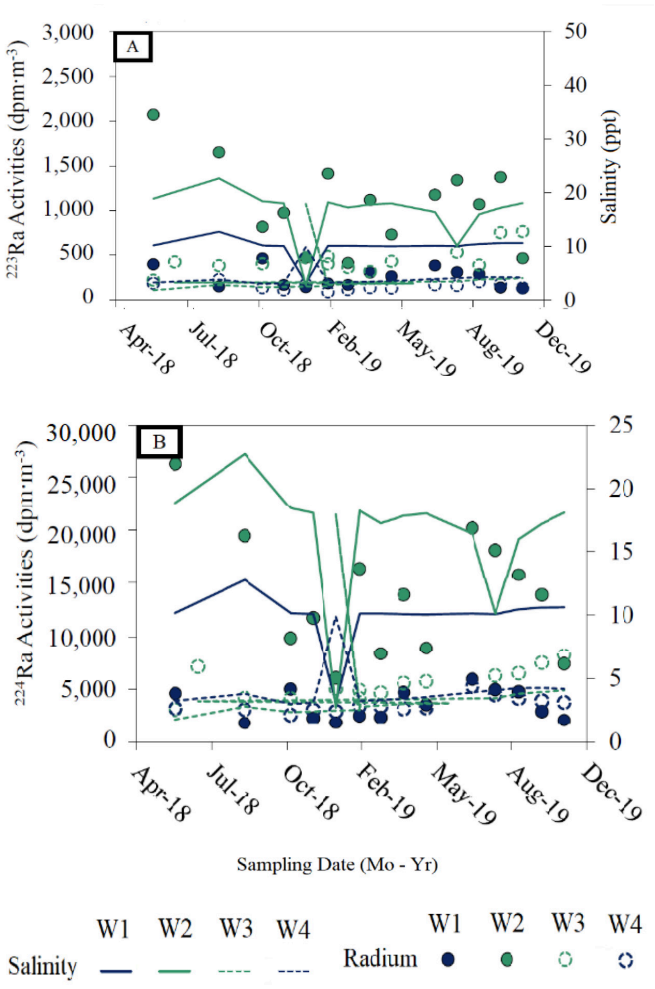

Figure 3. ^{223}Ra (**A**) and ^{224}Ra (**B**) activities and salinity over time for the riverside wells.

In the marine (island) environment wells, salinities ranged from 0.11 to 43.3 ppt overall, with a mean of 17.1 ppt. These wells are much deeper than the riverside wells, reaching a maximum depth of 12.8 meters compared to 6.7 for the riverside wells. Shallow well salinities were low, ranging from 0.16 to 11 ppt, with a mean of 4.3 ppt. Deep well salinities were significantly higher, ranging from 0.11 to 43.3 ppt, with a mean of 29.1 ppt. Values for pH ranged from 6.3 to 7.5 overall, with a mean median of 6.9. There did not appear to be a seasonal trend, though the deep well had a higher average pH of 7.0 compared to 6.8 in the shallow well.

Groundwater elevations were similar for both the deep and shallow marine wells, ranging from 0.61 meters to 1.83. The shallow well saw higher groundwater elevations overall, with a mean of 1.1 meters. The deep well averaged 0.93 meters. Groundwater elevations in the shallow well were highest in the fall months of October and November, reaching the maximum of 1.83 meters. Groundwater elevations for the deep well were not as consistent but also saw their highest elevations in the months of October and November. There did not appear to be a trend associated with local precipitation.

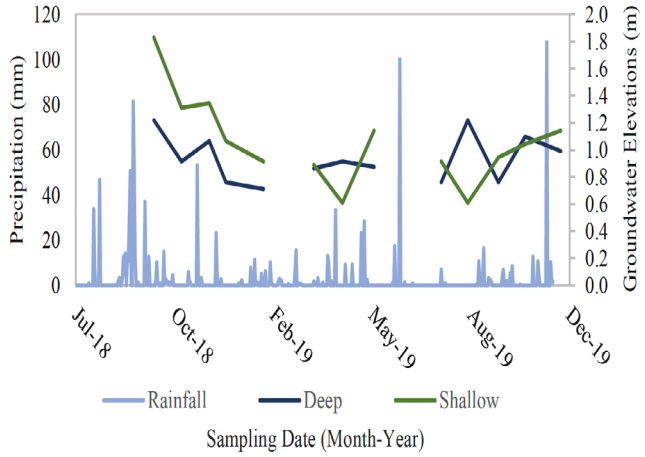

Figure 4. Precipitation depths (mm) with groundwater elevations (m above mean sea level) for the marine environment wells (deep and shallow).

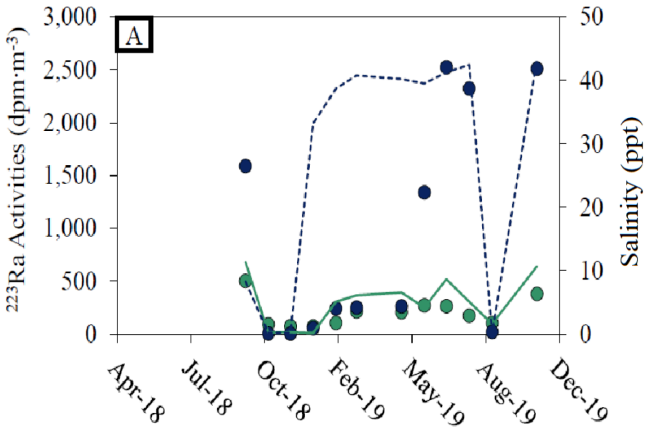

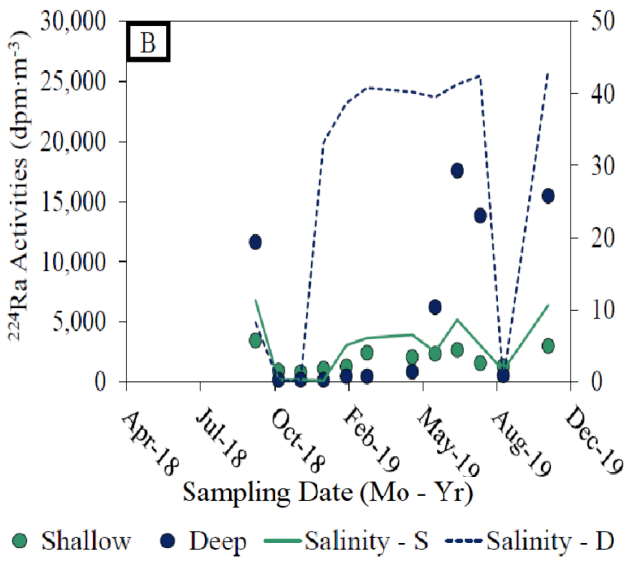

Figure 5. ^{223}Ra (**A**) and ^{224}Ra (**B**) activities and salinity for the deep and shallow marine/island environments

Lower radium and radon activities were measured in the island environment, despite of higher salinities overall. Activities of ^{223}Ra ranged between 5 to 2,524 dpm/m3, with a mean of 520 dpm/m3. Activities of ^{224}Ra ranged from 4.6 to 2,524 dpm/m3, with a mean of 3,427 dpm/m3 (**Figure 5**). Radon ranged from 124 to 129,250 dpm/m3 with a mean of 32,195 dpm/m3 .

In the island environment, a clear difference in radiogenic signature is observed between wells, which is consistent with degrees of salinity changes (**Figure 5**). This indicates that the two formations receive recharge and have separate hydrologic connections with the bay. Th shallow formation responds to precipitation events as indicated by lower and dropping salinity levels following rain events. Either salt-water intrusion or recirculation caused by tidal influence is visible both wells, but to a larger degree in the deeper well (**Figure 6**).

Overall more dramatic changes are observed in the deeper formation, as well as extremely high salinities and variations in radiogenic signatures. High salinities are expected to be associated with higher radium activities. This trend was generally observed throughout 2019 when lower precipitation volumes occurred (**Figure 4, 5**). However, between December 2018 and March 2019 when the lowest precipitation volumes were recorded, the deep and shallow formations displayed different responses, with the deeper greatly increasing in salinity despite radium activities remaining low until spiking later in the year. The shallow formation radium activities remained mostly constant, with high salinities accompanied by higher activities as expected. While there was an increase in salinity in the shallow well, it's an order of magnitude higher in the deep well where the salinity spike occurs sooner. Visually, no significant trends between radium isotopes and salinity exist for the two formations, though inverse correlations between salinity and the ^{224}Ra: ^{223}Ra activity ratios for the marine environment are obvious (**see Figure 7**).

In the river environment, there is a clear distinction between wells in terms of salinity and radium activities (**Figure 5**). Wells 3 (shallow) and 4 (deep), beside the river, have very low salinities while Wells 1 (deep) and 2 (shallow), near the evaporation pond, have much higher salinities. The riverbank Well 3 seemed unaffected by an event which affected both evaporation pond wells as well as the riverbank deep well. However, this well has much higher and more varied radium activities when compared to its deep counterpart in the flood plain environment. Each well is injected into different hydrostatic units and may receive recharge from precipitation, groundwater interaction with surface water sources (i.e., river and evaporation pond), or interaction with an adjacent aquifer, while a change in gradient may increase radium activities by causing groundwater movement. With an increase in precipitation in May 2019, radium activities went up in all wells. However, activities in shallow riverbank well continued to increase as all other wells displayed a decreasing trend after the rain event.

This indicates that both deeper formations in the two environments and the shallow one next to the evaporation pond respond to precipitation and recharge leading to lower radium activities. On the other hand, the shallow nearby river formation may be receiving recharge in the form of groundwater migration, which could explain the increase in activities following a rain event. The evaporation pond site shows the highest degree of variability in terms of salinity and radiogenic changes. In December 2018, groundwater in the wells next to the evaporation pond became nearly fresh, with salinities dropping below 5 and were accompanied by a drop in radium activities. The shallow pond well generally follows a similar trend to the deep but with much higher salinities and radium activities.

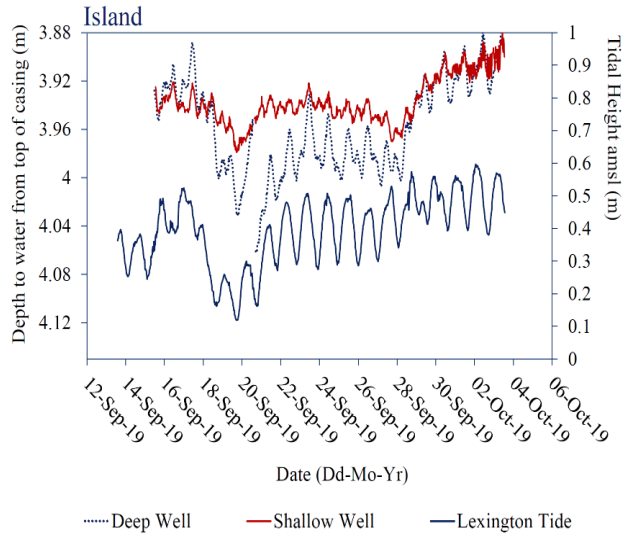

^{224}Ra activities were much higher than ^{223}Ra for all environments, as indicated by the ^{223}Ra/^{223}Ra activity ratios (AR) (**Figure 7**). For the river plain, both the deep and shallow wells showed no relationship between salinity and AR. Here, shallow groundwater signature seems to be influenced by nearby surface/river water. The deeper groundwater has a distinct signature, and only randomly shows some possible surface water influence (**Figure 7A**).

Radon also does not show any relationship with salinity, which is not surprising since radon is not salinity dependent but could change as aquifers receive recharge of fresher or saltier water (**Figure 7B**). Contrary to the river plain environment, a strong negative relationship is observed at the University Beach between salinity and AR (**Figure 7C**). The relationship is the strongest for the deeper formation, which indicates a direct connection with the Corpus Christi Bay. Salinities also indicate a marine influence, although other influences exist given the higher than seawater salinity levels observed at this horizon. In addition, surface water AR also confirmed the marine influence when the salinity-AR relationship is considered. The shallow water table characteristics, although change with salinity, do not show a marine influence.

Changes in water level or "groundwater elevation" between shallow and deep aquifers follow roughly the same trend in the river plain and are not correlated with either AR or radon (**Figure 7D, 7E**). An increase in groundwater level in this environment could be related to aquifer recharge, which, if associated with recent rain events, would be expected to dilute the radiogenic signatures. This would result in a negative correlation between radon and groundwater level, for instance. The island environment shows a negative correlation between the shallow formation water levels and AR, which is not found for the deeper formation. The shallow formation trend also corresponds with freshening (**Figure 7**).

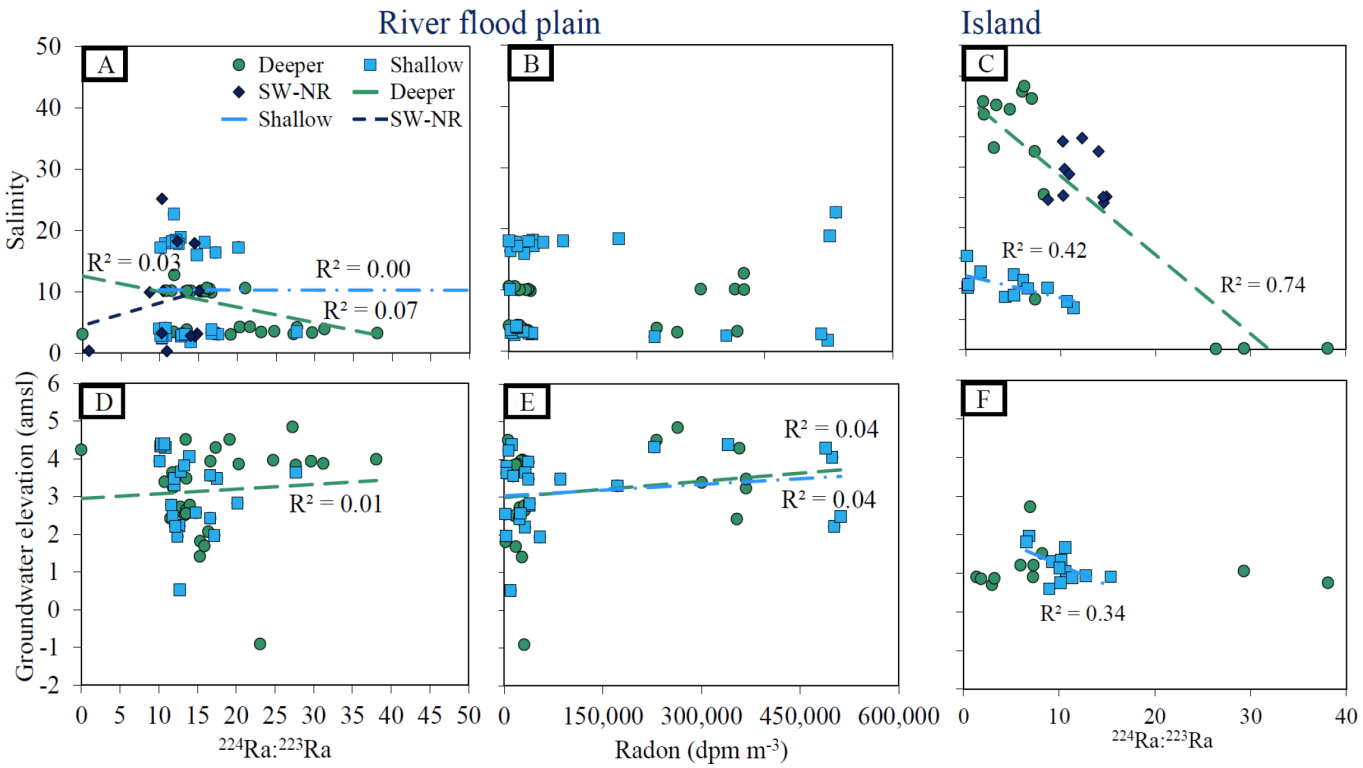

Figure 7. Hazel Bazemore Park wells and Nueces River Data. Figures (**7C, 7F**) display University Beach and Oso Bay surface water, University Well data. (**7A**) displays the ratio of ^{224}Ra:^{223}Ra vs Salinity. (**7B**) Radon activity vs salinity. (**7C**) ^{224}Ra:^{223} Ra vs Salinity ratio for University Beach surface water, and deep and shallow wells. (**7E**) Radon activity vs groundwater elevation (amsl) showing a weak positive correlation. (7**F**) Ratio of ^{224}Ra:^{223}Ra show a negative correlation for the shallow well.

Conclusion

Based on a preliminary evaluation of relationships between the short-lived isotopes and salinity, the following trends are observed: (1) overall radiogenic signatures vary by 1 to 3 orders of magnitude during the investigated period but are not always correlated with changes in salinity; (2) the most significant changes in radium activities as a function of salinity are found in the marine island environment in the deeper formation likely caused by the intrusion of radium depleted seawater; (3) changes with time at the river flood plain environment are different at the 2 locations with significant input of higher salinity and radium activity waters at the well pair near the evaporation pond, in the shallow formation.

The riverine influence is likely observed at the well pair located near the river where low salinity and radium activities were consistently measured in both shallow and deep formations. Large changes in radium activities are observed with time at all locations, in particular in the deep well in the nearshore island environment and in the shallow well near the evaporation pond. Since these two locations are also subject to major changes in salinities, the radium signature is also expected to fluctuate. Thus, an assumption of a constant groundwater endmember for estimation of advective groundwater fluxes to bays or rivers in semiarid areas is likely erroneous, leading to large errors.

Acknowledgements

A heartfelt thanks to the Center for Water Supply Studies and the hydrology team, Dr. Dorina Murgulet, Dr. Audrey Douglas, Cody Lopez and Will Wolfe. Thank you all for your abundance of guidance, granting me the opportunity to learn valuable skills and technical knowledge, to grow beyond what I thought possible, and to contribute to a better world for all through the study of Earth's most precious resource. Special thanks to the Corpus Christi section of the national McNair Scholars Program for encouraging me to exceed my own expectations, for believing in my success, and for providing myself and other atypical students a wealth of experiences that will drive future endeavors in academia and in life. Thank you Texas A&M University – Corpus Christi faculty and staff. I am forever grateful, proud, and delighted to be a TAMU-CC alumni, a great school that cares for its students academically and spiritually. Thank you all for giving myself and my fellow TAMU-CC students every opportunity to succeed. Islander pride!

References

Buesseler, K., Harvey, C. (1999, Sept. 30). *Investigating Contaminant Inputs via Submarine Groundwater Discharge to Coastal Waters Using Radium Isotopes.* Woods Hole Oceanographic Institution, Massachusetts Institute of Technology.

Burnett, W.C., Dulaiova, H. (2003) Estimating the dynamics of groundwater input into the coastal zone via continuous radon-222 measurements. *Journal of Environmental Radioactivity 69*, 21-35.

Burnett, William C., et al. (2008). Radon and Radium Isotopes as Tracers of Submarine Groundwater Discharge – Results from the Ubatuba, Brazil SGD Assessment Intercomparison. Estuarine, *Coastal and Shelf Science 76* (3), 501–511.

Cho, Hyung-Mi, and Guebuem Kim. (2016). Determining Groundwater Ra End-Member Values for the Estimation of the Magnitude of Submarine Groundwater Discharge Using Ra Isotope Tracers. *Geophysical Research Letters 43* (8), 3865–3871.

Dieter, C.A., Maupin, M.A., Caldwell, R.R., Harris, M.A., Ivahnenko, T.I., Lovelace, J.K., Barber, N.L., and Linsey, K.S. (2018). Estimated use of water in the United States in 2015. *U.S. Geological Survey Circular 1441* (65). Retrieved from https://doi.org/10.3133/cir1441.

Dimova, N., Burnett, W.C., Horwitz, E.P., Lane-Smith, D. (2007) Automated measurement of Ra-224 and Ra-226 in water. *Applied Radiation and Isotopes 65*, 428-434.

Victor & Brugnera, R. & Zuzel, G. (2016). Limits on uranium and thorium bulk content in GERDA Phase I detectors. Astroparticle Physics 91.

Hyung-Mi, C., and Guebuem, K. (2016). Determining groundwater Ra end-member values for the estimation of the magnitude of submarine groundwater discharge using Ra isotope tracers. *Geophysical Research Letters 43* (8).

Ito, M., Azam, S. (2010). Determination of Swelling and Shrinkage Properties of Undisturbed Expansive Soils. *Geotechnical and Geological Engineering 28*, 413-422.

Jing-yan, G., Xue-jing, W., Yan, Z., and Hailong, L. (2018). Estimating submarine groundwater discharge and associated nutrient inputs into Daya Bay during spring using radium isotopes. *Water Science and Engineering 11* (2), 120-130.

Kim, G., Burnett, W.C., Dulaiova, H., Swarzenski, P.W., Moore, W.S. (2001) Measurement of Ra-224 and Ra-226 activities in natural waters using a radon-in-air monitor. *Environmental Science & Technology 35*, 4680-4683.

Kontar, Y. Korotenko, K., Santiago, V. (2014). Assessment and Modeling of Dispersal Contamination Incoming with Submarine Groundwater Discharge (SGD) in Tsunami Affected Coastal Areas. *Tsunami Events and Lessons Learned* 55-88.

Lecher, Alanna, and Mackey, Katherine. (2018). Synthesizing the Effects of Submarine Groundwater Discharge on Marine Biota. *Hydrology 5* (60).

Lopez, C.*, Murgulet, D., Douglas, A*, and Murgulet, V. (2018). Evaluating Groundwater Inflow and Nutrient Transport to Texas Coastal Embayments, Phase III (Baffin Bay). Scientific report submitted to Texas General Land Office GLO Contract No. 16-060-000-9104 (105).

Mulligan, A., and Charette, M. (2006). Intercomparison of Submarine Groundwater Discharge Estimates from a Sandy Unconfined Aquifer. *Journal of Hydrology 327*, 3-4, 411–425.

Moore, W.S. (2006) Radium isotopes as tracers of submarine groundwater discharge in Sicily. *Continental Shelf Research 26*, 852-861.

National Cooperative Soil Survey, USA. (2010). "Beaumont Series." Keys to Soil Taxonomy, Eleventh Edition. Retrieved from https://soilseries.sc.egov.usda.gov/OSD_Docs/B/BEAUMONT.html

Sun, Y., Torgersen, T. (1998). The effects of water content and Mn-fiber surface conditions on Ra-224 measurement by Rn-220 emanation. *Marine Chemistry 62*(299-306).

U.S. Geological Survey. (n.d. -a). What is Groundwater? Retrieved from https://www.usgs.gov/faqs/what-groundwater?qt-news_science_products=0#qt-news_science_products

U.S. Geological Survey. (n.d. -b). Quality of Ground Water. Retrieved from https://pubs.usgs.gov/gip/gw/quality.html

U.S. Geological Survey (2016). Groundwater. Retrieved from: https://pubs.usgs.gov/gip/gw/index.html

Vienna: International Atomic Energy Agency. (2014). "The environmental behavior of radium." Techical Report Series ISSN 0074-1914(476).

The Water Quality Association. (2013). Radium Factsheet. Technical Application Bulletin.

Webster, I.T., Hancock, G.J., Murray, A.S. (1995)/ Modelling the effect of salinity on radium desorption from sediments. *Geochimica et Cosmochimica Acta 59*(2469-2476).

Weinstein, Y., Yechieli, Y., Shalem, Y., Burnett W. C., Swarzenski P. W., Herut, B. (2011, May 25). What is the role of fresh groundwater and recirculated seawater in conveying nutrients to the coastal ocean? *Environ Sci Technol 45* (12), 5195-5200. doi:10.1021/es104394r

Yan, Shao-Feng, et al. (2015, Aug. 11). Seasonal Variations in Groundwater Level and Salinity in Coastal Plain of Eastern China Influenced by Climate. *Journal of Chemistry 2015* (0AD), 1–8.

TEXAS A&M UNIVERSITY-CORPUS CHRISTI
A BRIEF HISTORY

Texas A&M University–Corpus Christi began in 1947 as the University of Corpus Christi (UCC) which was affiliated with the Baptist General Convention of Texas. In 1970, Hurricane Celia caused more than $1,000,000 dollars in damage to the campus. In 1971, the Baptist General Convention of Texas sold UCC to the state of Texas and the Texas Legislature authorizes the Texas A&I University System to establish a state-supported upper-level institution of higher education in Corpus Christi. In 1973, Texas A&I University at Corpus Christi opens its doors on 4 September 1973 to 969 students as an upper-level institution of higher education. In 1977, the Texas Legislature changes the name of the University to Corpus Christi State University. In 1989, Corpus Christi State University joins the Texas A&M University System. In 1993, the Texas A&M University System Board of Regents renames the institution Texas A&M University–Corpus Christi and a year later it becomes a four-year comprehensive university and enrollment increases to 5,000 students.

In 2004, the Board of Regents approves the College of Nursing
and Health Sciences which opened in 2005. In 2005, Dr. Flavius Killebrew becomes President/CEO and initiates Momentum 2015, a ten year plan to establish Texas A&M University–Corpus Christi as the flagship university of South Texas. In 2016, Dr. Killebrew announced his retirement and former Provost and Vice President for Academic Affairs Kelly Quintanilla was appointed interim president. Today the University has over 12,000 students.

Today Texas A&M University–Corpus Christi is not only a proud member of the Texas A&M University System but it is also the premier public university in the region and is currently the only university in the United States to be situated on an island. Texas A&M University–Corpus Christi is currently a member of the Southland Conference under the NCAA division I.

All information on this page can be found at http://www.tamucc.edu.

Please direct information to:

McNair Scholars Program
Texas A&M University- Corpus Christi
6300 Ocean Drive, Unit 5791
Classroom West
Corpus Christi, TX 78412
361-825-3835
mcnair.tamucc.edu

The McNair Research Journal is the official journal of the McNair Scholars Program (Ronald E. McNair Post-Baccalaureate Achievement Program) at Texas A&M University-Corpus Christi. Funding is through the U.S. Department of Education (Grant No. P217A170075).

TRiO
RONALD E. McNAIR POST-BACCALAUREATE ACHIEVEMENT PROGRAM

TRIO

RONALD E. MCNAIR POST-BACCALAUREATE ACHIEVEMENT PROGRAM

TEXAS A&M UNIVERSITY
CORPUS CHRISTI